UNIVERSIDADE ESTADUAL PAULISTA
"JÚLIO DE MESQUITA FILHO"
Campus de São José do Rio Preto

Natália Bueno Leite Slade

Estudos das Interações do Peptídeo Antimicrobiano Polybia MP1 com Membranas Modelo: Mecanismo de Ação e Especificidade

São José do Rio Preto

2014

Natália Bueno Leite Slade

Estudos das Interações do Peptídeo Antimicrobiano Polybia MP1 com Membranas Modelo: Mecanismo de Ação e Especificidade

Tese apresentada como parte dos requisitos para a obtenção do título de Doutor em Biofísica Molecular, junto ao Programa de Pós-Graduação em Biofísica Molecular, Área de Concentração- Biofísica Molecular, do Instituto de Biociências, Letras e Ciências Exatas da Universidade Estadual Paulista "Júlio de Mesquita Filho", Campus de São José do Rio Preto.

Orientador: Prof. Dr. João Ruggiero Neto

São José do Rio Preto

2014

Slade, Natália Bueno Leite.
Estudos das interações do peptídeo antimicrobiano Polybia MP1 com membranas modelo : mecanismo de ação e especificidade / Natália Bueno Leite Slade. -- São José do Rio Preto, 2014
117 f. : il., gráfs., tabs.

Orientador: João Ruggiero Neto
Tese (doutorado) – Universidade Estadual Paulista “Júlio de Mesquita Filho”, Instituto de Biociências, Letras e Ciências Exatas

1. Biologia molecular. 2. Biofísica. 3. Peptídeos antibióticos. 4. Dicroísmo circular. 5. Microscopia confocal. 6. Membranas (Biologia) I. Ruggiero Neto, João. II. Universidade Estadual Paulista "Júlio de Mesquita Filho". Instituto de Biociências, Letras e Ciências Exatas. III. Título.

CDU – 577.3

Ficha catalográfica elaborada pela Biblioteca do IBILCE
UNESP - Câmpus de São José do Rio Preto

Natália Bueno Leite Slade

Estudos das Interações do Peptídeo Antimicrobiano Polybia MP1 com Membranas Modelo: Mecanismo de Ação e Especificidade

Tese apresentada como parte dos requisitos para a obtenção do título de Doutor em Biofísica Molecular, junto ao Programa de Pós-Graduação em Biofísica Molecular, Área de Concentração- Biofísica Molecular, do Instituto de Biociências, Letras e Ciências Exatas da Universidade Estadual Paulista "Júlio de Mesquita Filho", Campus de São José do Rio Preto

Comissão Examinadora

Profa. Dra. Marcia Perez dos Santos Cabrera

UNESP - São José do Rio Preto

Prof. Dr.Amando Siuiti Ito

USP - Ribeirão Preto

Prof. Dr. Sebastião R. Taboga

UNESP - São José do Rio Preto

Prof. Dr. Manoel de Arcísio Miranda Filho

UNIFESP- São Paulo

Prof. Dr. João Ruggiero Neto

UNESP - São José do Rio Preto

Orientador

São José do Rio Preto

2014

Resumo

Peptídeos bioativos são de grande interesse como substitutos de antibióticos e quimioterápicos convencionais já que, alguns deles apresentam atividades antimicrobiana, antifúngica e/ou anticâncer. Eles são predominantemente catiônicos e sua atividade tem se mostrado ser modulada por interações eletrostáticas, contribuições hidrofóbicas e por características elásticas da membrana, o seu alvo. O peptídeo mastoparano Polybia MP1 (MP1) possui dois resíduos ácidos (D2 e D8) e três resíduos básicos (K4, K5 and K11), que somados ao C terminal amidado conferem a ele uma carga elétrica líquida relativamente baixa, Q= +2. Nesta tese, foi analisada a importância da sequência de aminoácidos do MP1, da sua carga elétrica líquida e da sua hidrofobicidade média na interação com distintas membranas modelo, já que a presença de resíduos ácidos é rara dentre os peptídeos bioativos e além disto, o MP1 apresenta elevadas atividades antimicrobiana e anticâncer sem ser hemolítico. Para entender a sua especificidade e o seu mecanismo de ação em células bacterianas e de câncer, a atividade e a afinidade do MP1 foi acessada através de espectroscopia de fluorescência e de dicroísmo circular, medidas de potencial eletrocinético e de espalhamento de luz dinâmico e microscopia confocal. Estas técnicas permitiram a observação da estruturação do peptídeo, da sua partição da água para a interface de membranas modelo, da sua atividade lítica e da agregação dos lipossomos devido a sua adição. Assim, foi possível estimar as contribuições energéticas envolvidas no sistema além das dimensões dos danos causados pelo MP1 na superfície da membrana. MP1 mostrou que sua baixa carga elétrica líquida e a presença de dois resíduos ácidos na sua sequência de aminoácidos apresentam um papel importante em modular a sua estruturação e a sua atividade em uma ampla gama de composições lipídicas. Isso é atribuído ao equilíbrio das contribuições eletrostáticas e não eletrostáticas e contribui para o entendimento da sua ação como peptídeo bioativo.

Palavras-Chave: Peptídeos Bioativos, Espectroscopia de Fluorescência, Dicroísmo Circular, Microscopia Confocal, Membranas-Modelo

Abstract

Bioactive peptides are of high interest as substitutes of conventional drugs since some of them present antimicrobial, antifungal and/or anticancer action. They are predominantly cationic and it has been shown that their activity is modulated by electrostatic interactions, hydrophobic contributions and the elastic features of the membranes their target. The mastoparan peptide Polybia MP1 (MP1) possesses two acidic residues (D2 and D8) and three basic ones (K4, K5 and K11), which together with the amidation of the C-terminal confers to it a relatively low net charge Q=+2. In this thesis, we analyzed the importance of the MP1 amino acid sequence, charge and hidrophobicity to the interaction with distinct model membranes, since the presence of acidic residues is a rare characteristic among the bioactive peptides and, beyond this, MP1 presents high antimicrobial and anticancer activities without being hemolytic. In search of understand its specificity and mechanism of action for bacteria and cancer cells, the activity and affinity of MP1 was assessed through circular dichroism and fluorescence spectroscopy, electrophoretic and dynamic light scattering measurements, and confocal microscopy. These techniques allowed the observation of the peptide structuration, the peptide partitioning from water to the model membranes interface, the peptide lytic activity, and the liposome aggregation due to peptide addition. From this, it was possible estimate the energetic contributions involved in the system, besides the dimension of the damages caused by MP1 on the membranes surface. MP1 showed that its low net charge and the presence of two acidic residues play an important role in modulating its structuration and activity in a wide range of lipid compositions, by equilibrating electrostatic and non-electrostatic contributions giving basis to understand its action as bioactive peptide.

Keywords: Bioactive Peptides, Fluorescence Spectroscopy, Circular Dichroism, Confocal Microscopy, Model Membranes.

Dedicatória

Dedico esta Tese aos meus pais, que não mediram esforços para que eu pudesse receber uma boa formação.

Dedico esta Tese ao meu esposo e ao meu filho, por fazerem a minha vida cada dia mais alegre.

Dedico esta Tese ao querido Professor Doutor Augusto Agostinho Neto (*in memória*), um exemplo de pessoa e de profissional; um grande incentivador do meu trabalho desde o período da graduação.

Agradecimentos

Agradeço à Deus pelo dom da vida!

Agradeço imensamente ao Professor Doutor João Ruggiero Neto por todo este período de aprendizagem, pelas oportunidades proporcionadas com a finalidade de contribuir para o meu crescimento profissional, pela paciência dedicada nos períodos de dificuldade e, especialmente, por ser uma inesgotável fonte de inspiração para o meu trabalho.

Agradeço à UNESP-IBILCE; pela excelente formação que me proporcionou.

Agradeço ao Programa de Pós Graduação em Biofísica Molecular; que através dos professores e funcionários possibilitou a execução deste trabalho.

Agradeço à Professora Doutora Marcia Perez dos Santos Cabrera, pela minha iniciação na área experimental.

Agradeço às minhas companheiras de laboratório Dayane, Luciana e Taísa; pelos momentos de companheirismo, descontração e trocas de experiência em técnica e análise.

Agradeço ao Doutor Paul Beales; por ter me recebido na Universidade de Leeds com muita vontade de realizar um bom trabalho.

Agradeço à Capes, CNPq e FAPESP por todo o apoio financeiro ao longo do doutorado.

Agradeço ao meus queridos colegas e amigos do departamento; que ao longo deste período fizeram parte dos maiores acontecimentos da minha vida e os tornaram, certamente, mais especiais.

Agradeço aos meus pais e irmão por todo o carinho, amor, paciência e apoio SEMPRE!!

Agradeço ao meu esposo (Gabriel) e meu filho (Estevão) por partilharem desta jornada comigo tornando tudo absolutamente melhor!

Content

ABBREVIATIONS

10k-AF647	10kDa Alexa Fluor 647-labelled dextran
3k-CB	3kDa Cascade Blue-labelled dextran
Φ	Polar face angle
ΔG_{ads}	Partition free energy
ΔG_{conf}	Conformational free energy
ΔG_{el}	Electrostatic free energy
ΔG_{ex}	Extra free energy
ACPs	Anticancer peptides
AFM	Atomic Force Microscopy
AMPs	Antimicrobial peptides
ANTS	Aminonaphtalene-1, 3, 6-trisulfonic acid sodium salt
CD	Circular Dichroism
CF	Carboxyfluorescein
CL	Cardiolipin
CPPs	Cell penetrating peptides
D	Aspartic Acid
D_H	Hydrodynamic diameter
DLS	Dynamic Light Scattering
DOPC	1,2-dioleoyl-sn-glycero-3-phosphocholine
DOPE	1,2-dioleoyl-sn-glycero-3-phosethanolamine
DPX	p-xylenebis (pyridinum) bromide
f_H	α-helix fraction
GUV	Giant Unilamellar Vesicle
<H>	Mean hydrophobicity
I	Isoleucine
K	Lysines
K_p	Partition coefficients
L	Leucine
L-CPL	Left circularly polarised light

LUV	Large Unilamellar Vesicle
MP1	Polybia MP1
MP2	Polybia MP2
MP3	Polybia MP3
MPX	Mastoparan X
NMP1	Polybia N2D-MP1
[P]/[L]	Threshold peptide lipid ratio
PC	L-α-Phosphatidylcholine
PG	L-α-Phosphatidyl-DL-glycerol
POPS	1-palmitoyl-2-oleoyl-sn-glycero-3-phosphoserine
Q	Peptide electric net charge
R-CPL	Right circularly polarised light
Rh-DOPE	1,2-dioleoyl-sn-glycero-3-phosphoethanolamine-N-(lissamine rhodamine B sulfonyl)
W	Tryptophan

Chapter 1

Introduction

1.1 Lipids and Biological Membranes

The lipids are water insoluble molecules which exhert many functions in biology. They are responsible for the energy storage and for the architecture of the biological membranes in a wide range of organisms (Nelson and Cox, 2011).

The structural lipids, known as phospholipids, are amphipathic molecules i.e. they are formed by a hydrophobic portion ("tail") and a hydrophilic one ("head"). The glycerophospholipids have tails made of two fatty acids sterified to glycerol, one of them is a 16 or 18 carbons saturated chain while the other is an unsaturated one with 18 or 20 carbons. The polar head is associated to the phosphate group and can be a simple group like –OH or other groups more complexes as shown in fig 1.1 (Nelson and Cox, 2011).

In the presence of water, these molecules tend to self-organize in such a manner that the heads are in contact with the water molecules and the tails are protected from them. This self-assembling leads the lipids to pack in bilayers exactly as they are found in the biological membranes. The lipid bilayer formation is favored when the cross sectional areas of the polar head groups and hydrophobic tails of the phospholipids are similar. It has a width of around 5 nm with a highly polar hydrophobic core that leads the hydrophobic edges to curve themselves by giving rise to a hollow sphere commonly known as vesicles (fig.1.2-b).

The biomembranes are composed by more than 100 species of lipids with distinct polar groups and hydrophobic portions, but the reasons for this diversity are not well understood (Gennis 1989). Each lipid leaflet of the plasmatic membrane is made up by distinct lipid compositions. In the case of the erythrocyte membranes, zwitterionic lipids containing choline groups are found in the outer leaflet while a mixture of zwitterionic and anionic lipids (phosphatidylethanolamine, PE, and phosphatidylserine, PS) are found in the inner layer, fig.1.2-c. Natural changes in these lipid compositions affect some of the membrane biological/biophysical features and can be indicative of specific diseases consequences; for example, when PS is externalized in human cells it signals destruction by programmed cell death as seen in leukemic, bladder and prostate cancer cells (Zwaal et al. 2005, Schweizer 2009).

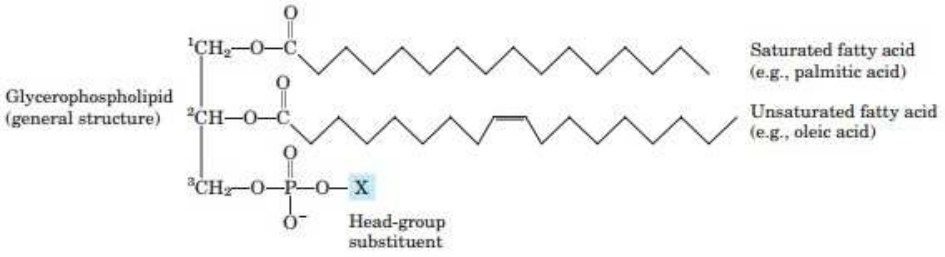

Name of glycerophospholipid	Name of X	Formula of X	Net charge (at pH 7)
Phosphatidic acid	—	—H	−1
Phosphatidylethanolamine	Ethanolamine	$-CH_2-CH_2-\overset{+}{N}H_3$	0
Phosphatidylcholine	Choline	$-CH_2-CH_2-\overset{+}{N}(CH_3)_3$	0
Phosphatidylserine	Serine	$-CH_2-CH(COO^-)-\overset{+}{N}H_3$	−1
Phosphatidylglycerol	Glycerol	$-CH_2-CH(OH)-CH_2-OH$	−1
Phosphatidylinositol 4,5-bisphosphate	*myo*-Inositol 4,5-bisphosphate	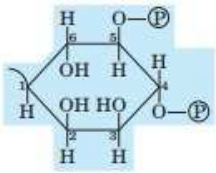	−4
Cardiolipin	Phosphatidyl-glycerol	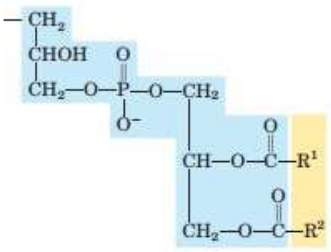	−2

Figure 1.1 Examples of glycerophospholipids (Nelson and Cox 2011).

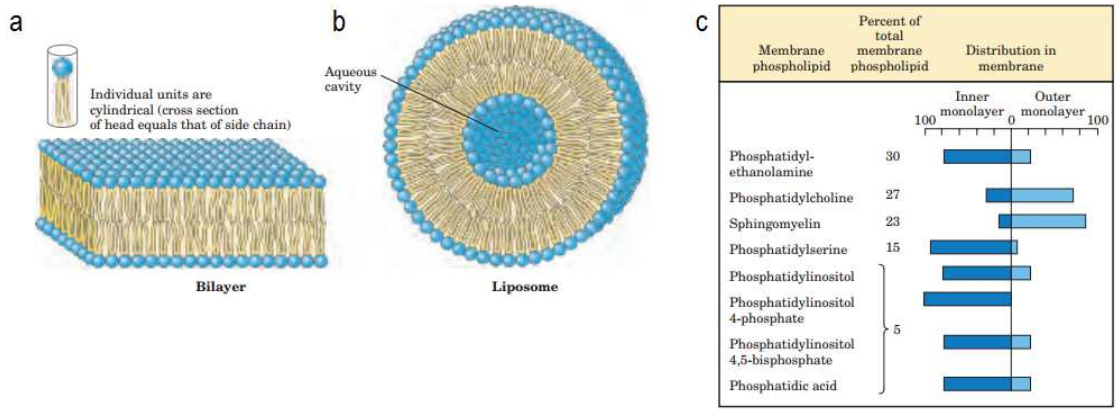

Figure 1.2 a- Lipid bilayer. **b-** Vesicle. **c-** Lipid distribution on the layers of the erythrocyte plasmatic membrane (Nelson and Cox 2011).

The cell membranes are a fluid mosaic of proteins that have high capacity of movement and displacement. In addition the membrane proteins display fundamental importance in holding and transporting selectively other molecules through the membrane. Sterols and glycerols are also found in some organisms and contribute to the membrane topology (Yeaman and Yount 2003). In a general way, the bacterial membranes are mainly composed by anionic lipids such as phosphatidilglicerol (PG), cardiolipin (CL) or phosphatidylserine (PS) (Cronan 2003). Among the bacteria there are two classes: the Gram negative and Gram positive with distinct cellular walls as shown in fig.1.3. In the first case, the cells are composed by one lipid bilayer (plasmatic membrane), one thin layer of peptidoglycan, and an outer bilayer rich in lipids, proteins and lipopolysaccharides. In the second case, they exhibit a single lipid bilayer (plasmatic membrane) and a thick layer of peptidoglycan.

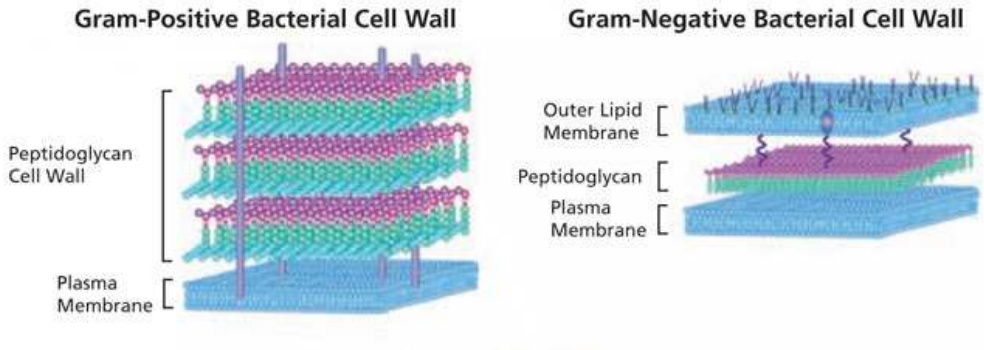

Figure 1.3 Representative scheme of Gram Positive and Gram Negative Bacteria cell wall.Lipid bilayer (Sigma Aldrich:http://www.sigmaaldrich.com/technical-documents/articles/biology/glycobiology/peptidoglycans.html).

The variety of lipids in a membrane influence many physical aspects such as: fluidity, surface charge density and curvature strains (Matsuzaki et al 1998). It occurs because of the wide range of existing polar head groups that exhibit differences in size and charge, and because of differences in the tails in terms of length and number and/or position of unsaturation. The curvature strain is related to the variations in symmetry between the hydrophilic and hydrophobic portions of a phospholipid. In the case of PE lipids, the cross section of the head group is smaller than the cross section of the tails and it shows a cone shape which favors negative curvature strain (fig.1.4), while PC lipids present a cylinder shape due to the perfect symmetry between the head and the tail volumes. As a consequence, they exhibit neutral curvature strain (fig. 1.4). Other lipids generate differences in the surface charge density of the membrane, since as seen in fig.1.1, there are differences in the charges of the polar head groups. Besides these, there are lipids with differences in phase transition temperatures due to the variety of unsaturation and the length of the hydrophobic tails which can affect the packing of the lipids leading to more or less fluid membranes.

Some of these aspects were explored in this thesis through the preparation of synthetic lipid vesicles in laboratory. These could be done by preparations including mixtures of lipids such as PC/PG (70:30), PC/PS (80:20), DOPC/DOPE/POPS (70:10:20) which are negatively charged, and PC or DOPC (100) and DOPC/DOPE (90:10) which are electrically neutral at physiological conditions. The changes in lipid composition showed to be important in the interaction between vesicles and cationic peptides. Differences in electrical charges could show

the importance of electrostatic effects by intensifying the interaction while the presence of PE has had the same final effect, but it showed the importance of curvature strains in this system.

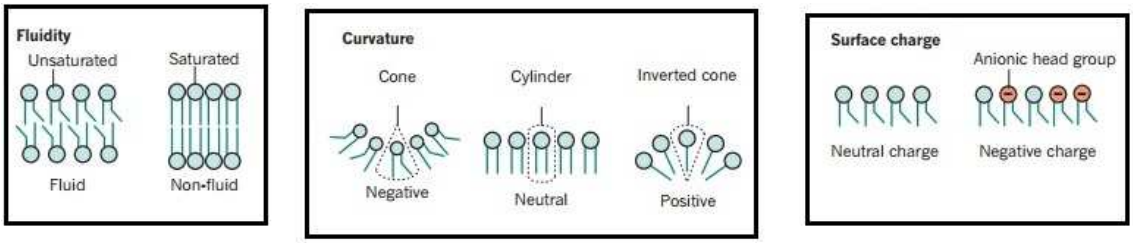

Figure 1.4 Example of changes in the membrane physical aspects due to lipids variety (Holthuis and Menon 2014).

1.2 Bioactive Peptides

Peptides are small molecules composed by sequences of amino acid residues covalently attached by peptidic bonds. Their molecular weight does not exceed 10000 Da. In general, twenty different amino acids are found in peptides and proteins. The differences between them rely on the lateral chains which vary in structure, size, water affinity and electrical charge. The figure 1.5 shows the 20 natural amino acids, their nomenclature and abbreviations.

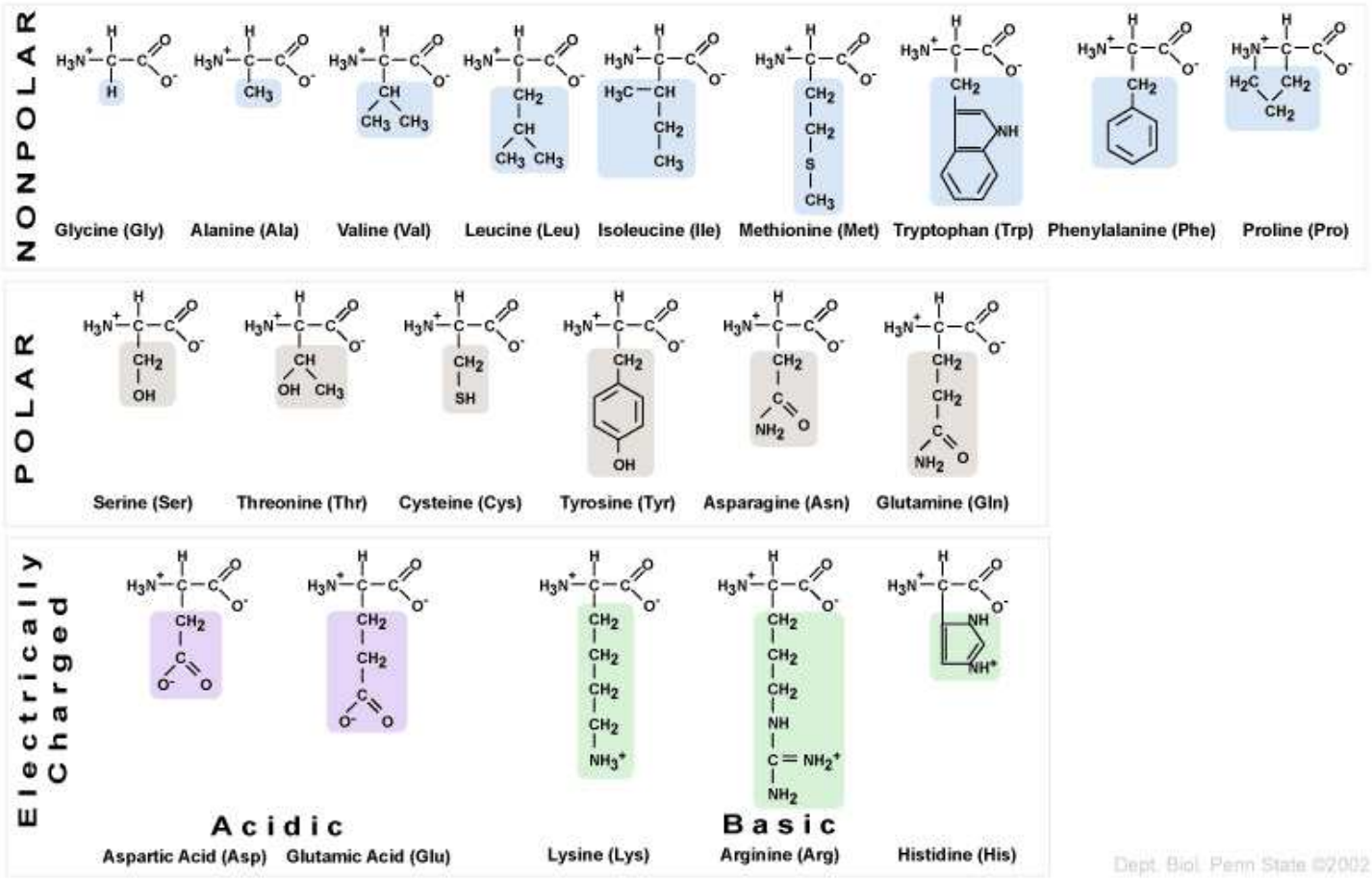

Figure 1.5 The twenty amino acids according to the residues characteristics: electrical charge and water affinity (polar or nonpolar) (https://wikispaces.psu.edu/download/attachments/40047576/image-1.jpg).

The bioactive peptides present up to 45 residues (Hancock and Lehrer1998), and can exhibit antimicrobial, antifungal, anticancer and/or hemolytic activity. For this reason, they became an object of many studies. All the cited activities are directly related to their interaction with the lipid membrane of the target organisms, since they act by promoting the disruption of the membrane surfaces through mechanisms not well established.

The antimicrobial peptides (AMPs) are found on the innate immune system of many organisms such as bacteria, insects, amphibians, birds, fishes, mammals, and plants (Wang and Wang 2004; Wang et al. 2009). They are good candidates in solving the problem of multidrug antibiotic resistance (Wimley and Hristova 2011) because they exhibit specific interactions with anionic groups of cell surface and are independent of receptors. The specificity towards anionic groups is attributed to their cationicity and the abundance of anionic lipids on the outerleaflet of prokaryotic cell membranes, a feature that has not changed along the evolution (Zasloff 2002). In consequence of this, the activity of these peptides is independent of chemical receptors and avoids that the organisms acquire resistance against them. Some natural peptides have been tested as drugs in trials for application as the case of candidiasis (Demegen Pharmaceuticals 2010), catheter-associated infections (Melo et al. 2006), and implant surface infections (Kazemzadeh-Narbat et al. 2010). Besides the disadvantage that they can exert hemolytic and/or mast cell degranulation activities, they also require high costs to be produced in comparison to the conventional chemical antibiotics. For these reasons, it is necessary the complete understanding of their mechanism of action to enable the development of novel peptides as short, as potent, and as simple as possible for pharmaco-applications (Wimley and Hristova 2011).

The AMPs are able to permeate the microbial cytoplasmic membrane by causing the cell disruption or cell death through leakage of the inner content. At the first stage of peptide-lipid interaction, the AMPs are in solution as random coil structures. They are attracted to the membrane surface due to electrostatic interactions between the cationic peptides and the anionic lipid head groups. Upon the adsorption to the membrane they assume a secondary structure. The predominat structure is amphiphatic helical generated because of their amino acid composition rich in basic and non polar residues, that tend to self organize by facing the polar ones to the water molecules while the non polar residues facing the lipids portion of the bilayer. After this step, many mechanisms have been proposed so far (Rapaport and Shai 1991; Ludtke et al. 1996; Gazit et al. 1996; Ostolaza et al. 1996; Epand and Epand 2009; and Yandek et al. 2007), among them are both transmembrane pore models and non pore models as shown in figure 1.6.

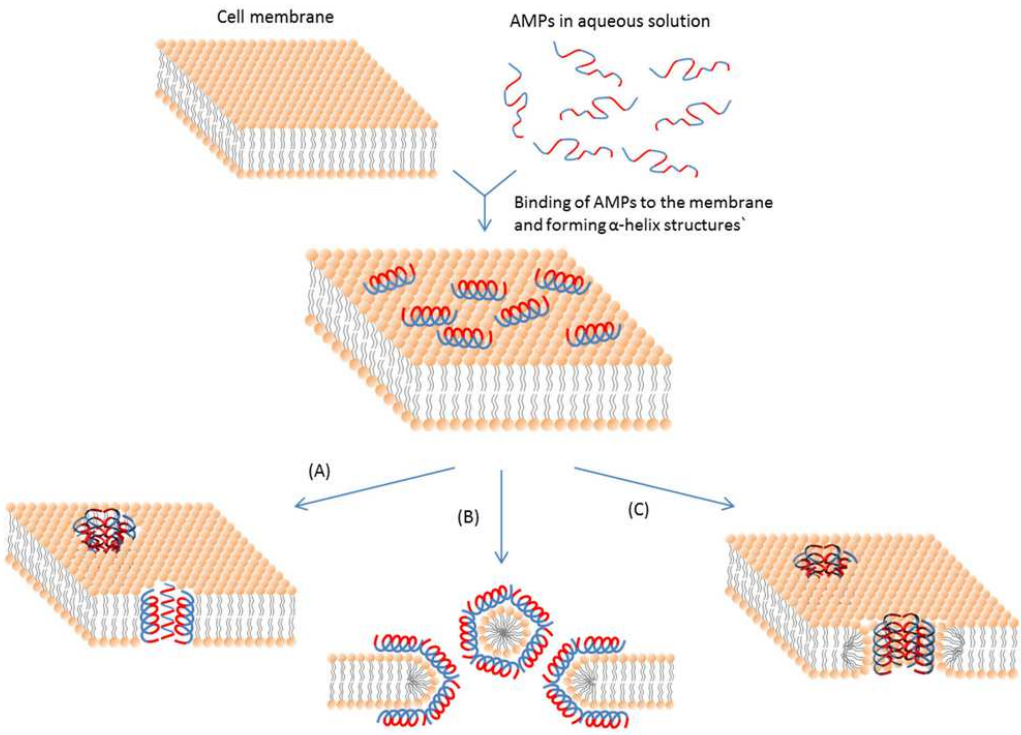

Figure 1.6 Schematic representations of mechanisms of action for AMPs. A: Barrel-Stave Pore mechanism. B: Non pore Carpet/Detergent Model. C: Toroidal Pore mechanism. (Bahar and Ren 2013).

In the pore formation models, the peptides adsorb on the membrane surface until reaching a critical concentration that disturb the lipids organization. An extra pressure is exerted on the membrane due to peptide accumulation that is relieved by opening pore like structures. The barrel stave pore (Huang 2000; Rapaport and Shai 1991) is made by the peptides insertion into the membrane followed by the formation of a channel all revested by them. The peptides interact laterally each other by stabilizing the lipid bilayer with the polar face in contact with the solvent while the non polar one is in contact with the lipid moiety. This type of pore requires specific properties of peptides such as length, helicity and amphipathicity (Pasupuleti et al. 2012) which makes of it a less frequent structure among the AMPs but well stabilished for alamethicin (Qian et al. 2008). On the other hand, there is no specific peptide-peptide interactions in the toroidal pore model (Wimley and Hristova 2011) since the peptides affect the local curvature of the membrane by inducing a positive curvature strain due to the adsorption process and yielding the pore structure. Different from the barrel stave model, this type of pore is stabilized by a mixture of lipids and peptides, does not require specific features for the AMPs, and has been shown for mellitin and magainin (Sengupta et al. 2008; Matsuzaki et al. 1997 and 1998).

Moreover, AMPs can act by the detergent (Ostolaza et al. 1996) or the carpet model (Gazit et al. 1996) in which the peptides insert parallel to the membrane surface and disturbs the lipid bilayer by causing its fragmentation and/or even micellization. It happens at high peptide concentrations and the dimension of this concentration is a particular feature for each AMP. The lipid clustering model (Epand and Epand 2009) assumes that, after adsorption on the membrane,

the peptides disturb the lipid packing by causing boundary defects such as lipid clusters and lipids phase separation. It enables passage of the cell inner contents to the external environment and can cause cell death. Some AMPs can even work by crossing the lipid bilayer of cellular membranes and killing pathogenic agents (Henriques et al. 2006). In this case, they work as cell-penetrating-peptides (CPPs) in which single peptides are able to cross the lipid bilayer as a manner to relieve the mass imbalance induced by their association on the external lipid layer (Yandek et al. 2007).

Among the biophysical features of AMPs that influences their antimicrobial activity are the peptides net charge (Q), the polar face angle (Φ), and the mean hydrophobicity (<H>). AMPs show net charges ranging from +2 to +11 as a consequence of the presence of lysines and arginines and the lack of acidic residues in their amino acid sequence (Yeaman and Yount 2003; Yount and Yeaman 2005). The cationicity has fundamental importance on the initial interaction between the peptide and the membrane surface where the electrostatic attraction takes place as the major contribution. Nevertheless, there is no direct relationship between charge and the peptide activity once that the excess of positive charges can affect the peptide structuration and reduce its activity due to intrachain and inter peptide-lipid electrostatic repulsion as shown by Tossi et al. (1994). The Φ is related to the amphiphatic helical structure found in the majory of the AMPs. These AMPs can be represented as a perfect α helix by helical wheel projections and from this one can obtain their polar face angle (fig. 1.7), described as the angle that covers the whole hydrophilic region of the peptide. The bigger the non polar face angle is the higher is the peptide affinity for mammalian cells (Yount and Yeaman 2005). For a molecule considerably hydrophobic it is unfavourable to remain in a highly polar environment. The mean hydrophobicity, <H>, is a quantity obtained from the arithmetic average intrinsic hydrophobicity of the residues. It can be obtained from many hydrophobicity scales such as the Eisenberg scale of consensus (Eisenberg et al. 1984) and the Wimley and White scale (Wimley and White 1996). The Eisenberg scale of gives to each amino acid a characteristic hydrophobicity value. For example, the most hydrophobic residue is isoleucine with 0.73, while the least hydrophobic is arginine with -1.76. The <H> increases with the quantity of hydrophobic amino acids in a sequence and can work by potentiating the interaction between the peptides and the non polar environment of the lipid bilayers. In the literature, there are studies showing that the lower is the φ, the higher is the effect of bilayer permeabilization (Uematsu and Matsuzaki 2000). There are others showing that the most stable pore structures are those observed for peptides with higher φs (Yeaman and Yount 2003). In another words, there is no consensus about the best relationship between AMPs charge/hydrophobicity and their activity. This makes peptides a challenging field for many scientists since, apart the

peptides features, we also have the membranes characteristics varying with the lipids composition and interfering on their action.

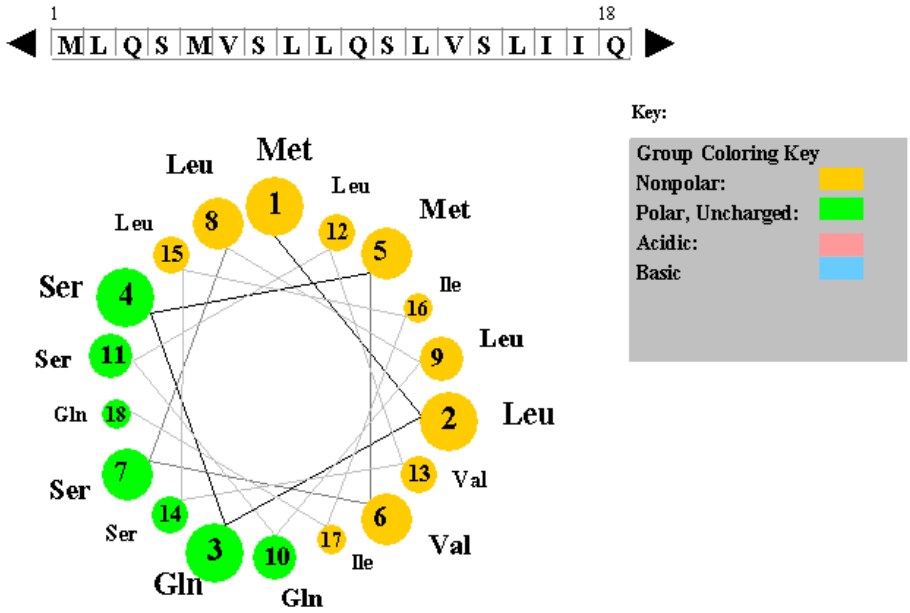

Figure 1.7 Example of helical wheel projection of an amino acid sequence. The residues are positioned as a perfect α helical structure. The polar non charged residues are shown in green while the non polar ones in yellow. It is an example of a perfect amphipathic helix since there is a clear separation of the polar face, indicated by the green residues side, and the non polar indicated by the yellow residues side. The figure is a snaphot of a Java Applet written by Edward K. O'Neil and Charles M. Grisham (University of Virginia in Charlottesville, Virginia). The applet is accessible athttp://cti.itc.Virginia.EDU/~cmg/Demo/wheel/wheelApp.html.

Recently, some AMPs have been studied as anticancer active peptides (ACPs) ((Papo and Shai 2005, Hoskin and Ramamoorthy 2008). Their affinity for cancer cells is attributed to differences on cell membranes due to the development of the disease. Cancer cell membranes are now known to lose the asymmetric transmembrane distribution of phospholipids that is observed in healthy cells (Zwaal et al 2005, Schweizer 2009). In healthy mammalian cells, the aminophospholipids, as phosphatidylserine (PS), are predominant in the inner membrane leaflet and the zwitterionic phospholipids in the outer leaflet of the membrane. In these cells, the phospholipid asymmetry is maintained by a family of aminophospholipid translocases APTLs, catalyzing the transport of PS from the outer to the inner membrane leaflets (Marconescu and Thorpe 2008). However in apoptotic and cancer cells, phophatidylserine is found to be also located in the outer monolayer in significant proportions (Zwaal et al 2005, Schweizer 2009). The ACPs mechanism of action involves the disruption of the plasma or mitocondria

membrane, the mechanisms of mediated immunity in which the peptides activate the imune system response (Wang et al, 2009a), cell receptors by regulating genes and developing the ability of treat the cancer (Leuschner and Hansel 2005), the DNA synthesis inhibition (Ourth 2011), and the anti-angiogenic effects (Koskimaki et al. 2009).

The focus of this thesis is to understand the specificity and mechanism of action of Polybia MP1 (MP1) using different model membranes. Because this peptide shows potent antimicrobial action against Gram-positive and Gram negative bacteria, chemotaxis to polymorphonucleated leukocytes, and it does not exhibit hemolytic activity in rat erytrocytes (Souza et al. 2005). MP1 also shows a selective inhibitory effect on proliferating bladder and prostate cancer cells (Wang et al. 2008), and against multidrug resistant leukemic cells (Wang et al 2009c). Recently, our group observed that this peptide is cytotoxic against leukemic T lymphocytes and very selective in recognizing these cells compared to health lymphocytes (dos Santos Cabrera et al. 2012).

The sequence of MP is rich in basic and acidic residues and is amidated at the C terminal, which confers an additional positive charge, at pH 7.4. These peptide remarks in an unstructured form in aqueous solution and acquires a helical structure when in contact with lipid bilayers. The macrodipole of this helical structure is oriented from C-terminal to N-terminal (Shoemaker et al 1985). The presence of an acidic residue, on the second position of the backbone, is seen as an stabilizing factor, responsible for the reduction of the electrostatic repulsion between the N-terminus NH3+ and the positive pole of the helical macrodipole. The acidic residues are scarcely present in most AMPs (Yount and Yeaman 2005) and the balance of the net charge due to the presence of acidic and basic residues has not been explored yet. In search of understanding the importance of these residues and the effects they cause in terms of hidrophobicity, helical stability, membrane affinity, and mechanism of action on the peptide lipid interactions, we have used distinct lipid compositions and different experimental techniques as a strategy to compare affinity and lytic activity of MP1 with analogs and other peptides with similar physico-chemical characteristics.

All the used peptides are mastoparans beeing MP1, Polybia MP2 (MP2), and Polybia MP3 (MP3) extracted from the venom sac of the wasp ***Polybia paulista***, Polybia-N2D-MP1 (NMP1) the synthetic analog of Polybia MP1 with the substitution N2D, and MPX extracted from the wasp ***Xanthopera***. The electrical net charges vary from +1 (MP3) to +4 (MPX), the mean hidrophobicities vary from -0.08 (MP2) to -0.11 (MP1), and the polar face angle from 60º (MP2 and MP3) to 120º (MP1 and NMP1). They are composed by 14 amino acid residues with the amidation on the C-terminus and present a tryptophan residue in the third position that works as a fluorophore and makes possible the use of fluorescence spectroscopy techniques to

investigate the positioning of the peptide in relation to the water /lipid bilayer. According to the biological assays performed by Souza et al. (2005 and 2009) the peptides extracted from ***Polybia paulista*** showed minimum inhibitory concentrations ranging from 6 to 62μM against the Gram negative ***E. coli*** and from 4 to 31μM against the Gram positive ***S.aureus*** besides minor or low degranulating activity in rat mast cells. The peptides' charge differences are related to the presence of lysine and aspartic acid in distinct quantities. The distribution of the aminoacids in the chain is such that they form amphipathic helical structures in adequate environments. A variety of lipid compositions was used enabling us to change the model membranes physical aspects such as: charge/ electrical potential, fluidity, and curvature strains and, consequently, to observe how these aspects could affect the peptides activity. The results of this thesis are separated in two published papers and one manuscript.

In the first paper, we compared MP1 with other four peptides to test their membranes' affinity and activity through circular dichroism and fluorescence spectroscopy. The peptides with lower net charges showed higher lytic activity and affinity in zwitterionic membranes, as an indicative that the electrostatic repulsion is a factor to be considered in the interaction of the most charged peptides with the electrically neutral vesicles. In the anionic vesicles, all the peptides showed increased activity which evidences the importance of the electrostatic contribution on the peptide-lipid interaction. The presence of acidic residues showed an important role in modulating the activity of the peptides by stabilizing the electrostatic interactions between the charged groups. This result was considerably dependent of the peptides mean hydrophobicity and it was especially demonstrated in the helix stabilization of MP1.

In the second paper, we compared MP1 action with its N2D mutant and MPX. They exhibit different net charges due to the decreased presence of acidic residues in their amino acid sequence. Their interaction with zwitterionic and anionic model membranes were investigated by fluorescence spectroscopy, electrophoretic mobility measurements and circular dichroism to estimate the free energies involved in these systems. The results showed the highest affinity in both anionic and zwitterionic environments for the peptides with lower net charge. The estimative of free energy was obtained separately according to each experiment i.e. the partition free energy was evaluated from the partition coefficients resulted from fluorimetric titrations, the electrostatic component was obtained from zeta potential results, and the conformational from the circular dichroism data. As expected, the electrostatic free energy increased with the peptides net charge. The sum of electrostatic and non- electrostatic contributions was incompatible with the total free energy (the partition free energy) given origin to an excess free energy. Even with lower electrostatic and conformational contributions, MP1 exhibited the major affinity for anionic vesicles with the highest excess free energy, which we suggest to be

likely due to other energetic contributions related to the presence of the acidic residue the second position (D2) of its amino acid sequence.

In the third part, the manuscript, since a lot have been explored about MP1 as an antitumor agent, we observed MP1 interaction with distinct lipid compositions to understand the affinity by cancer cells. To this end, giant and large unilamellar vesicles were formed with anionic (PS) and zwitterionic (PC) lipids with or without phosphatidilethanolamine (PE). The giant vesicles were observed by confocal microscopy, which enabled us to monitor the vesicles separately and study how the peptide could affect the membrane structure, taking into account the size of the pores opened through the use of three different sized dyes. The presence of PS and PE highly affected the permeation kinetics of MP1. PS helped the peptide-lipid interaction due to electrostatic attraction, which was reflected on the kinetics by the smallest lag times while PE containing vesicles allowed the equal entrance of the three dyes until the equilibrium with the background was reached. Experiments with large unilamellar vesicles (LUVs) were made by fluorescence spectroscopy and the re-quenching results revealed the all-or-none mechanism of leakage of MP1 in all the tested lipid compositions. It suggests that this peptide permeates the membrane trough the formation of pore like structures long lived enough to the fluorescent probes internalize in the vesicles until equilibrium is reached. This study shows how the lipid composition can affect the membrane permeation due to the action of MP1, since the presence of PE and PS affected the speed of the peptide permeation kinetics and consequently its specificity for tumor cells.

OBJECTIVES

The objective of this study is observe the interactions of the antimicrobial peptide Polybia MP1 (MP1) with distinct model membranes in search of understand its specificity and mechanism of action through experimental techniques such as: fluorescence and dichroism spectroscopy, electrophoretic mobility and dynamic light scattering measurements, and confocal microsopy.

The major objectives are:

I - Compare the activity and affinity of MP1 with other four mastoparan peptides, when in contact with zwitterionic and anionic model membranes, to observe how the peptides' electric net charge, mean hydrophobicity, and polar face angle modulates the peptide bilayer-specificity.

II - Investigate the impact of the aspartic acid residue, in the N-terminus of MP1, on MP1 affinity to anionic lipid bilayer through the comparison between MP1 and other two mastoparan peptides electrostatic and conformational free energies.

III - Observe the effects of lipid composition on the lytic activity of MP1 as a manner to understand the peptide affinity for tumor cells.

Chapter 2

Experimental Methods

Fluorescence Spectroscopy

Fluorescence is obtained through a process of three steps. It occurs in molecules known as fluorophores that, in science, are projected to be in a specific region of a molecule. The fluorescence process is showed in the Jablonski diagram (figure 1.7) and correspond to a simple diagram of electronic states transition (Haugland, 1996). At first the photon is excited with energy $h\nu_{ex}$ by an external energy source such as laser which is absorbed by the fluorophore and raises to a finite excited state (S_2) with energy E that lasts about $1\text{-}10x10^{-9}$ s. At this point, the fluorophore is able to experience from conformational changes to many interactions with the surrounding environment. As a result, the energy is able to be in part dissipated raising another excited state (S_1) from where the fluorescence emission takes place by returning to the fundamental level (S_0). In some cases, another process (collisional quenching and intersystem crossing) can occur and the excited state S_1 can lose some of its molecules to other states such as T_1 and T_2 demonstrated in figure 2.1a. Then, the frequency resultant of the transferring energy from the excited to the fundamental state can be converted to a wavelength and in a spectra (figure 2.1b), for polyatomic molecules, characteristic for specific fluorophores. For example, in the case of the AMPs used in this thesis, the tryptophan residue on the third position of the amino acid sequence presents fixed wavelengths of excitation and emission processes (280nm and 350nm respectively). It is highly sensitive to the polarity of the surrounding environment and spectral shifts are observed as a result of many phenomena (Lakowicz 1999). Changes on the peptide environment can be reflected by the tryptophan emission spectra, i.e. if the tryptophan changes from a polar environment like water to a non polar environment like the lipid bilayer the maximum wavelength of emission changes to values smaller than 350nm and resulting in a characteristic blue shift. In this way, the fluorescence spectroscopy is used as a powerful tool to monitor the peptides' adsorption to lipid bilayers (Ladokhin et al. 2000; Santos et al. 2002 and 2003). Other assays can be performed in the system with distinct fluorophores as the case of leakage and re-quenching assays. The later enables the estimative of peptide mechanism of leakage in model membranes.

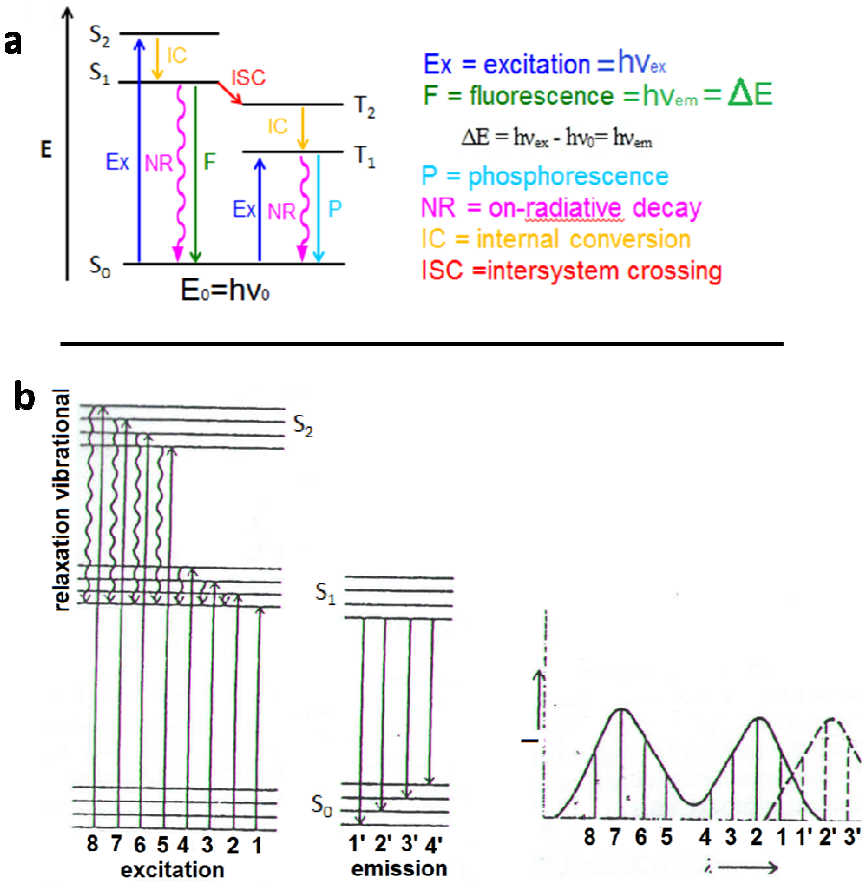

Figure 2.1 a General Jablonski diagram which shows the transition of the fundamental state to the excited state and the consequent process of emission. **b** The same transitions of panel (a) in spectra format, usually found for polyatomic molecules such as peptides. Panel (b) obtained from Perkin Elmer Ltd.

To estimate the peptides affinity for model membranes we obtain the partition coefficients, K_p, of peptide solutions that are titrated by adding aliquots of large unilamellar vesicles (LUVs) suspension. After each lipid vesicle addition, the tryptophan emission fluorescence spectra was collected with ISS PC1 spectrofluorometer (Urbana Champaign, IL, USA). The spectra were recorded from 300 to 450 nm with excitation at 280 nm and increment. The tryptophan zwitterion correction and Glan-Thomson polarizers, with excitation polarized at 90º and emission at 0º, were used to minimize the vesicle scattering effects as proposed by Ladokhin et al. (2000). Then, K_p was determined by fitting the plots of the normalized fluorescence intensities versus total lipid concentrations, [L], with the equation (Ladokhin et al. 2000):

$$\frac{I(L)}{I_0} = 1 + \left(\frac{I_{max}}{I_0} - 1\right)\frac{K_p[L]}{1+K_p[L]} \qquad (2.11)$$

I(L) and I_0 are the tryptophan fluorescence emission intensities in the presence and in the absence of vesicles respectively, I_{max} is the fluorescence intensity achieved at complete binding and [L] is the lipid concentration. Another manner to estimate the affinity of the peptide for

model membranes is by monitoring the spectral changes during the titration described above. It can be done by evaluating the observed blue shifts after each lipid addition, since the higher is the blue shift, the lower is the polarity of the tryptophan environment i.e. the peptide is effectively partitioning to the lipid bilayer interface.

Circular Dichroism

Circular Dichroism (CD) is defined as the difference between the absorption of left-handed circularly polarised light (L-CPL) and right-handed polarised light (R-CPL) by molecules which contain chiral chromophores (Chirascan User Manual). The chiral chromophores are molecules, with light absorbing groups, whose mirror images in mirrors are not super-imposable. Solutions of chiral molecules are anisotropic environments in which right and left circularily polarised light propagates at different speeds because of different extents of light absorbance. This enable the acquisition of CD spectra in function of a range of wavelengths. The degree of ellipticity (θ) is the obtained signal of a CD spectra. It occurs because, as we can see from figure 2.2a, before the sample we have the same magnitudes of R- and L-CPL. When these beams focus on the sample the magnitudes of the beams will change as a consequence of the molecules ability to deviate light after absorption. Then, we have distinct magnitudes of absorbed R-CPL and L-CPL for a given CD measure as shown in figure 2.2b. The subtraction and the sum of the absorbed light intensity can be used to construct an elliptically polarised beam , which is quantified by the tangent of the angle between the minor to major elliptical axis (Fig. 2.2c). The measures are made in the region of the UV/VIS in the electromagnetic spectra and monitor electronic transitions. After the circularly polarised light absorption the CD signal will be distinct from zero and generates a positive or negative signal depending on the orientation of the resultant elliptically polarised light. It means that, if the R-CPL is more intense than the L-CPL then the signal is positive.

CD spectroscopy is widely used for biophysical applications because it makes possible to evaluate the three dimensional structure of a peptide or a protein (Deber and Li 1995; Ladokhin et al. 2010; Souza et al. 2010). This is due to the fact that 19 from the 20 natural amino acids, responsible for these molecules composition, are chiral molecules and the CD spectra does not present sums of the individual amino acids spectra but patterns for the secondary structures like α-helix and β-sheets under wavelengths of 260nm (Fig. 2.2d). Examples of these patterns for secondary structures are the unfolded with a characteristic negative peak at 200nm, α-helix with two characteristics negative peaks at 222nm and 208nm, and β sheets with a characteristic negative peak around 216nm. In this way, this experimental strategy could be used in this study to observe the AMPs conformational changes in different environments and to estimate the affinity of the peptides for distinct vesicles.

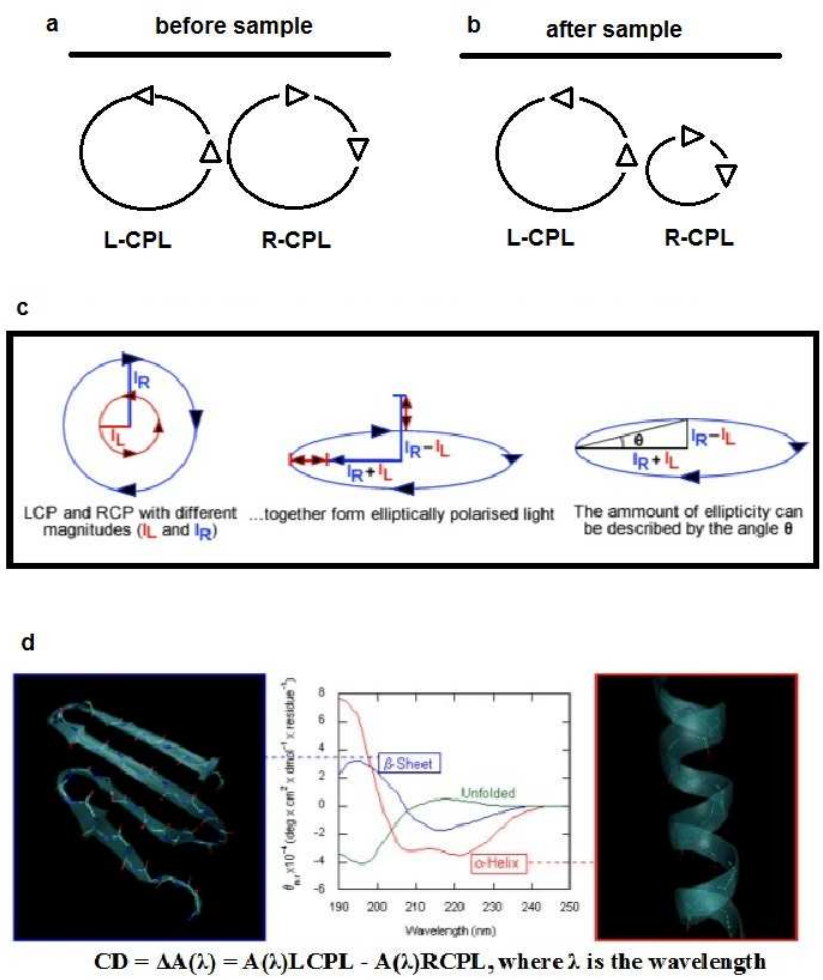

Figure 2.2 a- Right and left circularly polarised light representation (R-CPL or I_R and L-CPL or I_L respectively). **b-** The differences in magnitude in the R-CPL and L-CPL after the incidence on the sample with chiral absorbing groups. **c-** Scheme of the degree of ellipiticity obtained from the difference between the R- and L-CPL to quantify the degree of absorbed polarized light. Chirascan User Manual.**c d-** CD spectra patterns for secundary structures such as unfolded with a characteristic negative peak at 200nm, α helical with two characteristics negative peaks at 222nm and 208nm, and β sheets with a characteristic negative peak around 216nm.

CD spectroscopy was used both to assess structural changes of peptides and to estimate their affinities. For this, solutions of peptide were titrated with increasing lipid vesicles concentrations. After each lipid addition the CD spectra was collected from 260 to 190 nm with a Jasco-815 spectropolarimeter (JASCO International Co. Ltd., Tokyo, Japan). Following baseline correction, the observed ellipticity, θ (mdeg) was converted to mean residue ellipticity [Θ] (deg cm^2/dmol), using the relationship [Θ] = 100θ/(l c N), where "l" is the cuvette path length in centimeters, "c" is peptide milimolar concentration, and "N" the number of peptide residues. The α-helix fraction ($\boldsymbol{f_H}$) was evaluated from the observed mean residue ellipticity at 222 nm (Θ_{obs}) according to Deber and Li (1995) and Luo and Baldwin (1997). Plots of the normalized molar ellipticity (Θ_{obs} /Θ_0) as a function of the lipid concentration could be fitted with the equation:

$$\frac{\Theta_{obs}}{\Theta_0} = 1 + \left(\frac{\Theta_H}{\Theta_0} - 1\right)\left(\frac{K_p[L]}{1+K_p[L]}\right) \quad (2.2)$$

Θ_0 is the molar ellipticity per residue in 222 nm in the absence of LUVs and [L] is the lipid concentration.

Electrophoretic Mobility

Charged particles in solution that are under an electric field tend to move with velocity proportional to the applied field according to:

$$v = u_E E \tag{2.1}$$

where u_E is the electroforetic mobility and E is the intensity of the applied electric field. In this situation, the viscosity of the medium also exerts a force on the particles. It can be evaluated by the Stokes relationship by relating the environment viscosity, the temperature, and the particles radius. Experimentally, it can be measured by using the Doppler velocimetry method in which a laser beam is splitted into two beams that will focus on mirrors to be reflected under the sample. One of the mirrors is able to move by modulating the beam frequency. When light passes through the sample, the particles in movement promote its scattering by changing the beam frequency from ν_0 to ν_S with a frequency displacement $\Delta\nu$, that is dependent on the particles velocity, the incident wavelength (λ_0), and the scattering angle (θ).

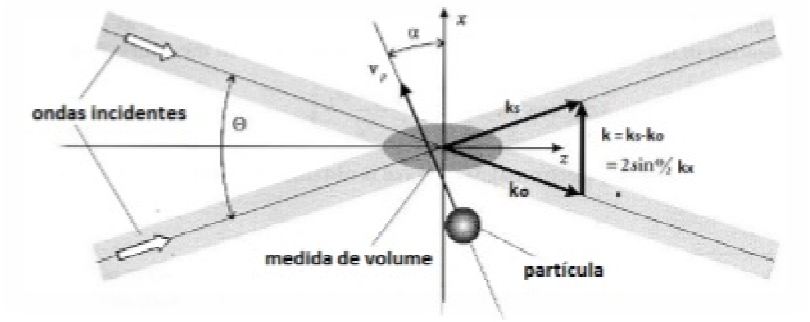

Figure 2.3- Double beam configuration (Kalker and Kaiser, Phys 137).

by considering the incident and the scattering vectors respectively, $\overrightarrow{k_0}$ and $\overrightarrow{k_S}$, and the vector $\vec{k}$= $\overrightarrow{k_S} - \overrightarrow{k_0}$ one can relate the Doppler frequency displacement and the velocity by:

$$2\pi\Delta\nu = \overrightarrow{k}.\vec{v} \tag{2.2}$$

since n is the refraction index of medium and λ_0 is the wavelength of the incident beam, the scattering vector can be written as:

$$\overrightarrow{k} = \frac{4\pi n}{\lambda_0}\sin\frac{\theta}{2} \tag{2.3}$$

and the Doppler frequency displacement rewritten by substituting the wavelength vector:

$$\Delta v = \frac{2nv}{\lambda_0}\sin\frac{\theta}{2}\cos\frac{\theta}{2} = \frac{nv}{\lambda_0}\sin\theta \tag{2.4}$$

From the expression above we obtain $v = \frac{\Delta v \lambda_0}{n\sin\theta}$ that gives us from equation 2.1:

$$u_E = \frac{\Delta v \lambda_0}{n\sin\theta}\frac{1}{E} \tag{2.5}$$

The electrophoretic mobility can be related to the zeta potential according to the Smulochowski equation:

$$u_E = \frac{2\zeta\varepsilon f(\kappa a)}{3\eta} \tag{2.6}$$

ζ is the zeta potential, ε is the medium dieletric constant, f(κa) is the Henry's function, κ is the Debye length, a the particle radius, and η is the medium viscosity. The Henry's function f(κa) is considered to be 1.5 for solutions containing more than 10^{-3} M of salt according to the Smulochowski approximation, where the particle radius is much bigger than the Debye length, and f(κa)= 1.0 in environments of low polarity according to the Huckel approximation, where the particle radius is smaller than the Debye length.

The zeta potential through electrophoretic measurements has been intensively used for peptide-lipid interaction studies (Klocek et al. 2009; Freire et al. 2011; dos Santos Cabrera et al. 2011). From this, it is possible to characterize the surface potential of the liposome and monitor how it changes due to peptides interaction. The peptides association to charged lipid gives insights of the electrostatic interactions involved in the system. It could be done by titrating liposome suspensions with increasing concentrations of peptide by using a Zetasizer Nano ZS90 equipment with detection angle θ = 90◦, incident light λ_0=0.6328 μm, and refractive index n=1.4. The surface potential was calculated from the zeta potential using the expression (Hunter 1981):

$$tanh\left(\frac{Z}{4}\right) = tanh\left(\frac{y_0}{4}\right)e^{-\kappa r} \tag{2.3}$$

where Z is the reduced zeta potential (eζ/kT) and y_0 is the reduced surface potential (eψ$_0$/kT), k is the Boltzmann constant, T temperature, e is the proton charge, κ is the inverse Debye length and r=0.2 nm is the position of the shear plane where zeta potential was measured.

Dynamic Light Scattering

Dynamic Light Scattering (DLS) gives the size of particles in solution due to the measurement of their Brownian motion. It is possible because particles in liquid solution are constantly moving, due to collisional effects with the neighbourhood molecules, and when illuminated scatter light in all directions proportionally to their sizes. A pattern of light scattered is generated by a set of illuminated particles and it can be registered by positioning a screen or a receptor to receive it, as shown in figure 2.4a. This pattern is composed by areas with and without light detection as bright and dark speckles, resulted of the destructive and constructive phase additions of the scattered light. The light scattered pattern generated varies with the particles motion by giving raise to different intensities of light for each pattern. In practice, the rate of the fluctuation of the scattered light intensity from a sample can be measured through it illumination in a couple of minutes. Decay rates are obtained from the correlation function as a function of time. They are converted to the average size of the particles in the sample due to the existence of specific decay rates for a number of size classes (5nm to 10μm), since large particles move slowly and small particles move quickly (Fig.2.4b). Then, the size distribution can be obtained from the rate in which the correlation function decays as shown in Fig. 2.4b and c. In this work, this technique has been used to monitor the liposome size changes due to the peptides interaction and verify the possibility of aggregates formation.

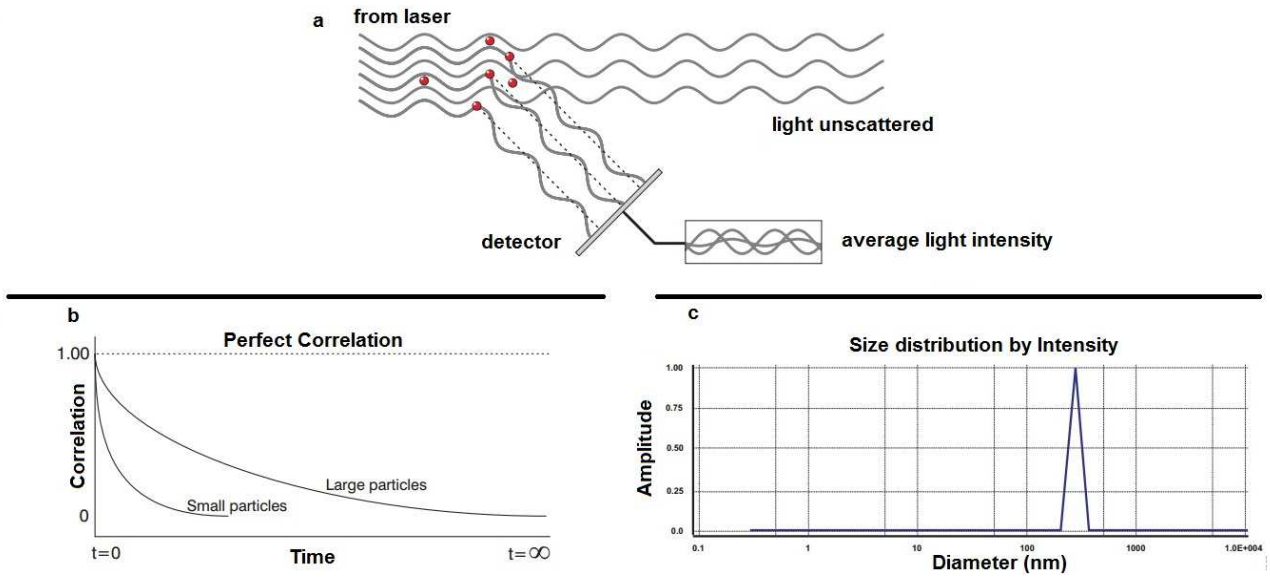

Figure 2.4 a- Representation of the mechanism of particle light scattering and the acquisition of generated scattering pattern. **b-** Examples of rates in which correlation function decays for large and small particles. **c-** The size distribution intensity given by the plot of diameter ***vs*** amplitude i.e. the distribution of size classes as a function of the relative intensity of the scattered light (Zeta Sizer Nano Series- User Manual).

The hydrodynamic diameter (D_H) of vesicles could be determined by DLS using a ZetaSizerNano ZS90 (Malvern Instruments Ltd, Worcestershire, U.K.). D_H was calculated from the diffusion coefficient (D) using Stokes Einstein relation: $D_H=kT/3\pi\eta D$, where η is the solvent viscosity. These assays could be performed by titrating vesicles with the peptides and the peptides with vesicles. The samples were prepared in vials in which the hydrodynamic diameter was determined after 30 minutes equilibration time. The correlation function was fitted with cumulants expansion up to second order to obtain the intensity size distributions.

Confocal Microscopy

Microscopy is basically obtained by simple optical concepts. Its objective is to generate larger images of samples that are barely seen to human eyes. A simple microscope is mainly composed by one light source and two convex lenses called objective and ocular and the steps to obtain increased images of a sample are showed in the figure 2.5. This approach has been used for many scientists for observation of important systems in biology and biophysics. The development of the machinery generated fantastic improvement of images acquisition with high resolution both in liquid and solid samples with or without fluorescence facilities. In the Confocal Microscopy it is possible to use spatial filtering techniques to eliminate out-of-focus light in samples whose thickness exceeds the immediate plane of focus (Claxton et al. 2006). Besides this the equipments can present more than 3 types of laser systems which improves the regulation of wavelength and excitation intensity (Claxton et al. 2006), and enables the precise use of distinct fluorophores in one sample simultaneously. This technique allows the observation of AMPs effect on single giant unilamellar vesicles different from the methods cited above in which the activity of the peptides could be observed in a set of vesicles resulting in average information of the system. This approach also enabled us to observe how the AMPs affect the vesicles morphology and helps to evaluate the peptide-lipid interactions with liposome of the same size of real cells like fungus and red blood cells with diameters around 5µm and 10µm respectively (Hristova and Wimley 2011). In this work, it was used to observe the dye entrance of three different fluorescent probes with distinct sizes to estimate the size of pores and the kinetic of the defects that might be generated on the vesicles due to peptide addition.

To this end, vesicle samples were imaged at room temperature by using the Zeiss LSM 510 META (Jena, Germany) inverted confocal microscope. Giant unillamelar vesicles (GUVs) solution and buffer were incubated for 15 minutes prior to imaging to allow the GUVs to sediment to the bottom of the sample. The fluorescent probes were diluted in buffer and were added carefully to the top of the sample. Images and movies of the vesicles in the mixture with buffer and the dyes were recorded as a control experiment. For the quantitative analysis of the dye influx process, the concentration of dye in the interior of the vesicles was normalized on a scale of 0-1 according to the equation $c(t) = (b_{interior,\ t} - b_{interior,\ control}) / (b_{exterior} - b_{interior,\ control})$. $b_{exterior}$ is the average pixel intensity in a region of the bulk solution; $b_{interior\ t}$ is the average pixel intensity of dyes in the interior of GUVs after t seconds after peptide addition and $b_{interior,\ control}$ is the average pixel intensity of the dyes in the interior of GUVs in the unleaked control samples (i.e. the background signal). This procedure allowed us to monitor leakage events of individual GUVs for a period of up to 30 min after peptide addition and to quantify the permeability of GUVs during leakage events.

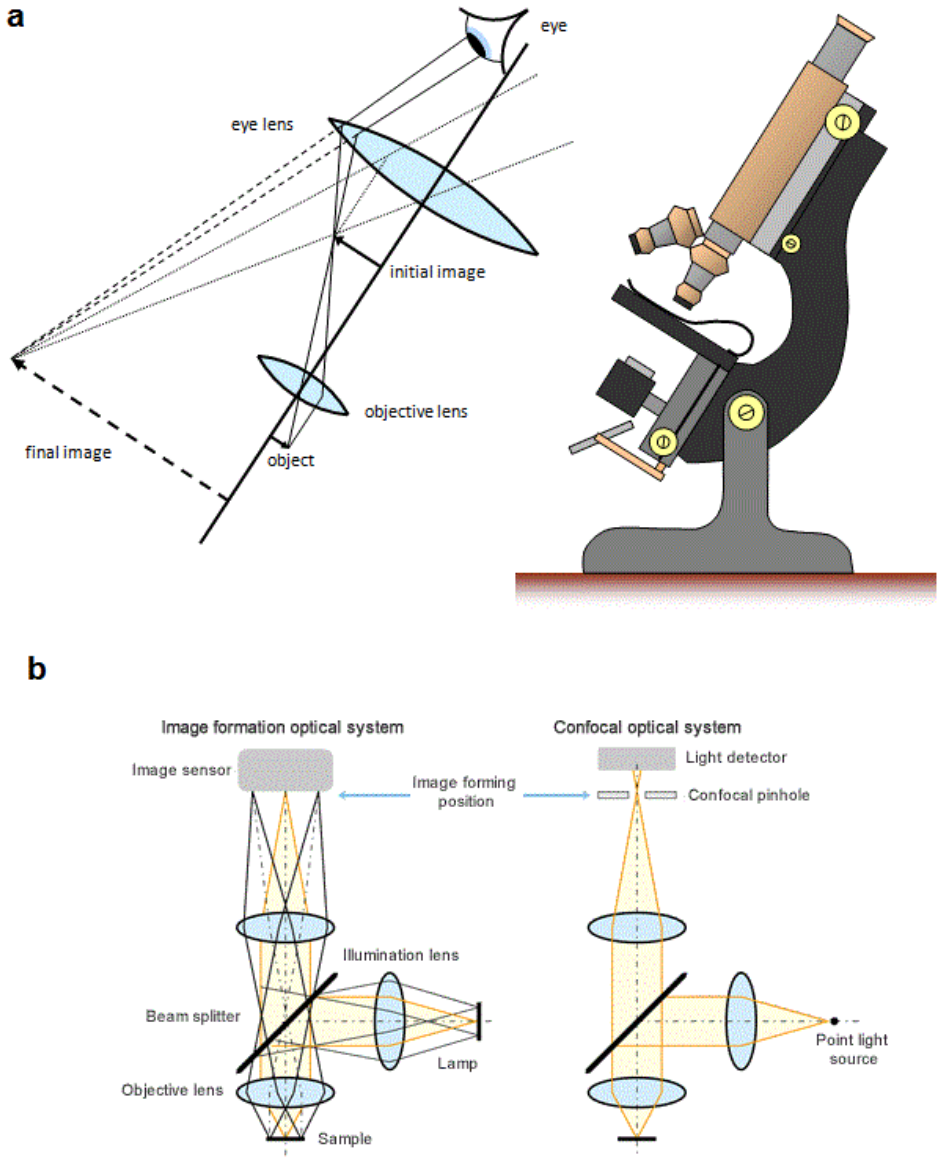

Figure 2.5 **a-** Image formation in a optical system, the light illuminates the sample and the objective lens is responsible for forming its image, which acts as the object for the ocular lens. Next, this object has its size increased by the ocular lens which works as a magnifying glass resulting in the final image. **b-** Image formation in the confocal system, laser emitted from the light source is radiated by the objective lens and the light converges to one point on the sample by reducing unnecessary scattered light from the environment and improving contrast compared with simple optical microscopes. The light reflects on the sample, goes back along the same optical path, is separated by the beam splitter, and converges on the pinhole. The pinhole is a circular aperture to detect exclusively light at the focused position. It blocks the reflected light from places other than the focal position at the pinhole by forming a perfectly focused clear image with good contrast (http://www.olympus-ims.com/en/knowledge/metrology/lext_principles/basic/).

Chapter 3

The effect of acidic residues and amphipathicity on the lytic activities of mastoparan peptides studied by fluorescence and CD spectroscopy

Natália Bueno Leite[1], Laiana Cristina da Costa[1], Dayane dos Santos Alvares[1] Marcia Perez dos Santos Cabrera[1], Bibiana Monson de Souza[2], Mário Sérgio Palma[2], João Ruggiero Neto[1] *

1- Department of Physics IBILCE – São Paulo State University -UNESP;

2- Center of Studies of Social Insects/Dept. Biology/ IB – São Paulo State University - UNESP

Amino Acids (2011) 40:91-100

DOI 10.1007/s00726-010-0511-9

Summary

Bioactive peptides are predominantly cationic and it has been shown that their activity is modulated by electrostatic interactions, hydrophobic contributions and the elastic features of the membranes they target. A novel family of peptides extracted from the venom sac of the wasp Polybia paulista, however, present acidic residues in the N-terminus (Souza et al. 2005 and 2009). Biological activity assays with Gram-positive and Gram-negative microorganisms revealed a mild to intense antimicrobial activity. Like other peptides extracted from the venom sac of wasps, they present degranulating activity in rat mast cells. They showed low hemolysis in rat blood cell and chemotaxis. However comparisons of the biological activities of the sequences with aspartic acid residue in the N-terminus instead of asparagine show that they differentiate in these activities. The peptides with IDWL in the N-terminal showed lower degranulating and hemolytic activities than their analogs with N2D substitution, and some of them present very high antimicrobial activity (Souza 2007). The presence of acidic and basic residues determinates the peptide net charge which have been shown to modulate both, the peptide affinity for the bilayer and the lytic activity (Dathe and Wieprecht, 2002). Besides the presence of the acidic residue at the N-terminus and the net charge, these peptides differentiate in their hydrophobicities and the angle of polar face, which have also been shown to act synergistically in modulating the lytic and biological activities and consequently the peptide bilayer-specificity (Taheri-Araghi et al. 2007).

We compared the activity and affinity of MP1 with other four mastoparan peptides with distinct net charges (ranging from +1 to +4) and mean hydrophobicity (ranging from -0.11 to 0.08). The interaction with zwitterionic (PC) and anionic (PC/PG) model membranes was observed to evaluate their membranes affinity and activity through circular dichroism (CD) and fluorescence spectroscopy techniques. The circular dichroism spectra showed that all the peptides are in random coil structure in buffer, but in contact with lipid bilayer they assume a CD spectra characteristic of helical structures. The helical content for each peptide in buffer, anionic and zwitterionic vesicles was evaluated and showed a significative increase in the presence of negatively charged lipids. The activity of these peptides was monitored by fluorescence spectroscopy through dye leakage experiments. All the peptides showed cooperative dose response curves meaning that there is a particular concentration (threshold peptide lipid ratio, [P]/[L]) for each peptide to disturb the lipid bilayer in which the vesicles with dye entrapped start to leak. The peptides with lower net charges showed higher lytic activity by presenting smaller [P]/[L] ratios, an effect that was barely changed with the addition of anionic lipids in the vesicle composition. On the other hand, the most charged peptides showed reduced [P]/[L] ratios in PC/PG vesicles compared with the PC ones, by indicating that the electrostatic contribution takes an important place in the interaction. Fluorescence

spectroscopy was also used to monitor the tryptophan residue in the membrane environments. For this, we used lipid titrations to estimate the wavelength blue shift and the fluorescence quenching by acrylamide to evaluate the accessibility of the quencher to tryptophan. All the results showed that the amino acid residue is somehow protected from the aqueous environment, which was more pronounced in the presence of anionic lipids.

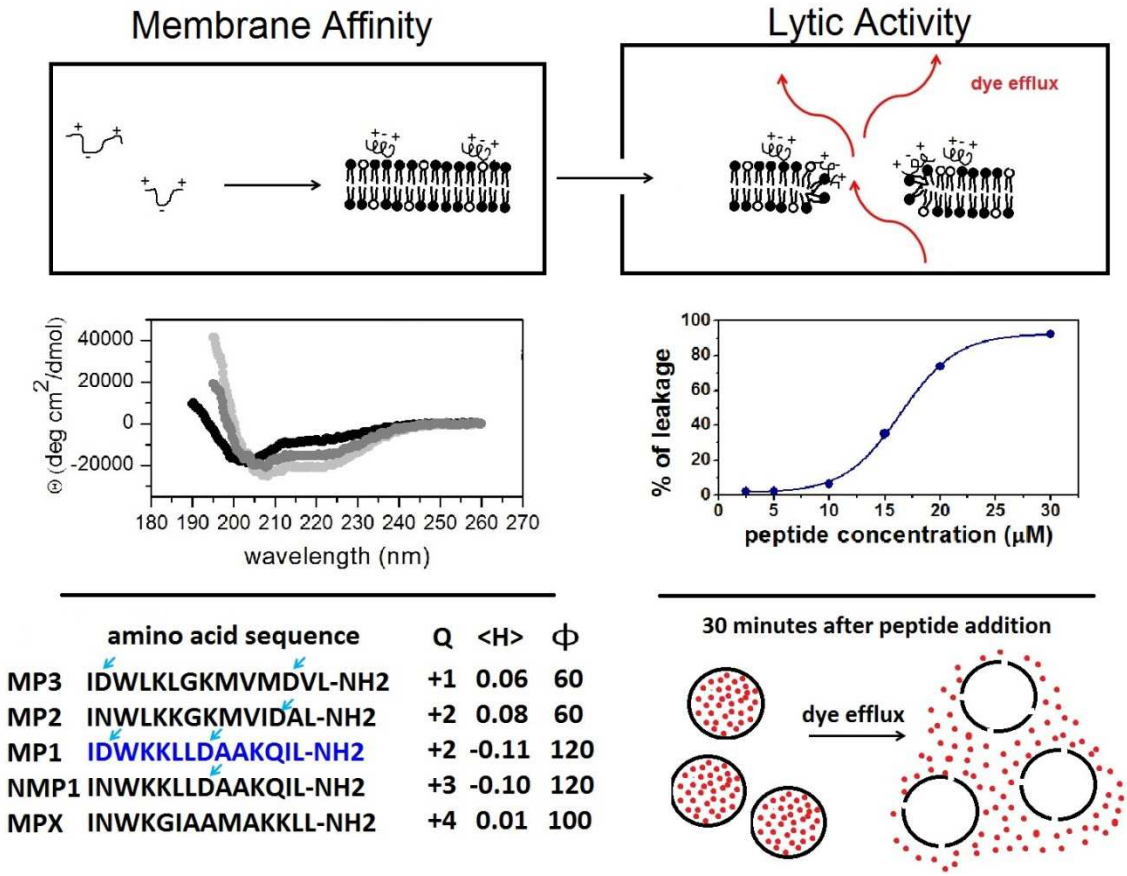

Figure 3.1 - Schematic representation of the experimental carried out to quantify the affinity and lytic activity in model membranes. This study compares the activity and affinity of MP1 with four more peptides with distinct amino acid sequence, net charges, and hidrophobicities features. The lytic activity was observed through dye leakage experiments, in which the model membranes were prepared with entrapped dye and submitted to increasing concentrations of peptide that enabled the leakage of the inner content in a cooperative pattern. Besides fluorescence spectroscopy, the affinity was studied through the peptides helical stabilization due to their amino acid composition, electric net charge (Q), mean hydrophobicity (<H>), and polar face angle (Φ).

The peptides with net charges +1 and +2 showed the highest affinity for zwitterionic membranes, as an indicative that the electrostatic repulsion is a factor to be considered in the interaction of the most charged peptides with the neutral vesicles. This observation was confirmed in the presence of anionic vesicles where all the peptides showed increased activity.

The peptides with lower net charge presents 1or 2 acidic residues. Their affinity and activity showed that the presence of negatively charged residues has an important role in modulating their action by stabilizing the electrostatic interactions between the charged groups. There is the possibility of the acidic and basic residues positioned as the third and the fourth nearest neighbors act by stabilizing the helical conformation by the formation of salt bridges. Besides this effect, the differences in the peptides hydrophobicity were also accounted in modulating the interaction with vesicles. The existence of the acidic residue in a hydrophobic peptide played an important role in modulating their affinity and lytic activity toward neutral vesicles, which is different from the acidic residue in a hydrophilic peptide with higher affinity and lytic activity in anionic ones. The data showed that the interplay especially between the acidic residue in the N-terminus and peptide hydrophobic/hydrophilic balance drives the peptide bilayer specificity and consequently its lytic and biological activities.

3.1 Introduction

Peptides of mastoparan family belong to the immune system of social wasps. Due to the positioning and the presence of basic and hydrophobic amino acid residues on their sequences, they assume a helicoidal amphipathic structure in membranar environments and display important biological activities such as: antimicrobial, mast cell degranulation and hemolytic (Nakajima 1986).

Generally, these peptides are composed by fourteen amino acid residues in their sequences, being unexceptional find the specific group of amino acids INW, at N-terminus, followed by a lysine or a leucine. While at C-terminus, the last two residues are predominantly hydrophobics and the leucine is frequently found as the last one (Nakajima 1986).Mostof the times, C-terminus is protected by amidation, which increases helical stability due to an extra hydrogen bonding(Sforça et al. 2004) and also helps to protect against proteolytic degradation (Andreau and Rivas 1999). Some mastoparan peptides present one or more acidic residues, in general an aspartic acid at the N-terminus instead of asparagine, and it differentiate the activity of the peptides. The presence of the acidic residues could contribute with a stabilizing effect to the helical structure by increasing the helical macrodipole and providing na extra hydrogen bonding or salt bridge between lateral chains specially aspartic acid and lysine at positions i and i+4 or i+3 (Marqusee and Baldwin 1989).

Recently a novel family of peptides, with acidic residues in the N-terminus, was extracted from the venom sac of the wasp Polybiapaulistaas described by Souza et al. 2005 and 2009. Biological activity assays with Gram-positive and Gram-negative microorganisms revealed a mild to intense antimicrobial activity. Like other peptides extracted from the venom sac of wasps, they present degranulating activity in rat mast cells. They showed low hemolysis in rat blood cell and chemotaxis. However comparisons of the biological activities of the sequences with aspartic acid residue in the N-terminus instead of asparagine show that they differentiate in these activities. The peptides with IDWL in the N-terminal showed lower degranulating and hemolytic activities than their analogs with N2D substitution, and some of them present very high antimicrobial activity (Souza 2007). The presence of acidic and basic residues determinate the peptide net charge which have been shown to modulate both, the peptide affinity for the bilayer and the lytic activity (Dathe and Wieprecht, 2002). Besides the presence of the acidic residue at the N-terminus and the net charge, these peptides differentiate in their hydrophobicities and angle of the polar faces, which have also been shown to act synergistically in modulating the lytic and biological activities and consequently the peptide bilayer-specificity (Taheri-Araghi et al. 2007).

The presence of acidic and basic groups allows not only for the helical stabilization by intra-molecular salt and hydrogen bonding, but also for the formation of bridges and bonds with the lipid polar head groups (Sakai and Matile 2003; Pantos et al. 2008). Studies by molecular dynamics of a cell penetrating peptide, Tat HIV, showed that the peptide translocation is strongly influenced by these types of hydrogen bonding (Herce and Garcia 2007). Recently it was proposed that the mechanism of action of mastoparans is similar to transportan, a cell penetrating peptide, which involves the same type of translocation (Almeida and Pokorny 2009; Pokorny et al. 2009).

To understand the role played by the acidic residue at the N-terminus, the net charge, the hydrophobicity and the lytic activities of four peptides derived from Polybiapaulista wasp venom extract we report the results obtained with a series of experiments with these peptides exploring the influence of the structural parameters, such as net charge, hydrophobicity and broadness of the polar face, in modulating their affinity to and their lytic actvity in model phospholipid membranes with their biological activities.

3.2 Materials and Methods

Chemicals

Lipids egg phosphatidylcholine and phosphatidylglycerol were purchased from Avanti Polar Lipids (Alabaster, AL) and carboxyfluorescein (CF) from Sigma Chemical Co (S. Louis, MI). Unless otherwise indicated other chemicals were of high quality analytical grade. Buffers: Tris/H_3BO_3 5 mM, 0.5 mM Na_2EDTA, pH 7.5 for CD and Tris/HCl 10 mM, 1mM Na_2EDTA, pH 7.5, either containing 25 mM CF (vesicles formation) or 150 mMNaCl for the leakage experiments and fluorescence spectroscopy experiments.

Peptide synthesis and purification

Polybia MP-1, Polybia MP-2, Polybia MP-3, the synthetic analoguePolybiaNMP-1 and Mastoparan (MPX)were synthesized and purified by Professors M.S. Palma research group from UNESP-Rio Claro, as described by Souza et al. (2005 and 2009).

Vesicle preparation

Liposome composed respectively by L-α-phosphatidylcholine(PC) and 70% L-α-phosphatidylcholine and 30% L-α-phosphatidyl-DL-glycerol (PC/PG(70/30)) have been prepared according to general procedures with slight modifications. Shortly phospholipids dissolved in chloroform have been dried under N_2 flow on round bottom flasks. The lipid film was completely dried under vacuum for at least three hours and afterwards hydrated with Tris buffer (Tris/H_3BO_3 5 mM, 1mM Na_2EDTA, pH 7.5 or with Tris/HCl 10 mM, 1mM Na_2EDTA, pH 7.5, either containing 25 mMcarboxyfluorescein (CF) for leakage experiments or 150 mMNaCl for fluorescence spectroscopy. In both preparations the final lipid concentration was around 10 mM. The suspension was sonicated under N_2 flow, in ice/water bath, for 50 min, or until clear, to produce small unilamellar vesicles (SUVs), necessary for the CD measurements. Titanium debris has been removed by centrifugation. Large unilamellar vesicles (LUVs), used in dye release experiments and tryptophan fluorescence spectroscopy, were obtained by two extrusion steps using anAvanti Mini-Extruder (Alabaster, AL) and double stacked polycarbonate membrane (Nuclepore Track-etch Membrane, Whatman):firstly 6 times through 0.4 μm and then 11 times through 0.1 μmmembranes.For the dye-entrapped LUVs free dye was separated by gel filtration on a Sephadex G25M column (Amersham Pharmacia, Upsala, Sweeden). Vesicles were used within 48 hours of preparation. The lipid concentration was determined by phosphorus analysis (Rouser et al. 1970). Laser light scattering measurements with Zeta SizerNano NS-90 (Malvern Instruments, Worcestershire, U.K.) have revealed homodisperseLUV suspensions, with an average diameter of 100.0-110.0 ± 0.2 nm among several preparations.

Dye leakage

To complete a final volume of 1.2 mL, an aliquot of fresh LUV suspension was injected into a 1 cm quartz cell, containing magnetically stirred peptide solutions in Tris/HCl buffer at different concentrations, ranging from 0.25 till 9 μM, according to the permeabilizing efficiency, to reach around 100% leakage within 20 to 30 minutescontact time. CF release from the vesicles was monitored fluorimetrically by using a ISS PC1 spectrofluorometer (Champaign, IL, USA) at 520 nm, 0.5 nm slit width, (excited at 490 nm, 1 nm slit width) by measuring the decrease in self-quenching at 25°C. Percentage of dye leakage was determined after regular time intervals, and calculated with the equation:

$$percentage\ of\ leakage = 100\mathrm{x}(F - F_0)/(F_{100} - F_0) \quad (3.1)$$

where F is the observed fluorescence intensity, F_0 and F_{100} correspond, respectively, to the fluorescence intensities in the absence of peptides and to 100 % leakage, as determined by the addition of 20 μL of 10% Triton X-100 solution. F_{100} has been corrected for the corresponding dilution factor. The observed release of CF from vesicles is described by a single exponential function as proposed by Schwarz and Robert (1990). However, in the present study the curves of the leakage time course could only be fitted, with correlation factors above 0.97, by using the relationship:

$$leaked\ fraction = L_{max} - L_i \exp(-kt) \quad (3.2)$$

where L_{max} represents the maximum (steady state) leakage, or the fraction of CF released at the rate k, L_i is a constant that accounts for the leakage that occurs immediately at vesicle addition, i.e. when at t ~ 0, L ≠ 0, t is the time elapsed after the addition of vesicle and k is a constant measuring the rate of leakage. The influx function is given by:

$$E(t) = 1 - leaked\ fraction \quad (3.3)$$

and was employed to obtain the apparent average pore number (p*), as:

$$p^* = -\ln E(t) \quad (3.4)$$

which is based on the assumption that vesicles are homogeneous in size (Schwarz and Robert 1990).

Circular Dichroism measurements

CD spectra were obtained at 20 μM peptide concentration in different environments: Tris/H_3BO_3 buffer or in the presence of zwitterionic PC and in anionic PC/PG (70/30) SUVs at 100 μM concentration. In buffer the peptide and lipid concentrations have been chosen to minimize noise to signal ratio and light scattering. CD spectra were recorded from 260 to 190 nm with a Jasco-710 spectropolarimeter (JASCO International Co. Ltd., Tokyo, Japan), which was routinely calibrated at 290.5 nm using d-10-camphorsulfonic acid solution. Spectra have been acquired at 25ºC using 0.5 cm path length cell, averaged over sixscans, at a scan speed of 20 nm/min, bandwidth of 1.0 nm, 0.5 s response and 0.1nm resolution. Following baseline correction, the observed ellipticity, θ (mdeg) was converted to mean residue ellipticity [Θ] (deg cm^2/dmol), using the relationship [Θ] = 100θ/(l c n), where "l" is the path length in centimeters, "c" is peptide milimolar concentration, and "n" the number of peptide residues. The α-helixfraction (f_H) was evaluated from the observed mean residue ellipticity at 222 nm ($\Theta^{obs}{}_{222}$) according to Deber and Li (1995):

$$f_H = \frac{\left(\Theta^{obs}_{222} - \Theta^{0}_{222}\right)}{\left(\Theta^{100}_{222} - \Theta^{0}_{222}\right)} \tag{3.5}$$

where :$\Theta^0{}_{222}$ is zero and $\Theta^{100}{}_{222}$ is given by:

$$\Theta^{100}_{222} = -39500\left(1 - \frac{2.57}{n}\right) \tag{3.6}$$

where n is the peptide length, n= 14 in the present study.

Fluorescence spectroscopy

Tryptophan emission fluorescence spectra were collected using quartz cell with 1 cm path length, at 25ºC with ISS PC1 spectrofluorometer (Urbana Champaign, IL, USA). The spectra were recorded from 300 to 450 nm with excitation at 280 nm, and increment of 1 nm, averaging in 5 scans. Excitation and emission bandwidth were set at 1 nm and at 0.5 nm, respectively. The Trp emission spectra were recorded after one hour of sample preparation. Correction for scattering was carried out by using cross polarization, parallel at emission and perpendicular at excitation (Ladokhin et al. 2000), and/or subtracting spectra obtained for each vesicle composition from blank of peptide samples. Blue shifts ($\Delta\lambda_{max}$) were calculated as the

differences, in wavelength, of the maxima in emission spectra of the peptide acquired in the presence and in the absence of vesicles. Standard deviation for the blue shift was 1 nm.

Acrylamide Fluorescence Quenching

Acrylamide fluorescence quenching experiments were performed by adding aliquots of a 2.77 M acrylamide aqueous solution in a 5.0 μMpeptide solution in Tris/HCl 10 mM buffer in the absence and in the presence of 500 μM lipid vesicles at 25°C . The suspension was constantly stirred.The tryptophan emission fluorescence spectra were collected from 310 to 450 nm and excited at 285 nm. The fluorescence quenching data were analyzed according to the Stern-Volmer equation for collisional quenching:

$$F_0 / F = 1 + K_{SV}[Q] \tag{3.7}$$

where F_0 and F are fluorescence intensities, measured manually with the cursor at the maximum intensity peak, in the absence and in the presence of quencher respectively. K_{SV} is Stern-Volmer constant for a collisional process and [Q] is the quencher concentration. In the case of static quenching the equation used for the numerical fitting was:

$$F_0 / F = 1 + K_{SV}[Q]\exp(V[Q]) \tag{3.8}$$

where V is a static quenching constant (Eftink and Ghiron 1976).

3.2 Results

Dye leakage

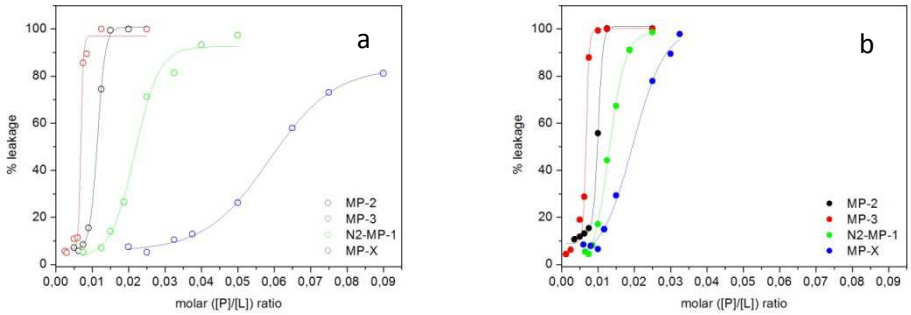

Figure 3.1. Dose-response curves:% leakage after 10 min as a function of peptide to lipid molar ratio ([P]/[L]). **a**Zwitterionic vesicle at 100µM. Thresold [P]/[L] values are 0.006 for MP-3, 0.0085 for MP-2, 0.0137 for NMP-1 and 0.33 for MPX.**b**Anionic vesicle at 100µM. Thresold [P]/[L] values are 0.0055 for MP-3, 0.0084 for MP-2, 0.079 for NMP-1 and 0.009 for MPX. Continuos line fitted with Boltzmann sigmoidal equation.

Vesicle permeabilization has been used as a model system to explore the lytic activity of bioactive peptides. Since the antimicrobial and hemolytic functions are centered at the lipidic phase of the bilayer. The lipid composition of the cell membrane has been shown to work as a selective barrier for peptides action, once that anionic lipids are preponderant in prokaryotic outer leaflet, while in mamalian membranes zwitterionic lipids are more abundant (Yeaman and Yount 2003; Zasloff 2002). Then, we used zwitterionic PC and anionic PC/PG (70/30) as model systems to mimic mammal and bacterial membranes, respectively.

Fluorescent dye release induced by the five studied peptides was monitored by the fluorescence de-quenching. The dose response curves are obtained by the percentage of leakage as a function of the ratio between the peptide and the total lipid molar concentrations, [P]/[L]. It showed sigmoid profiles for all the peptides in both zwitterionic and anionic vesicles as shown in the Fig 3.1.a and b. The lytic activity of the peptides is characterized by a threshold [P]/[L] value, above which, cooperative dye release takes place. The threshold ratio, the leakage efficiency and the cooperativity are found to be dependente on the density charge of the vesicle surface and on the peptide net charge. In zwitterionic vesicles it is observed that the threshold [P]/[L] ratios increase with the peptide net charge. As the net charge increases the dose response curves become less cooperative. By comparing the percentage of leaked dye after a peptide-lipid contact time of 10 min, we have also found that the less charged peptides induced a higher leaked fraction. In anionic PC/PG vesicles the behavior seems to be similar to the observed for

zwitterionic vesicles. The dose response curves for the less charged peptides (Q= +1 and +2) are characterized by low threshold [P]/[L] ratios, slightly higher than those found in neutral PC vesicles; nevertheless, the leakage is more cooperative in anionic vesicles. For peptides with higher net charges (Q= +3 and +4) the threshold [P]/[L] ratios are lower for anionic vesicles as compared with neutral ones with more cooperative dye release and achieving higher percentage of leaked dye.

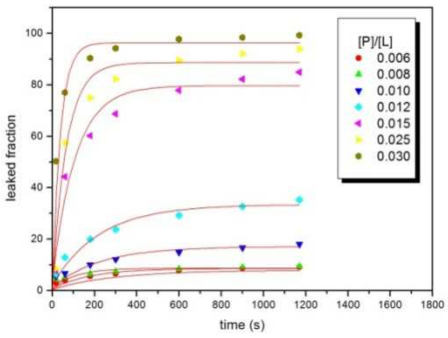

Figure 3.2. Time course curves of dye release for MPX in PC/PG (70/30) for each [P]/[L] used on the dose response curve at t = 17s, 60s, 180s, 300s, 600s, 900s and 1700s after peptide addition.

Figure 3.2 shows some examples of the time course curves of dye release, which were well fitted for all the peptides in both zwitterionic and anionic vesicles by using the Eq. 3.2. The release kinetics were fitted with correlation factor above 0.97, mostof them around 0.99 in the range of peptide concentrations tested. The influx ratio given by Eq.3.3 at different [P]/[L] ratios was used to estimate the average pore number, p*. Figure 3.3 a and b shows the dependence of this parameter in function of [P]/[L] in zwitterionic and anionic vesicles, respectively. For Polybia MP-3 and MP-2 in electrically neutral vesicles, it can be observed that the dependence of the apparent average pore number with [P]/[L] increases cooperatively above threshold [P]/[L] values, suggesting a cooperative process of pore formation. This behavior is somewhat diferente from that observed previously for Polybia MP-1 for which the apparent pore number increases linearly with [P]/[L] ratios, suggesting a process of pore inactivation (dos Santos Cabrera et al. 2008). The leakage process for PolybiaNMP-1 and MPX was observed to be similar, but less cooperative as compared to Polybia MP-2 and MP-3. In anionic vesicles, it was also observed that the apparent pore number increases with the [P]/[L] ratio in a cooperative way. For the most charged peptides, the cooperativity showed to be considerably higher than the observed for electrically neutral vesicles. The values of the threshold [P]/[L] ratiosand the respective average pore numbers obtained from these experiments are summarized in the Table 3.1.

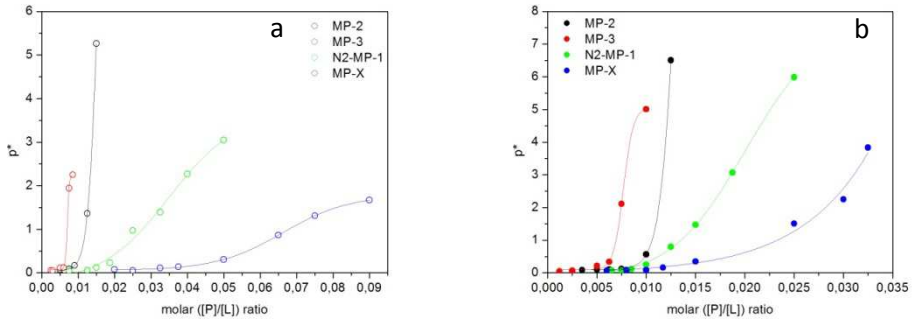

Figure 3.3. Apparent average pore number p* as a function of peptide to lipid ratio [P]/[L]. **a**Zwitterionic vesicle addition at 100 μM. **b**Zwitterionic vesicle addition at 100 μM. Continuous line fitted with Boltzmann sigmoidal equation.

Circular dichroism

Circular dichroism spectra of the peptides in SUVs showed two negative dichroic bands at 222 and 208 nm characteristic of helical structure, while they were observed to be random coil in buffer, as shown in Fig. 3.4. The Polybia MP-3 and MP-2 CD spectra in zwitterionic vesicles showed a more intense dichroic band at 222 nm than at 208 nm suggesting a slight tendency to aggregation in these vesicles, but not in anionic vesicles.The helical content, summarized in Table 3.1, was observed to be dependent on the peptides net charge. In zwitterionic vesicles, the less charged peptides Polybia MP-3, MP-2 and MP-1 showed higher helical contents, parameter that decreased for the most charged Polybia NMP-1 and MPX. In anionic vesicles, it was observed higher helical content compared to the electrically neutral vesicles, suggesting that the helix induction is modulated by electrostatic interaction between lipid head groups and the charged residues in the peptides. The comparison of the helical fraction of Polybia MP-3 and MP-2 indicates that the substitution of the acidic residue at position 2 by asparagine reduces the helical contentby 11 and 36% in zwitterionic and in anionic vesicles, respectively. The same substitution in Polybia MP-1 leads to a decrease of 20% in eletrically neutral vesicles, but in anionic ones the helical content increased significantly suggesting that the N-terminus substitution N2D and consequent increase in net charge mighthave different effects on the helical content when peptides are hydrophobic, as Polybia MP-2, or hydrophilic, as Polybia NMP-1. The electrostatic contribution, however, seems not to be the mandatory factor modulating the helical content, when peptides are hydrophobic: the less charged peptide Polybia MP-3 presents higher helical content in anionic vesicle than the two peptides with net charge +2.

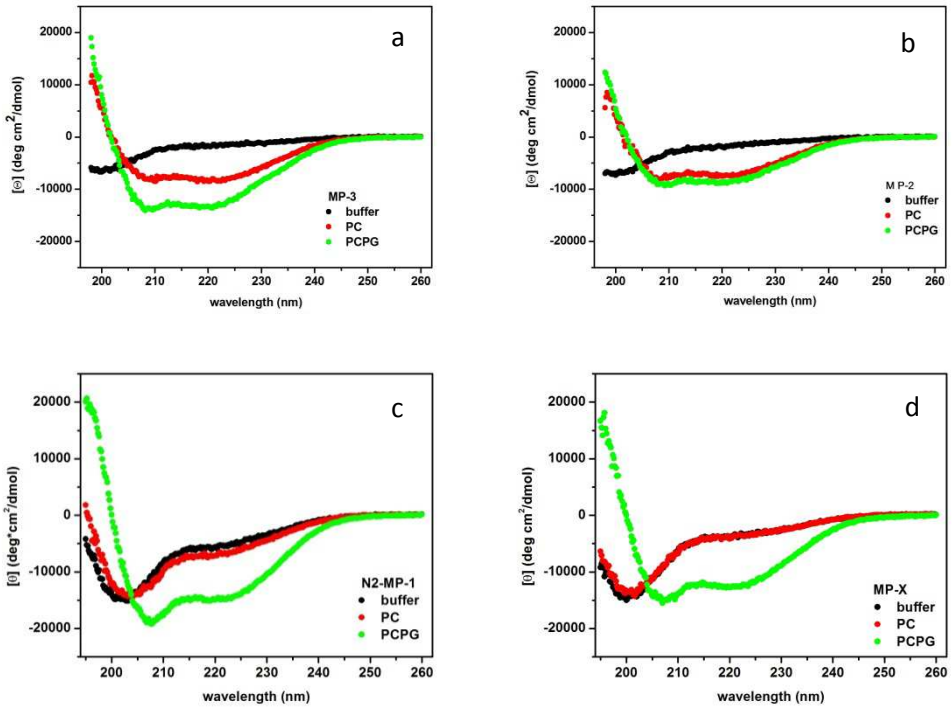

Figure 3.4. Circular dichroism spectra of the peptides at 20 µM. Spectra were recorded in the absence and in the presence of SUVs at 100 µM in Tris H_3BO_3 5mM, 150 mM Na_2EDTA, pH 7.5, at 25ºC.**a**Polybia MP-3. **b**Polybia MP-2.**c**Polybia NMP-1. **d**MPX.

Fluorescence Spectroscopy

Tryptophan fluorescence emission spectra for the five peptides, in the presence of vesicles, showed significant spectral blue shift compared with the respective spectra in buffer, indicative that upon interaction with bilayers the tryptophan residue moves to a more hydrophobic environment. In Fig 3.5 the differences between the positions of the tryptophan spectral peaks in the presence and in the absence of lipids were displayed as a function of the total molar lipid concentration. In zwitterionic vesicles the largest spectral shifts were observed for the less charged peptides, suggesting that the peptide affinity to neutral vesicles decreases with the net charge, in very good agreement with the results obtained by circular dichroism and dye leakage. It is intriguing that for Polybia MP-3 and MP-2 the blue shift increases quickly when a minimum amount of vesicle was added. It could be an indicative that besides peptide adsorption another process, such as peptide aggregation induced by the lipid bilayer, takes place. Nevertheless, tryptophan self-quenching was not observed, which should be expected in the peptide aggregated state. The less charged peptides Polybia MP-3 and MP-2 also showed greater blue shifts in anionic vesicles followed by the others peptides in good agreement with the leakage data.

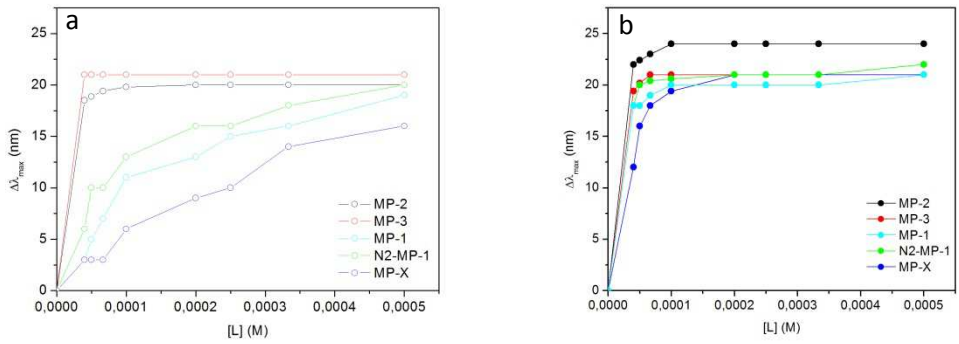

Figure 3.5. Tryptophan blue shift with increasing lipid concentration of the five peptides at 5 μM incubated with different lipid concentrations up to 500 μM in 10mM Tris/HCl, 1mM EDTA, 0.15 NaCl, pH 7.5 at 25ºC during 1h for equilibration.**a**Zwitterionic lipid. **b**Anionic lipid.

The significant blue shift observed for tryptophan suggests that this residue penetrates in the bilayer. Fluorescence quenching experiments were performed to quantify the extent of this penetration in the hydrophobic phase. Water soluble acrylamide was used as a quencher for tryptophan fluorescence and the loss of the fluorescence intensity, due to the addition of this quencher, was analysed with Stern-Volmer plots as shown in Fig 3.6.The Stern-Volmerplots for the peptides in buffer were not linear. It suggests that besides the process of collisional quenching there is a static one, which is possibly due to the presence

of acrylamide adjacent to the tryptophan when it is excited (Eftink and Ghiron 1976).In the presence of vesicles the static quenching was reduced and the relative change in the fluorescent intensities increased linearly with the quencher concentration. The values of Stern-Volmer constants were obtained from the slopes of the linear plots according to Eq. 3.7 and from the numerical fitting of nonlinear plots using Eq. 3.8. The Stern-Volmer constants in the presence of vesicles have shown that the bilayer protects the fluorophore from the quencher; however this screening effect was not complete. To compare the quenching data, the Stern-Volmer constants for each peptide (K_{SVL}) in vesicles were normalized by the respective value in buffer (K_{SVB}) and the results are shown in Table 3.1. Since acrylamide is accessible to all tryptophan species in solution, with exception to those buried in the lipidic phase of the bilayer (Mishra et al. 1994), these normalized constants represent the fraction of fluorescence intensity remained after the incorporation of the fluorophore in the bilayer and qualitatively estimates the peptide-bilayer affinity. Notwithstanding the similarity of the constants for Polybiamastoparans it is possible to observe that tryptophan residues in these peptides were differently shielded in zwitterionic and anionic vesicles.

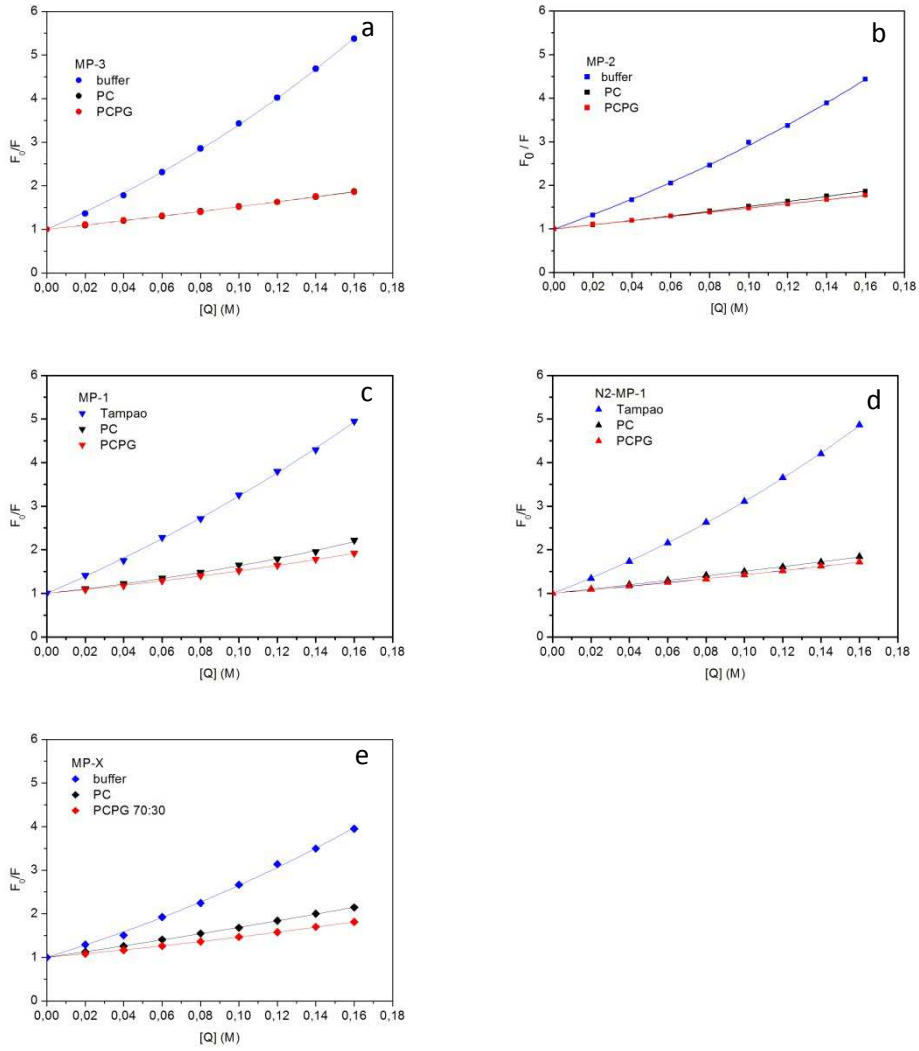

Figure 3.6. Stern-Volmer plots of the peptides tryptophan fluorescence quenched by acrylamide in buffer and in the presence of LUVs.Liposome were composed of PC and PC/PG. The concentration of lipid was 500 μM in a total volume of 1300 μL of 10 mM Tris/HCl, 1 mM EDTA, 0.15 NaCl, pH 7.5. Continuous lines are the best fit obtained with Eq.3.7 for the linear plot and Eq. 3.8 for the non-linear plot.**a**Polybia MP-3. **b**Polybia MP-2.**c**Polybia MP-1.**d**Polybia NMP-1. **d**MPX.

Table 3.1- Structural and physico-chemical features, biological activity data compared to the quantitative parameters of the lytic activity, and spectroscopy data of the interaction of Polybiamastoparans with zwitterionic and anionic vesicles.

Polybia MP3	Ile-**Asp**-Trp-Leu-Lys-Leu-Gly-Lys-Met-Val-Met-**Asp**-Val-Leu-**NH_2**
Polybia MP2	Ile-Asn-Trp-Leu-Lys-Leu-Gly-Lys-Met-Val-Ile-**Asp**-Ala-Leu-**NH_2**
Polybia MP1	Ile-**Asp**-Trp-Lys-Lys-Leu-Leu-**Asp**-Ala-Ala-Lys-Gln-Ile-Leu-**NH_2**
Polybia N2D MP1	Ile-Asn-Trp-Lys-Lys-Leu-Leu-**Asp**-Ala-Ala-Lys-Gln-Ile-Leu-**NH_2**
MPX	Ile-Asn-Trp-Lys-Gly-Ile-Ala-Ala-Met-Ala-Lys-Lys-Leu-Leu-**NH_2**

	Polybia MP-3		**Polybia MP-2**		**Polybia MP-1**		**Polybia NMP-1**		**MPX**	
Q	+1		+2		+2		+3		+4	
<H>	0.06		0.08		-0.11		-0.10		0.01	
M	0.26		0.27		0.24		0.25		0.2	
Φ	60		60		120		120		100	
	PC	**PCPG**	**PC**	**PCPG**	**PC**	**PCPG**	**PC**	**PCPG**	**PC**	**PCPG**
[P]/[L]	0.006	0.0055	0.0085	0.0084	0.15[b]	0.25[b]	0.0137	0.079	0.033	0.009
p*	0.084	0.17	0.13	0.13	0.23[b]	0.15[b]	0.13	0.075	0.1	0.093
Δλ (nm)	21.0	21.0	20.0	24.0	19.0	22.0	20.0	21.0	18.0	21.0
K_{SVL}/K_{SVB}	0.27	0.35	0.25	0.26	0.32	0.27	0.27	0.29	0.38	0.28
f_h	0.26	0.42	0.23	0.27	0.27[b]	0.36[b]	0.21	0.48	0.12	0.40
MIC(μM) *E. coli*	62[a]		8[a]		8[a]		5.8		Na	
MIC(μM) *S. aureus*	31[a]		4[a]		15[a]		7.8		Na	
EC_{50} (μM) WRRBC	50[a]		50[a]		nh		26		Na	

Sequences and structural characteristics of Polybia peptides in comparison with MPX. Negatively charged Asp residues are shown in bold. Net electrostatic peptide charge, Q; average hydrophobicity per residue,<H> and mean hydrophobic moment μ, obtained from Eisenberg et al. (1984) consensus scale, averaged over the number of residues; angle subtended by the polar face (polar, charged residues), estimated from the helical wheel projection, Φ. Lytic activity on zwitterionic, PC, and anionic, PCPG, vesicles:threshold concentration ratio, [P]/[L], and the respective average number of pore, p*, in zwitterionic and anionic vesicles; Spectroscopy data on zwitterionic, PC, and anionic, PCPG, vesicles: blue shift, Δλ (nm); Stern-Volmer constants ratio in vesicles (K_{SVL}) and in buffer (K_{SVB}); α-helical content, f_h. Biological activity: minimum inhibitory concentration (μM), MIC, in Gram-negative (E. coli) and Gram-positive (S. aureus) bacteria and hemolytic activity, EC_{50} (μM),in washed rabit red blood cells (WRRBC).

nh, not hemolytic; na, not available; ([a]) Souza et al. 2009 and ([b]) dos Santos Cabrera et al. 2008.

3.3 Discussion

Besides the difference in the net charge, four of the five peptides used in the present study show the presence of acidic residues, two of them (Polybia MP-3 and MP-1) with an aspartic acid residue in the N-terminus (D2). This is not a ubiquitous aspect among linear peptides, that present antibacterial activity and to which the cationic charge is accepted to play an important role in the specificity to the bacterial anionic outer leaflet membrane. Previous results in biological activity have shown that the peptides with smaller net charges present multi-functional activity, including reasonable antibacterial activity against ***E. coli*** and ***S. aureus***, relatively low hemolytic effect compared with mellitin and mast cell degranulation activity (Souza et al. 2005; Souza et al. 2009).

The lytic activities of these peptides were evaluated in model zwitterionic and anionic membranes in assays of fluorescent dye released from vesicles. Two parameters have been used: the threshold peptide to total lipid molar ratios needed to start the cooperative dye leakage, and the average pore number at these critical ratios. This evaluation showed that the less charged peptidePolybia MP-3 presents very low threshold ratios with approximately the same threshold [P]/[L] for neutral or anionic vesicles. The average pore number, however, showed that this peptide displays preference for electrically neutral vesicles which is in good agreement with its low antibacterial and mild hemolytic activities. For Polybia MP-2 with the substitutions: N2D, I11M and A13V, it was observed that the critical [P]/[L] and the average pore number were the same for zwitterionic and anionic vesicles. The biological activity showed that this peptide presented lower values of minimum inhibitory concentration for Gram-positive and Gram-negative bacteria and similar hemolytic efficacy compared with Polybia MP-3 (Table 3.1). Estimative of the helical propensities for Polybia MP-1 and MP-2 based on Chou-Fasmancalculations (Chou and Fasman 1974), reveals that excepting the N2D substitution in Polybia MP-2, the other two, I11M and A13V, maintain the same helical propensity (P_α=120)for the segment K8 to L14. Asparagine is less helicogenic than aspartic acid according to the Chou-Fasmanhelix propensity scale. Otherwise the increase in the helical macrodipole, due to the acidic residue in the N-terminus and a possible hydrogen or saline bond between this residue and the lysine in anadjacent position, helps to stabilize the helix in Polybia MP-1 in bothzwitterionic and anionic vesicles. Beyond its relatively high helical content, influenced by the presence of the acidic residue at the N-terminal,Polybia MP-3 is slightly lower hydrophobic with mean hydrophobicity <H>=0.06, according to the Eisenberg consensus scale (Eisenberg et al. 1984) compared to Polybia MP-2 with <H>=0.08, while their mean hydrophobic moments are approximately the same <μ>=0.26 and <μ>=0.27 for Polybia MP-3 and -MP-2 respectively. They are characterized by broad hydrophobic face and Φ, the angle subtended by the positive

charges, is estimated in 60° according to the helical wheel projection shown in fig. 3.7. These characteristics: relatively high helical content in zwitterionic vesicles, hydrophobicity and broad hydrophobic face were responsible for the higher lytic activity in zwitterionicvesicles as well as the hemolytic activity. Studying peptides designed to vary one of these parameters, Kiyota et al. (1996) and Dathe et al. (2002) showed that association of hydrophobicity, low polar angle and high helicity results in more hemolytic activity. The smaller net charge in Polybia MP-3 contributed to the lower affinity in anionic vesicles, as indicated by its K_{SVL}/ K_{SVB} constant ratio (Table 3.1), despite its higher helical content, hydrophobicity and the broad hydrophobic face. Electrostatic net charge and consequently the binding affinity have been shown to be more important in modulating the activity in anionic vesicles (Dathe 1999; Sitaran and Nagaraj 1999; Seelig 2004). The spectral shifts and the normalized Stern-Volmer constants support the lower affinity of Polybia MP-3 for anionic vesicles and similar affinities for neutral and anionic vesicles for Polybia MP-2. The greater net charge and higher hydrophobicity of Polybia MP-2 acted in concert tomodulate its affinity for neutral and anionic vesicle.

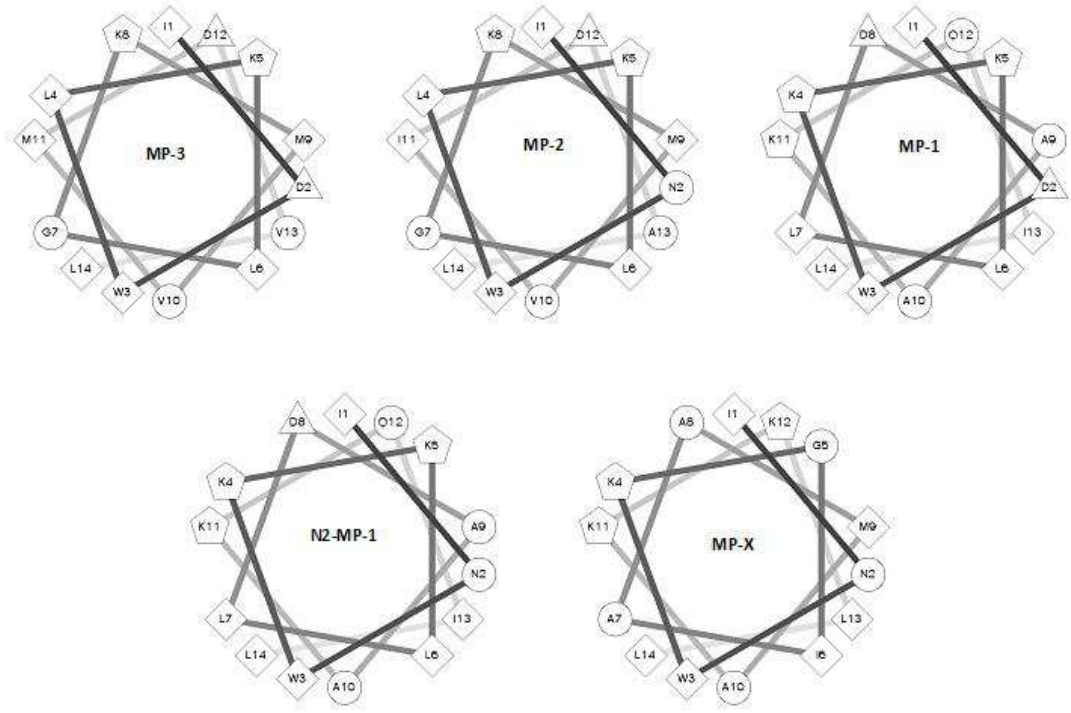

Figure 3.7. Helical wheel projections of the peptides. The representations of the residues are the following: ***circles*** hydrophilic, ***diamonds*** hydrophobic, ***triangles*** the potentially negative and ***pentagon*** potentially positive. Helical wheels were prepared by the software Helical Wheel projections: wheel.p1, version 1.3 (Zidovevetzki et al. 2003).

Compared to Polybia MP-2, the two extra charged groups in the N-terminalin Polybia MP-1, one acidic (D2) and one basic (K5), increased the width of the polar face (Φ=120°) and the differences in the sequence resulted in a hydrophilic peptide with a mean hydrophobicity <H> = - 0.11. As a result, the threshold [P]/[L] and the average pore number for Polybia MP-1, points out for a more efficient lytic activity in anionic vesicles judging from its average pore numbers and from the less cooperative dose response curve for zwitterionic vesicles (dos Santos Cabrera et al. 2008). Notwithstanding the higher threshold [P]/[L] ratio in anionic vesicles, the [P]/[L] at 50% leakage normalized by the threshold [P]/[L] was 1.08 in anionic vesicles and 1.7 in thezwitterionicshowing that the lytic process is more cooperative and efficient in anionic vesicles. In Polybia MP-1,hydrophilicity and a broader hydrophilic face contributed to a decrease in the lytic activity in zwitterionic vesicles. The same characteristics modulated positively this activity in anionic vesicles and also the peptide affinity to these vesicles, as supported by the blue shifts and Stern-Volmer constants. The substitution D2N in PolybiaNMP-1 resulted in a slightly less hydrophilic peptide with higher net charge and with the same width of the estimated polar face. The Chou-Fasman calculations show a segment of 10 residues from K5 to L14 with high helical propensity with P_{α}=120. Although the D2N substitution in PolybiaNMP-1 is outside this helical segment, the loss of the acidic residue decreased the helical content in electrically neutral vesiclesprobably due to the extra charge and hydrophilicity, which increased the helical fraction in PC/PG vesicles, when compared to its parent peptide MP-1. As a result of these characteristics,Polybia NMP-1 presented higher lytic activity in anionic vesicles with smaller average pore number at the threshold [P]/[L] ratio. The Stern-Volmer constants and the spectral shifts, however, are quite similar in neutral and anionic vesicles. It is worth noting that this substitution resulted in a relatively higher antimicrobial and hemolytic activities compared with Polybia MP-2 and MP-1. The reversion of the bilayer specificity due to the increase in the electrostatic net charge beyond a critical value in the same sequence leading to a simultaneous increase in the antimicrobial and hemolytic activity was also observed in magainin (Dathe et al. 2002).

MPX the higher charged of the studied peptides, with three basic groups, is not hydrophilic, <H> =0.01, with slightly narrower polar face (100°) than Polybia MP-1. Its mean hydrophobic moment is the smaller between the studied peptides <μ>=0.2. This peptide has the segment from A7 to L14 with high propensity and the Chou-Fasman calculation shows a P_{α}=128. The helical content in zwitterionic vesicles is the smallest between the peptides studied, probably due to its net charge and its smaller hydrophobic moment, which consequently modulated its lower affinity to the electrically neutral vesicles and lead to the higher [P]/[L] ratio. The greater net charge favored the interaction with anionic vesicles resulting in higher

helical content and lower critical [P]/[L] ratio. The higher affinity to anionic vesicles was also observed in the spectral shift and Stern-Volmer constants.

The results reported above have emphasized that the presence of an acidic residue in the N-terminus stabilized the peptide helical conformation by increasing the helical macrodipole (Schoemaker et al. 1985). The conformation stabilizing effect could be improved if this residue could be salt bridged with a basic residue as the third or fourth nearest neighbor. The present study shows that the acidic residue in a hydrophobic peptide plays important role in modulating their affinity and lytic activity toward neutral vesicles, which is different from the acidic residue in a hydrophilic peptide with higher affinity and lytic activity in anionic vesicles. The data showed that the interplay between the acidic residue in the N-terminus and peptide hydrophobic/hydrophilic balance drives the peptide bilayer specificity and consequently its lytic and biological activities.

References

Almeida PF, Pokorny A (2009) Mechanism of antimicrobial, cytolytic and cell-penetrating peptides: From kinetics to thermodynamics. Biochemistry 48: 8083-8093.

Andreu D, Rivas L (1999) Animal antimicrobial peptides: An overview. Biopolymers 47: 415-433.

Chou PY, Fasman GD (1974) Prediction of protein conformation. Biochemistry 13: 222-245.

Dathe M, Wieprecht T (1999) Structural features of helical antimicrobial peptides: their potencial to modulate activity on model membranes and biological cells. Biochim. Biophys. Acta 1462: 71-87.

Dathe M, Meyer J, Beyermann M, Maul B, Hoischen C, Bienert M (2002) General aspects of peptide selectivity towards lipid bilayers and cell membranes studied by variation of the structural parameters of amphipathic helical model peptides. Biochim Biophys Acta 1558: 171.

Deber CM, Li S-C (1995) Peptides in membranes: Helicity and hydrophobicity. Biopolymers 37: 295-318.

Dos Santos Cabrera MP, Costa ST, Souza BM, Palma MS, Ruggiero JR, Ruggiero Neto J (2008) Selectivity in the mechanism of action of antimicrobial mastoparan peptide Polybia-MP1.

Eur Biophys J 37: 879.

Eftink MR, Ghiron CA (1976) Fluorescence quenching of indole and model micelle systems. Phys. Chem. J 80 (5), 486-493.

Eisenberg D, Schwarz E, Komaromy M, Wall R (1984) Analysis of membrane and surface protein sequences with the hydrophobic moment plot. J. Mol. Biol. 179:125-142.

Herce HD, Garcia AE (2007) Molecular dynamics simulations suggest a mechanism for translocation of the HIV-1 TAT peptide across lipid membranes. Proc. Natl. Acad. Sci. USA 104: 20805-20810.

Kiyota T, Lee S, Sugihara G (1996) Design and synthesis of amphiphilic α- helical model peptides with systematically varied hydrophobic-hydrophilic balance and their interaction with lipid- and bio-membranes. Biochemistry 35:13196-13204.

Ladokhin AS, Jayasinghe S, White SH (2000) How to measure and analyze tryptophan fluorescence in membranes properly, and why bother? Anal Biochem 285:235-245.

Marqusee S, Baldwin RL (1989) Helix stabilization by Glu^{-}... Lys^{+} salt bridges in short peptides of ***de novo*** design. Proc. Natl. Acad. Sci.USA 84: 8898-8902.

Mishra VK, Palgunashari MN, Segrest J, Anantharamaiah GM (1994) Interactions of synthetic peptides analogs of class A amphypathic helix with lipids. J. Biol. Chem 269:7185-7191.

Nakajima, T. (1986). Pharmacological biochemistry of Veside venom. In: "Venom of the Hymenoptera - Biochemical, Pharmacological and behavioral Aspects" (Piek, T.; Ed), Ac. Press, London, 309 - 327.

Pantos A, Tsogas I, Paleos CM (2008) Guanidinium group: A versatile moiety inducing transport and multicompartimentalization in complementary membranes. Biochim. Biophys. Acta 1778: 811-823.

Rouser G, Fleischer S, Yamamoto A (1970) Two dimensional thin layer chromatographic separation of polar lipids and determination of phospholipids by phosphorous analysis of spots. Lipids 5: 491-496.

Schwarz G, Robert CH (1990) Pore formation kinetics in membranes determined from the release of marker molecules out of liposomes or cells. Biophys. J. 58: 577-583.

Schoemaker KR, Kim PS, Brems DN, Marqusee S, York EJ, Chaiken IM, Stewart JM, Baldwin RL (1985) Nature of the charged group effect on the stability of the C-peptide helix. Proc Natl. Acad. Sci USA 82:2349-2353.

Sforça ML, Oyama Jr. S, Canduri F, Lorenzi CCB, Pertinhez TA, Konno K, Souza BM, Palma MS, Ruggiero Neto J, de Azevedo Jr, WF, Spisni A (2004) How C-terminal carboxyamidation alters the biological activity of peptides from the venom of the Eumenine solitary wasp. Biochemistry 43, 5608.

Sitaram N, Nagaraj R (1999) Interaction of antimicrobial peptides with biological and model membranes: structural and charge requirements for activity. Biochim. Biophys. Acta 1462: 29-54.

Seelig J (2004) Thermodynamics od lipid-peptide interactions. Biochim. Biophys. Acta 1666: 40-50.

Souza BM, Mendes MA, Santos LD, Marques MR, Cesar LMM, Almeida RNA, Pagnocca FC, Konno K, Palma MS (2005) Structural and functional characterization of two novel peptide toxins isolated from the venom of the social wasp ***Polybia paulista*** Peptides 26: 2157-2164.

Souza BM (2007) Estrutura a função de mastoparanos dos venenos de vespas. Dissertation. Universidade Estadual Paulista, Rio Claro, Brazil.

Souza BM, Silva A.R, Resende VMF, Arcuri HA, dos Santos Cabrera MP, Ruggiero Neto J, Palma MS (2009) Characterization of two novel polyfunctional mastoparan peptides from the venom of the social wasp ***Polybia paulista*** Peptides 30: 1387-1395.

Taheri-Araghi S, Ha B-Y (2007) Physical basis for membrane-cherged selectivity of cationic antimicrobial peptides. Phys. Rev. Lett. 98: 168101.

Yandek LE, Pokorny A, Almeida PF (2009) wasp mastoparan follow the same mechanism as the cell-penetrating peptide transportan 10. Biochemistry 48: 7342-7351.

Yeaman MR and Yount NY (2003) Mechanisms of antimicrobial peptide action and resistance. Pharmacol Rev 55: 27-55.

Zasloff M. Antimicrobial peptides of multicellular organisms. Nature 2002;415:389-95.

Zidovevetzki, R, Rost, B, Armstrong DL, Pecht I (2003) Transmembrane domains in the functions of fc receptors. Bioplys. Chem. 100: 555-575.

Chapter 4

The effect of the aspartic acidic D2 on the affinity of Polybia MP1 to anionic lipid vesicles

Natália Bueno Leite[1], Dayane dos Santos Alvares[1], Bibiana Monson de Souza[2], Mário Sérgio Palma[2], João Ruggiero Neto[1].

1- Department of Physics IBILCE – São Paulo State University -UNESP;

2- Center of Studies of Social Insects/Dept. Biology/ IB – São Paulo State University – UNESP.

European Biophysical Journal (2014) 43:121-130

DOI 10.1007/s00249-014-0945-1

Summary

The mastoparan peptide MP1 extracted from the Brazilian wasp ***Polybia paulista***, possesses two acidic residues (D2 and D8) and three basic residues (K4, K5 and K11). With the amidation of the C-terminal, the peptide has a relatively low net charge Q=+2 and shows a broad spectrum of bactericidal activities without being hemolytic and cytotoxic (Souza et al. 2009). This peptide also showed a selective inhibitory effect on proliferating bladder and prostate cancer cells (Wang et al. 2008), and also to act against multidrug resistant leukemic cells (Wang, 2009), and specificity in recognizing leukemic T lymphocytes (dos Santos Cabrera et al. 2012). We had observed, last chapter, that the D2 residue plays an important role in modulating the activity of MP1. Its substitution by asparagine, D2N, resulted in the higher efficiency against both types of bacteria, however, the hemolytic activity increased significantly (EC_{50}=26 μM) making the peptide less selective (Leite et al. 2011). We investigated the impact of the aspartic residue, in the N-terminus of MP1 on its affinity to anionic lipid bilayer. The electrostatic and the folding conformational free energies of the peptides MP1, its D2N mutant and MPX in the zwitterionic (PC) and anionic (PC:PG) interfaces were calculated and compared with the free energies of partitioning these peptides into the bilayers.

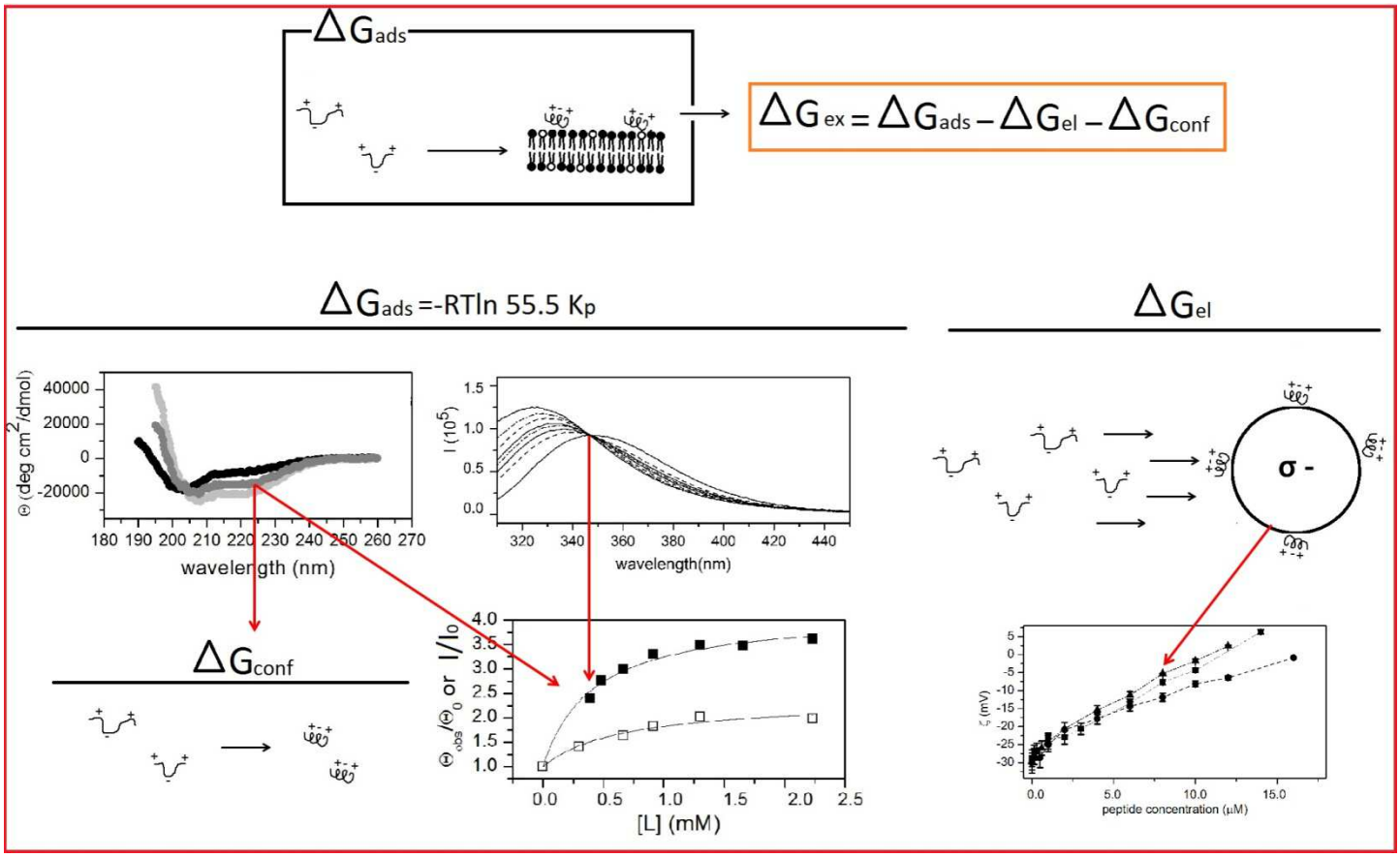

Figure 4.1 - Schematic representation of the experiments performed in the studied system and the obtained results. The total energy of the system is defined as the partition free energy ΔG_{ads}, which involves the process of the peptide partitioning from the aqueous environment to the membrane interface. The excess free energy, ΔG_{ex}, is obtained for systems in which electrostatic and conformational contributions are not additive. ΔG_{ads} can be evaluated from the partition coefficients resulted from spectroscopy titrations. ΔG_{conf} is evaluated from the peptide helical content through CD measurements and ΔG_{el} is resulted from the peptide's accumulation on the model membranes surface which is obtained from electrophoretic measurements.

The energetic contributions were assessed through the peptides interaction with vesicles by circular dichroism (CD), fluorescence spectroscopy, and zeta potential measurements. Both the fluorimetric and zeta potential titrations showed that MP1 has higher affinity to anionic vesicles than its D2N mutant and even than MPX, which is in contrast to the less favorable electrostatic (coulombic) contribution due to the MP1 lower net charge. Fluorimetric measurements allowed the evaluation of the partition coefficients (K_p), in which the peptides adsorb to the outer monolayer of vesicles. The K_p values were used to estimate the partition free energy of transferring the peptide from buffer to the vesicle interface. In the case of anionic vesicles, adsorption of the peptide also has an energetic component due to the work of the electrostatic potential. The electrostatic energetic contribution was obtained from the surface potential calculated from zeta potential measurements and it increased with the peptides' net

charge. The circular dichroism data showed that all the peptides assume helical conformation in contact with vesicles, by indicating that the peptide adsorption is accompanied by its folding in the lipid interface. The helical content was evaluated and MP1 showed the highest value in zwitterionic environment, which barely changed in the presence of PG, since the acidic residue in the N-terminus is able to reduce the repulsive charge-helix macrodipole interaction (Fairman et al. 1989) by stabilizing the MP1 helical conformation. The folding free energy of the peptides at the bilayer interface was obtained from the helical content and showed to be probably the main hydrophobic contribution to the adsorption. The sum of the electrostatic and conformational energies was less than the partition free energy showing that these energetic contributions are not compatible for the peptides. It means that other energetic contributions, with different origin, such as non-coulombic electrostatic due to the solvation of the peptide, thermodynamic contributions of the bilayer itself, and changes in lipid packing, must play important role. It resulted in an extra energetic contribution which increased with the peptides net charge decrease, by indicating that the D2 residue turns these extra energetic contributions more favorable for MP1 than its D2N mutant and MPX in 1.2 kcal/mol and 1.5 kcal/mol respectively.

4.1 Introduction

Mastoparans belong to a family of peptides extracted from the venom sac of wasps. They are in general tetradecapeptides containing one to four basic residues and they are rich in hydrophobic and non-polar residues (Nakajima et al. 1986). Isoleucine and asparagine is frequently found at positions 1 and 2 of the N-terminus. The third residue is generally hydrophobic, such as tryptophan which works as an intrinsic fluorescent probe in some of these peptides. The amidation of the C-terminus is frequently found as well. This terminal protection prevents proteolytic digestion (Andreu and Rivas 1999) and provides an extra hydrogen bond, increasing the stabilization of the helical structure (Sforça et al. 2004). By adsorbing to lipid bilayer or a bilayer-mimetic, like surfactant micelles, these peptides become an amphipathic helical structure.

Some mastoparans display broad-spectrum of antimicrobial activities against Gram-positive and Gram-negative bacteria. They are fungicide, and in some cases, they are also hemolytic and mast cell degranulators (Palma 2006). Their biological activities are strongly related to both the amino acid content and to the lipid membrane composition. These peptides are cationic and the outer leaflet in prokaryotic cells is anionic while in mammalian ones it is rich in zwitterionic lipids (Yeaman and Yount 2003).

The mastoparan peptide Polybia MP1(IDWKKLLDAAKQIL-NH2), or simply MP1, extracted from the Brazilian wasp ***Polybiapaulista***, possesses two acidic residues (D2 and D8) and three basic residues (K4, K5 and K11). With the amidation of the C-terminal, the peptide has a relatively low net charge Q=+2. Despite their low net charge they have broad spectrum of bactericidal activities without being hemolytic and cytotoxic (Souza et al. 2009). MP1 also showed a selective inhibitory effect on proliferating bladder and prostate cancer cells (Wang et al. 2008), and against multidrug resistant leukemic cells (Wang, 2009). Recently, we have observed that this peptide is cytotoxic against leukemic T lymphocytes and very selective in recognizing these cells compared to health lymphocytes (dos Santos Cabrera et al. 2012).

The D2 residue plays an important role in modulating the selectivity of MP1. Its substitution by an asparagine (D2N mutant) resulted in the higher efficiency against both types of bacteria, however, the hemolytic activity increased significantly (EC_{50}=26 μM) making the peptide less selective (Leite et al. 2011). In addition, the substitutions of the aspartic residues by lysines, and the glutamine by arginine in the MP1 resulted in higher toxicity to human cells (Wang et al. 2009). Molecular dynamics simulation in TFE (dos Santos Cabrera et al. 2008) suggested an important role played by the acidic residue in the N-terminus as well as the relative positioning of acidic and basic residues on the charge-hydrophobic balance. Those simulations showed that each acidic residue is ion-paired with two amines: D2 with N-terminus NH_3^+ and K5 and D8 with K4 and K11. Besides charge balance these ion-pairing contribute to the stabilization of the helical structure. The acidic residue in the N-terminus would reduce the repulsive interaction of the N-terminus with the helix macrodipole (Marqusee and Baldwin 1987, Fairman et al. 1989).

In the present study we investigated the impact of the aspartic residue, in the N-terminus of MP1 on its affinity to anionic lipid bilayer. The electrostatic and the folding conformational free energies the peptides MP1, its D2N mutant and MPX in the zwitterionic (PC) and anionic (PC:PG) interfaces were calculated and compared with the free energies to partitioning these peptides into the bilayers. These energetic contributions were assessed by CD, fluorimetric and zeta potential titrations in LUVs. These titrations showed that the less charged peptide MP1 has higher affinity to anionic vesicles than its D2N mutant and even than MPX. The higher affinity of MP1 to anionic vesicles is in contrary to the less favorable electrostatic (coulombic) contribution due to the lower net charge and hydrophobic energetic contribution, due to the folding of the peptides in the bilayer interfaces. Most likely extra energetic components contribute to the higher affinity of MP1. For MP1 in anionic vesicles, these extra energetic components are more favorable by 1.2 kcal/mol compared with its D2N mutant and 1.5 kcal/mol compared to MPX.

4.2 Materials and methods

Chemicals

L-α-phosphatidylcholine and L-α-phosphatidyl-DL-glycerol were purchased from Avanti Polar Lipids (Alabaster, AL). Tris-hydroxymethyl-aminomethane and NaCl from Merck Darmstadt-Germany; EDTA from Sigma-Aldrich (S. Louis MI). Unless otherwise indicated other chemicals were of high quality analytical grade. The water used was deionized and doubly distilled in quartz with a conductivity 0.6 μS/m.

Peptide synthesis and purification

Polybia MP-1, PolybiaN2-MP-1, and Mastoparan (MPX) were synthesized and purified by Professors M.S. Palma research group from UNESP-Rio Claro, as described by Souza et al. (2005 and 2009).

Solutions

Peptides were dissolved in water under gentle agitation and the concentrations were determined spectrophotometrically through the optical density in 280 nm and tryptophan molar absorptivity $\varepsilon = 5580\ M^{-1}cm^{-1}$. Buffers: TRIS buffer 1 (TB1): TRIS/H_3BO_3 5 mM, 1mM Na_2EDTA, 150mM NaF, pH 7.5 for fluorescence titrations experiments. TRIS buffer 2 (TB2): TRIS/HCl 10 mM, 1mM Na_2EDTA, 150 mMNaCl, pH 7.5 for zeta potential experiments.

Vesicle preparation

Liposomes of pure L-α-phosphatidylcholine (PC) and mixed composed of 70% L-α-phosphatidylcholine and 30% L-α-phosphatidyl-DL-glycerol (PC:PG (70/30)) have been prepared according to general procedures with slight modifications. Shortly phospholipids dissolved in chloroform have been dried under N_2 flow on round bottom flasks. Traces of organic solvent were removed under vacuum for at least three hours. The lipid films were afterward hydrated with TB1 for CD and fluorescence titrations or with TB2 for zeta potential titrations. In both preparations the final lipid concentration was around 9.0 mM. Large unilamellar vesicles (LUVs) were obtained by two extrusion steps using an Avanti Mini-Extruder (Alabaster, AL) and double stacked polycarbonate membrane (Nuclepore Track-etch Membrane, Whatman): firstly 6 times through 0.4 μm and then 11 times through 0.1 μm membranes. Only fresh vesicles were used in the experiments. The lipid concentration was determined by phosphorus analysis (Rouser et al. 1970).

Circular Dichroism measurements

Solution of peptide at 10 μM in TB1 buffer was titrated with increasing lipid concentrations of zwitterionic PC or anionic PC:PG (70/30) LUVs up to 2.3 mM. The highest lipid concentration used is greater than $10/K_p$ which assures that all the peptides are bound in anionic and zwiterionic vesicles (McKeown et al 2011). After each lipid addition the CD spectra were collected from 260 to 190 nm, at 25ºC, with a Jasco-815 spectropolarimeter (JASCO International Co. Ltd., Tokyo, Japan), which was routinely calibrated at 290.5 nm using d-10-camphorsulfonic acid solution, using 0.2 cm path length cell. For MPX, the CD spectra were also collected at 5.0 mM of lipids using a 0.1 cm path length. The spectra were averaged over 15 to 30 scans, at a scan speed of 50 nm/min, bandwidth of 1.0 nm, 1.0 s response and 0.2 nm resolution. Following baseline correction, the observed ellipticity, θ (mdeg) was converted to mean residue ellipticity [Θ] (deg cm^2/dmol), using the relationship [Θ] = 100θ/(l c N), where "l" is the path length in centimeters, "c" is peptide milimolar concentration, and "N" the number of peptide residues. The α-helix fraction (f_H) was evaluated from the observed mean residue ellipticity at 222 nm (Θ_{obs}) according to Luo and Baldwin (1997) :

$$f_H = \frac{\Theta_{obs} - \Theta_C}{\Theta_H - \Theta_C} \tag{4.1}$$

Θ_C is molar ellipticities per residue for the peptide as random coil (Θ_C = 1500 deg.$cm^2 dmol^{-1}$) and Θ_H for a complete helix and is given by (Luo and Baldwin 1997):

$$\Theta_H = (-44000 + 250T)\left(1 - \frac{x}{N}\right) \tag{4.2-a}$$

x = 3 is the number of non H-bonded CO groups in a caboxylated peptide and T is the temperature in degree Celsius. The plots of the normalized molar ellipticity (Θ_{obs} /Θ_0) as a function of the lipid concentration were fitted with the equation:

$$\frac{\Theta_{obs}}{\Theta_0} = 1 + \left(\frac{\Theta_H}{\Theta_0} - 1\right)\left(\frac{K_p[L]}{1 + K_p[L]}\right) \tag{4.22-b}$$

Θ_0 is the molar ellipticity per residue in 222 nm in the absence of LUVs and [L] is the lipid concentration.

Fluorescence Spectroscopy Titrations

Peptide solutions at 5 μM were titrated, in a quartz cell with 1 cm path length, by adding aliquots of lipid large unilamellar vesicles (LUVs) up to a total lipid concentration of 1.3 mM at 25ºC. After each lipid vesicle addition, the tryptophan emission fluorescence spectra were collected with ISS PC1 spectrofluorometer (Urbana Champaign, IL, USA). The spectra were recorded from 300 to 450 nm with excitation at 280 nm and increment of 1 nm, averaging in 10 iterations. Excitation and emission bandwidth were set at 2.0 nm. The tryptophan zwitterion correction, eq.3, and Glan-Thomson polarizers, with excitation polarized at 90º and emission at 0º, were used to minimize the vesicle scattering effects as proposed by Ladokhinet al. (2000):

$$I_{pep}^{corr} = I_{pep}\frac{I_{trp}^{buff}}{I_{trp}([L])} \tag{4.3}$$

I_{trp} and I_{pep} are the fluorescence intensities of the tryptophan zwitterion and the peptide respectively at a given lipid concentration [L], and I_{trp}^{buff} is the fluorescence intensity of the tryptophan zwitterion in the buffer. Partition coefficients were determined by fitting the plots of the normalized fluorescence intensities versus total lipid concentrations with the equation (Ladokhin et al. 2000):

$$\frac{I(L)}{I_0} = 1 + (\frac{I_{max}}{I_0} - 1)\frac{K_p[L]}{1+K_p[L]} \tag{4.4}$$

I(L) and I_0 are the tryptophan fluorescence emission intensities in the presence and in the absence of vesicles respectively, I_{max} is the fluorescence intensity achieved at complete binding and [L] is the lipid concentration.

Zeta Potential measurements and Dynamic Light Scattering

Zeta potential of PC/PG (70/30) large unilamellar vesicles, at 40 μM total lipid concentration, in the absence and in the presence of different concentrations of peptides, were determined from the electrophoretic mobility using a ZetaSizerNano ZS90 (Malvern Instruments Ltd, Worcestershire, U.K.). Vesicles were prepared in TB1 buffer and electrophoretic mobilities were determined from three measurements of 30 consecutive runs using DTS1060 (Malvern) disposable cells with golden electrodes at 25°C.

The surface potential was calculated from the zeta potential using the expression (Hunter 1981):

$$tanh\left(\frac{Z}{4}\right) = tanh\,(\frac{y_0}{4})e^{-\kappa r} \tag{4.5}$$

where Z is the reduced zeta potential ($e\zeta/kT$) and y_0 is the reduced surface potential ($e\psi_0/kT$), k is the Boltzmann constant, T temperature, e is the proton charge, κ is the inverse Debye length and r=0.2 nm is the position of the shear plane where zeta potential was measured.

Dynamic Light Scattering

The hydrodynamic diameter (D_H) of LUVs was determined by DLS using a ZetaSizerNano ZS90 (Malvern Instruments Ltd, Worcestershire, U.K.). D_H was calculated from the diffusion coefficient (D) using Stokes Einstein relation: $D_H=kT/3\pi\eta D$, where η is the solvent viscosity. These experiments were performed in two experimental situations. In the first, vesicles were added to a 5 μM peptide solution. In the second, aliquots of peptide were added to a vesicle suspension. When vesicles were titrated, light scattering and zeta potential measurements were performed using the same procedure described in dos Santos Cabrera et al. (2012). The samples were prepared in vials in which aliquots of peptides were added to vesicle suspensions such that after the peptide additions the final total lipid concentration in each vial was 40 μM. After 30 min. of equilibration at 25ºC, the hydrodynamic diameter was determined from 15 consecutive runs of 10 s. The correlation function was fitted with cumulants expansion up to second order to obtain the intensity size distributions. Afterward the suspension was transferred to the DTS disposable cuvette and the zeta potential was measured.

4.3 Results

Table 4.1 Sequence and characteristics of the peptides: Sequence; net charge (Q) molecular weight (MW), Residues number (N_R), and α-helix fraction f_H determined from CD titrations.

	Q	MW (Da)	N_R	f_H[b] PC	f_H[b] PCPG
MP1:IDWKKLLDAAKQIL-NH_2	+2	1583	14	0.83	0.85
D2N-MP1:INWKKLLDAAKQIL-NH_2	+3	1580	14	0.66	0.88
MPX:INWKGIAAMAKKLL-NH_2	+4	1556	14	0.70[a]	0.72[a]

[a] obtained from titrations up to 5.0 mM lipid concentration

[b]Leite et al 2014

Circular Dichroism

Circular dichroism spectra of the peptides Polybia MP1, its D2N mutant and MPX, in buffer, displayed two negative bands in 220 and 205 nm which indicates that in buffer the peptides have already a reduced helical content. In the presence of zwitterionic or anionic LUVs these bands were displaced to 222 and 208 nm fig. 4.1-a, characteristic of helical structure, indicated that the adsorption of the peptides to the bilayer is accompanied by the peptide folding. The use of short path length cuvette allowed to collect CD spectra of LUVs up to 1.3 mM of total lipids with good signal to noise ratio, from 260 to 205 nm. The 208 nm band was more intense than the 222 nm one suggesting that the peptides are monomeric in the range of lipid concentration from 0.2 to 2.5 mM (Matsuzaki et al 1994 and Lau et al 1984). However, should be mentioned that in PCPG LUVs and at lipid to peptide molar ratios [L]/[P] <15 it was observed that the 222 nm band of MP1 became ~10-15% more intense than 208 nm band that could be a consequence either peptide aggregation (Blondelle et al. 1997) or vesicle aggregation. Titrations were performed in a broad range of lipid to peptide [L]/[P] ratios (from 4 to 120) to detect changes in the vesicle size by DLS. It was observed, as shown in the fig 1-b, that the three peptides were able to induce increase in the size of anionic vesicles at high [P]/[L] ratios. Decreasing this ratio by adding lipid resulted in the decrease of the vesicle size and for [P]/[L] < 0.05 the vesicles diameter remained equal to that of pure vesicles, evidencing the particle dissociation. Aggregation was not observed using LUVs at [L]/[P] ≥ 20.

The normalized molar ellipticities (Θ_{obs}/Θ_0) of these peptides increase hyperbolically with the total lipid concentration as also shown in fig. 4.1-c for MP1, 4.1-f and 4.1-i for D2N and MPX. The continuous lines in these plots are the best fits obtained with the eq. 4.2-b. The values of the helical fractions (f_H) are shown in the table 4.1. In PC LUVs, MP1 showed higher helical content (f_H = 0.75) compared to the D2N mutant (f_h = 0.64) and MPX (f_h = 0.70) while in PC:PG LUVs, the helical contents of MP1 and D2N mutant are virtually the same (f_h = 0.85 and 0.88) and f_h = 0.72 for MPX. The helical fraction obtained for MPX in PC LUVs and TRIS buffer with 150 mM NaF. is lower than that measured by McKeown et al (2011). They found f_h = 0.86 in phosphate buffer without added salt. The partition coefficients of the peptides in PC and PC:PG LUVs, obtained from the best fitting with eq. 42-b, indicate that MP1 has higher affinity to zwitterionic and anionic bilayers than its D2N mutant and MPX.

Fluorimetric titrations and partition coefficients

The tryptophan emission spectra obtained from the fluorimetric titrations of peptides with zwitterionic and anionic LUVs, evidence both blue shift and increase in the emission intensities upon vesicle addition, indicating that the tryptophan changes to less polar environment when the peptides interact with the lipid bilayer, as shown in the fig. 4.2-a for Polybia MP1 and in 4.2-c/d for D2N mutant and 4.2-e/f MPX respectively. The positions of the fluorescence emission maxima are shown in the table 4.2. The plots of the normalized fluorescence emission intensity I/I_0 vs lipid concentration are shown in the fig. 4.2-b, -d, and -e for the three peptides in PC and PC:PG LUVs respectively. I/I_0 increased with the lipid concentration in a hyperbolic way and was fitted using eq. 4.4. The best fits are shown as continuous line in the Fig. 4.2-b and -c and the partition coefficients K_p and I_{max}/I_0 obtained are shown in the table 4.2. These partition coefficients correspond the adsorption of the peptide to the outer monolayer of LUVs. The first lipid addition was done in order to avoid high peptide to lipid [P]/[L] ratios for which were observed, by DLS measurements, non-ideal behavior due to vesicle aggregation for the three peptides as shown in fig 4.1. This might cause I/I_0 value to be near the saturation especially in PC/PG LUVs, however it was possible to fit the eq. 4.4 to the experimental data with high correlation and low residual sum. The values of the partition coefficients showed that the MP1 has higher affinity to anionic LUVs compared to D2N mutant and MPX, while in PC LUVs the affinity of the D2N mutant is only slightly higher than MP1 and MPX.

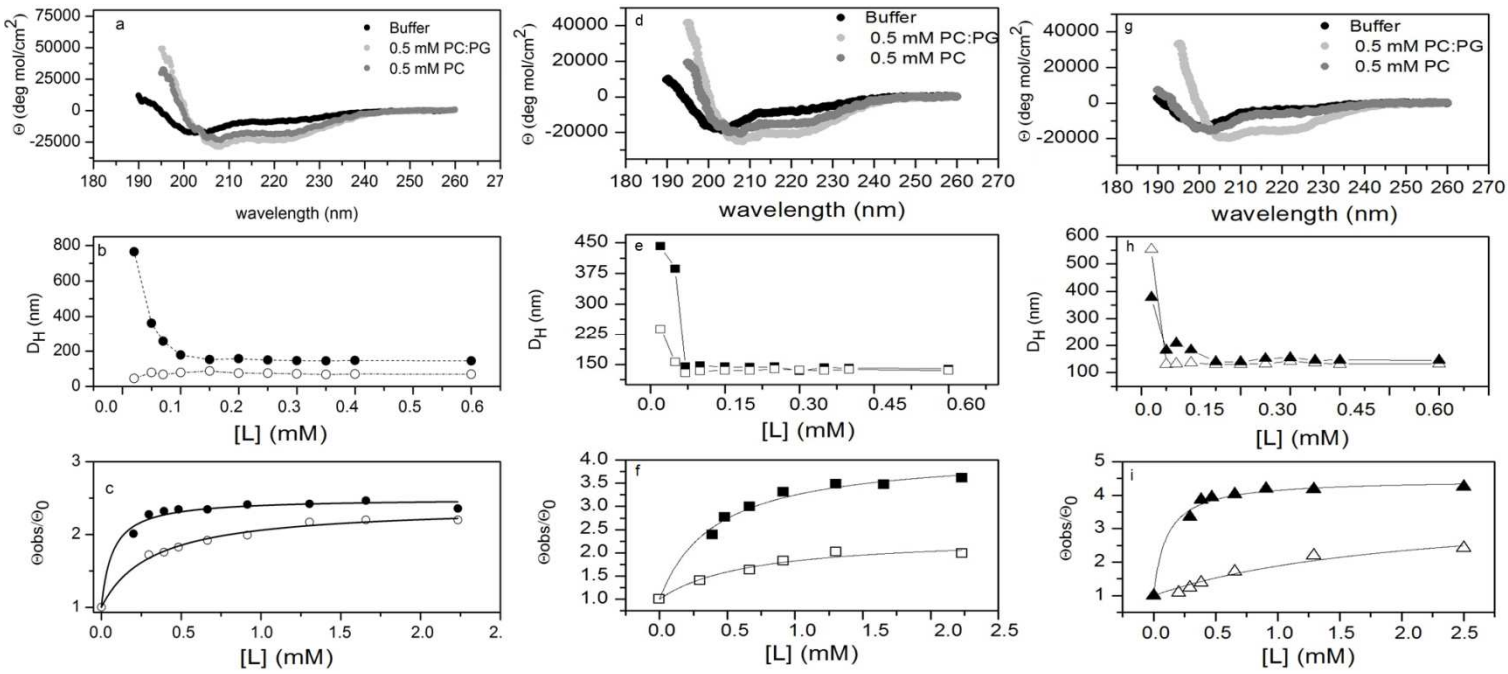

Fig. 4.1 a, d and e - Circular dichroism spectra of MP1, N2DMP1 and MPX respectively at 10µM. Spectra were recorded in the absence and in the presence of 0.5 mM of PC:PG (70/30) and PC LUVs in tris H_3BO_3 5mM, 0.15 M NaF, 0.5 mM Na_2EDTA , pH 7.5, at 25 ^oC .**b, e and g** - Hydrodynamic diameters (D_H) were obtained from the diffusion coefficient (D), using the Stokes-Einstein equation, $D_H = kT/3\pi\eta D$, where k is the Boltzmann constant and T the absolute temperature by dynamic light scattering of the peptide titration for MP1, N2DMP1, and MPX respectively. **c** Molar ellipticity normalized at 222 nm as a function of the lipid concentration. For MP1, N2DMP1 and MPX, respectively, at 10 µM titrated with zwitterionic (open symbols) and anionic (closed symbols) lipids. Solid lines: non-linear fit using eq. 4.2-b.

The partition coefficient of MPX in zwitterionic vesicles in 150 mMNaClK_p=2200 M^{-1} is around 30% smaller than that obtained by Arbuzova and Schwarz (1999) in DOPC and 107 mMNaCl and by Yandek et al. (2009) in 100 mM KCl. With anionic vesicle the partition coefficient of MPX is in a reasonable agreement with that determined by Schwarz and Reiter (2001) for the slow binding mode. Using kinetic measurements, these authors observed two binding modes, fast and slow. Our experiments were carried out at equilibrium. Therefore, our results would be comparable to the slow binding mode. The partition constant for MPX found by Schwartz and Reiter is K_p = 22500 M^{-1}in vesicles with 90% POPC and 10% POPS and 107 mM NaCl. In our experiments, we found a partition constant K_p = 45000 M^{-1} in vesicles with three times more anionic lipids and 150 mMNaCl, therefore in reasonable agreement with those

authors. A very unusual behavior was observed, in anionic vesicles, K_p increased with the decrease of peptides net charge, suggesting that the peptide partitioning into the lipid bilayer is driven by non-coulombic interactions.

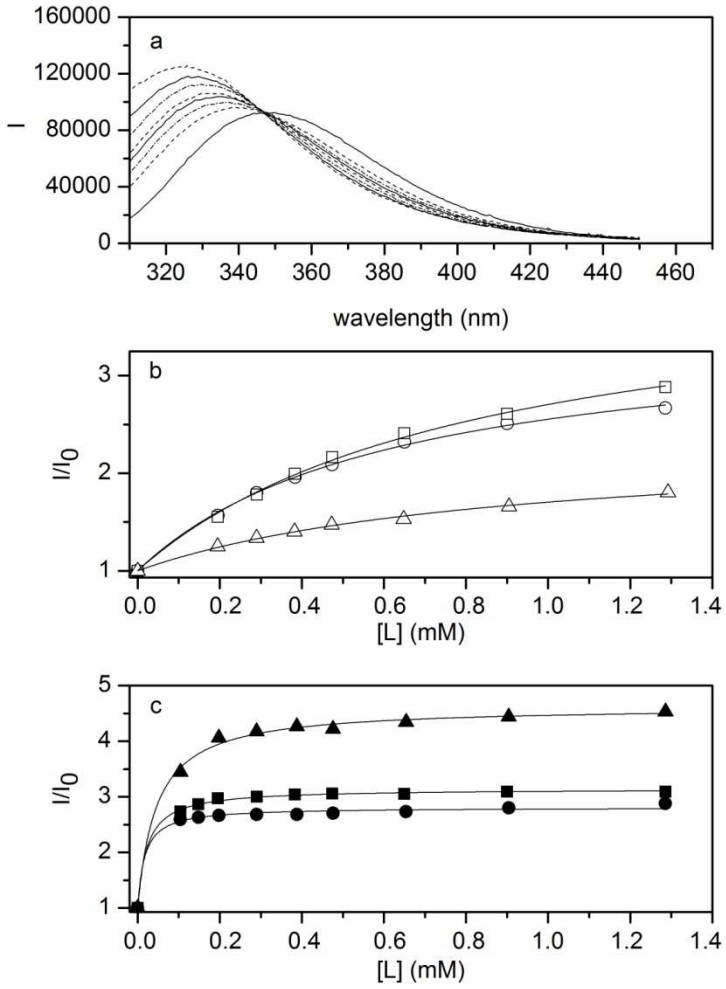

Fig. 4. 2 a Fluorescence emission spectra of MP1 5 μ M in tris H_3BO_3 5mM, 0.15 M NaF, 0.5 mM Na_2EDTA , pH 7.5, at 25 ^oC in the presence of PC LUVs, from bottom to top in 325 nm: 0, 0.2, 0.29, 0.38, 0.475, 0.65, 0.9, 1.3 mM of lipid. **b** Normalized fluorescence emission intensity as a function of the lipid concentration. MP1, N2DMP1, and MPX at 5 μM titrated with zwitterionic (open symbols) and anionic (closed symbols) lipids. Solid lines: non-linear fit using eq.4.4.

Table 4.2 Blue Shifts and Partition coefficients.Position of the maxima emission intensities of tryptophan (λ_{max}); partition coefficients K_p and I_{max}/I_0 obtained from nonlinear fits of eq.4.2 to the experimental plots.

	λ_{max}(nm) PC	λ_{max}(nm) PC/PG	$K_p(M^{-1})^a$ PC	I_{max}/I_0	K_p $(M^{-1})^a$ PC/PG	I_{max}/I_0
MP1	327	327	2400 ± 100	2.3	130000 ± 14000	2.8
D2N-MP1	326	325	3200 ± 200	4.1	80000 ± 4000	3.1
MPX	328	323	2200 ± 100	3.5	45000 ± 2000	4.6

[a] Partition coefficients refer to the adsorption to the outer monolayer of LUVs

Zeta Potential Measurements

The adsorption of the peptides to PC/PG (70/30) vesicles was also monitored by changes in the zeta potential. The zeta potential values of vesicles, at 40 μM total lipid, in the absence and in the presence of increasing peptide concentrations were shown in the fig. 4.3-a. In the absence of peptides the vesicle zeta potential was about -29 mV. After peptide addition, the zeta potential increased up to zero. Further peptide addition led to positive potential values. From the fig. 4.2-a one can also observe how the zeta potential changes for each peptide. For the highly charged peptides MPX and its D2N mutant the changes in the zeta potential is characterized by a smooth, almost linear, increase of ζ with the peptide concentration up to its inversion. However, for the low charged Polybia MP1 (Q=+2) peptide, there is an initial steep increase of ζ at small peptide concentration, [P]/[L] < 1/20. The insert of fig. 4.3-a, shows that at [P]/[L]=1/40, Polybia MP1induced greater relative changes in the zeta potential than the other two more cationic peptides. This result indicates that, at low [P]/[L] ratios, the less charged peptide has higher affinity to anionic vesicles reinforcing the affinity order obtained from the CD and fluorescence titrations. The steeper increase observed in the MP1 titration, at low peptide concentrations, was followed by a plateau, in which peptide addition induced smaller potential changes and the peptide concentration to invert the zeta potential signal was higher than for the other peptides. The hydrodynamic diameters assessed concomitantly with the zeta potential revealed that the plateau observed for Polybia MP1 is due to the increase in vesicle size as shown in the fig. 4.3-b. However, it is noticeable that the increase of the peptide concentration, so that [L]/[P] becomes less than 10 the aggregation, was hardly observed in the titrations with the other two peptides.

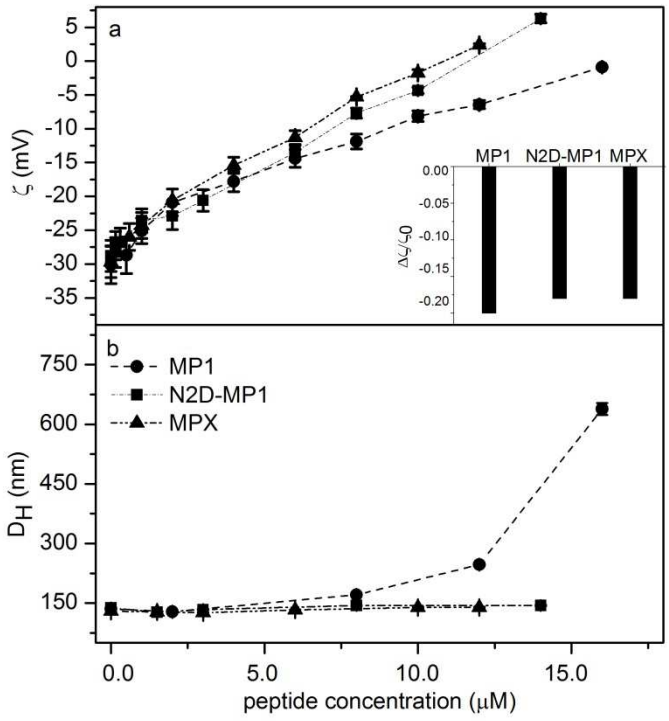

Fig. 4.3 a Zeta potential measurements of vesicles PC/PG, in the presence of different peptide concentrations, was measured by electrophoretic mobilitythrough laserDoppler velocimetry using Malvern ZetasizerNano ZS90. Total lipid concentrations 40 μM in 10 mMTris/HCl, 1 mM EDTA, 0.15 MNaCl, pH 7.5 at 25 ^{o}C.**b**Hydrodynamic radii of vesicles as a function of the lipid concentration. Hydrodynamic radii were determined by dynamic light scattering of the vesicles at the same experimental conditions as zeta potential measurements

Thermodynamics calculations

Aiming to understand the origin of the unusual higher affinity of the less charged peptide to anionic vesicles, we compared the free energies to partitioning the peptides into PC and PCPG vesicles, the energetic cost to fold the peptide in these bilayer interfaces and in the electrostatic (coulombic) component in the case of anionic vesicles.

The partition free energy was calculated by using the partition coefficients (K_p) obtained from the fluorimetric titrations:

$$\Delta G_{obs} = -RTln55.5K_p$$

RT is the thermal energy and 55.5 is the water molar concentration and take into account the cratic correction.

The energetic cost to transfer the completely unfolded peptide from water to the zwitterionic (POPC) bilayer interface was calculated using the package MPEx (Jaysinghe et al 2009The transfer of unfolded MP1 to the POPC interface involves a small unfavorable (positive) energy of 0.03 kcal/mol while the transfer of the other two peptides is favorable (negative) with energies -0.78 kcal/mol and -2.08 kcal/mol for the D2N mutant and for MPX respectively. The CD experiments showed that the adsorption of the peptide is accompanied by its folding in the bilayer interface. The energetic cost to fold the peptide in the membrane interface is given by (Ladokhin et al 1999):

$$\Delta G_{conf} = \delta g f_H N$$

δg is the free energy per residue for folding the peptide in the membrane interface, f_H is the maximum helical fraction obtained from the CD titrations of the peptides with LUVs and N is the number of residues. The free energy per residue was determined by Ladokhin et al (1999), McKeown et al. (2011) and Almeida et al. (2012) as δg = -0.4 kcal/mol. These energetic components are also shown in the table 4.3. In PC LUVs, the energetic cost to folding MP1 is -4.65 kcal/mol that represents 66% of the partition free energy while for its mutant it represents 50 %. Thus the partition of a peptide into the bilayer must involve other energetic contributions, as pointed by White and Wimley (1999). These energetic contributions are related to solvation, loss of motional freedom of the peptide in the membrane and thermodynamics contributions of the bilayer itself among others.

In the case of anionic vesicles the adsorption of the peptide has also an energetic component due to the work of electrostatic potential. The electrostatic free energy to the adsorption of the peptide to the anionic bilayer given by:

$$\Delta G_{el} = z_p F \psi_0$$

wherez_p is the peptide net charge, F is the Faraday constant and ψ_0 is the vesicle surface potential calculated from the zeta potential using the eq. 4.5. The surface potential was calculated using the zeta potential value at [P]/[L]=1/40. The electrostatic free energies obtained are shown in the table 4.3. The electrostatic free energies, shown in table 4.3, are also very small compared with the adsorption free energies, e.g., for MP1 it is around 20% while for MPX it is 40% of the adsorption free energy. In these calculations we have used the peptides net charges, however applying the Gouy Chapman model to the experimental condition one obtain the effective chargesz_{eff}=1.8, 2.6 and 2.9 for MP1, D2N mutant and MPX respectively, and the electrostatic components are even smaller. For this, the zeta potential titrations were analyzed using the protocol suggested by Klocek et al (2009). The analysis assumes that both peptides and ions are adsorbed ideally on the lipid bilayer, and that the peptide concentration immediately above the vesicle surface (C_M) is a function of bothz_{eff}andthe vesicle surface potential (Ψ_0), as described below:

$$\boldsymbol{C_M = C_F \exp\left(-z_{eff} F \Psi_0 / RT\right)} \tag{4.6}$$

where, C_F is the bulk peptide concentration, defined as theremaining peptide concentration in solution after its adsorption on the vesicle surface; F is the Faraday constant, and RT is the thermal energy. The surface charge density, σ, of the vesicle with X_{PG} mole fraction of PG,in the presence of X_B and X_{Na} mole fractions of bound peptide and sodium ions respectively is given by:

$$\boldsymbol{\sigma = \left(e_0 / A_L\right)\left(\left(-X_{PG}\left(1 - X_{Na}\right) + z_{eff} X_B\right)/\left(1 + \left(A_P / A_L\right)X_B\right)\right)} \tag{4.7}$$

where e_0 is the elementary charge, A_L is the area of lipid molecule (70 $Å^2$) and A_P is the peptide area in the membrane (135 $Å^2$). Themolar fraction of adsorbed peptide is $X_B = n_B/n_L = C_B/C_L$ where n_B and n_L the number of moles of bound peptides and lipids, C_B and C_L are the respective molar concentrations, and X_{na} is given by assuming Langmuir adsorption for sodium ions:

$$\boldsymbol{X_{Na} = \left(\left(K_{Na} C_{MNa}\right)/\left(1 + K_{Na} C_{MNa}\right)\right)} \tag{4.8}$$

K_{Na} is the sodium adsorption constant taken as 0.6 M^{-1} and C_{MNa} is the sodium ion concentration under the influence of the vesicle surface potential:

$$\boldsymbol{C_{MNa} = C_{Na} \exp\left(-F\Psi_0 / RT\right)} \tag{4.9}$$

The surface charge density can also be given by the Grahame equation:

$$\sigma^2 = 2000\varepsilon_0\varepsilon_r RT\sum C_i\left(e^{\left(z_i F\Psi_0/RT\right)}-1\right) \quad (4.10)$$

ε_0 is the vacuum dielectric permittivity, ε_r is the relative dielectric constant for water C_i is the bulk concentration for the i^{th} ionic specie with valence z_i. Then, numerical solutions for z_{eff} were found by varying X_B and Ψ_0 until obtain a reasonable solution by the mathematical equality of the eqs 4.7 and 4.10.

Together the electrostatic and conformational free energies comprise 70% and 83% of the adsorption free energy of MP1 and its D2N mutant respectively. The electrostatic and hydrophobic components are not always additive especially in the case of interfacial peptide (Ladokhin and White 2001). We have not verified whether these interactions are additive or not for the peptides used, however, the higher affinity of MP1 compared to its D2N mutant is in contrast with the more favorable electrostatic and conformational contributions observed for the mutant. It is likely that other energetic contributions of different origin would be responsible for the higher affinity of MP1. In this sense, one is tempted to attribute the extra free energy of partition to energetic contributions of other origins, such as non coulombic electrostatic due to peptide solvation or the thermodynamic contribution of the bilayer itself as suggested by Ladokhin et al. 2001 and Wimley and White 1999. These extra energetic contributions calculated as:

$$\Delta G_{ex} = \Delta G_{ads} - \Delta G_{el} - \Delta G_{conf}$$

The extra free energy contribution, shown in the table 4.3, is -2.7 kcal/mol for MP1 and -1.5 kcal/mol for D2N mutant. These values disclose that the extra free energy for MP1 is 1.2 kcal/mol more favorable compared to its D2N mutant and 1.5 kcal/mol compared to MPX.

Table 4.3 Free energies to partitioning peptides into vesicles. Partition free energy (ΔG_{ads}), free energy to transfer a completely unfolded peptide to POPC interface (ΔG_{uif}), Electrostatic free energy (ΔG_{el}), and conformational free energy , (ΔG_{conf}). $\psi_{0,}$ is the vesicle surface potential at [P]/[L]=1/40 calculated from zeta potential by eq.4.3.

Zwitterionic	**PC**					
	ΔG_{ads}	**ΔG_{uif}[a]**	**ΔG_{conf}**			
MP1	-7.03 ± 0.02	0.03	-4.65 ± 0.05			
D2N-MP1	-7.16 ± 0.03	-0.78	-3.70 ± 0.04			
MPX	-6.96 ± 0.02	-2.08	-3.92 ± 0.04			
Anionic	**PC/PG**					
	ΔG_{ads}	**ΔG_{uif}[a]**	**ΔG_{conf}**	**ΔG_{el}**	**ΔG_{ex}**	**Ψ_0 (mV)**
MP1	-9.35 ± 0.06	0.03	-4.76 ± 0.09	-1.85 ± 0.03	-2.7 ± 0.07	-40.0 ± 0.8
D2N-MP1	-9.06 ± 0.03	-0.78	-4.90 ± 0.08	-2.63 ± 0.03	-1.5 ± 0.03	-38.0 ± 0.5
MPX	-8.72 ± 0.03	-2.08	-4.00 ± 0.09	-3.60 ± 0.05	-1.1 ± 0.03	-39.0 ± 0.6

([a])calculated with MPEx

4.4 Discussion

The effect of the acidic groups on the affinity of Polybia MP1 and its D2N mutant to zwitterionic and anionic PC/PG (70:30) lipid vesicles was evaluated and compared to the mastoparan MPX. These peptides have homologous sequence with three lysines and amidated C-terminus and 8 hydrophobic residues. The main characteristic is that Polybia-MP1 has two aspartic acids concomitantly with the three lysine residues with net charge +2. The D2N substitution in the synthetic analog lead to a net charge Q=+3. In previous work, the effects of these peptides were investigated using observation of giant unilamellar vesicles (GUVs) by phase contrast and fluorescence microscopy (dos Santos Cabrera et al. 2011). This study suggested that these peptides present some interfacial actions, inducing controlled loss of phase contrast and the formation of dense fluorescence regions suggesting the formation of domains. Measuring the effect of these peptides on the size of anionic vesicles we had observed that they induced vesicle aggregation at concentrations near the zeta potential signal inversion. Aggregation of vesicles is a characteristic behavior of peptides with interfacial action (Wimley 2010). Besides binding affinity of these peptides to zwitterionic and anionic vesicles, the conformation and the ability to induce vesicle aggregation were also evaluated.

The light scattering experiments where vesicles were titrated with the peptides and also peptide solutions were titrated with liposomes indicated vesicle aggregation for large peptide to lipid ratios near the peptide concentration to induce liposome charge inversion as observed previously. At the initial points of these titrations some liposomes received a large amount of peptides and the large vesicle coverage induced its charge inversion and consequent interaction with oppositely charged vesicles. Similar process was observed for penetratin an important vector carrier (Persson et al. 2001).

The conformational analysis by CD showed that the partition of the peptides in LUVs is accompanied by its folding to the helical conformation. MP1 showed higher helical content (f_h = 0.83) in zwitterionic vesicles compared to its D2N mutant (f_h = 0.66). The energetic cost to folding the peptide in PC interface showed in the table 3 reveals that the folding of MP1 is 0.95 kcal/mol more favorable than its mutant. Scholtz et al (1993) showed that the Glu – Lys salt bridge in TFE costs around 400 cal/mol. Thus our result suggests an important role played by the acidic residues on the stabilization of the helical conformation in PC vesicle through possible ion-pairing similar to that observed from molecular dynamics simulations in 40% TFE. In addition, the acidic residue in the N-terminus region reduces the repulsive charge-helix macrodipole interaction (Fairman 1989) stabilizing the helical conformation. In anionic vesicles MP1 and its D2N mutant have almost the same helical contents f_h = 0.85 and 0.88 respectively.

The D2N mutant should have higher helical content in anionic vesicle because the asparagine has higher propensity of helical formation than the aspartic acid (Rohl and Baldwin 1996), in addition, the electrostatic interaction with anionic vesicles is expected to increase due to the higher peptide net charge (Q=+3). These results have evidenced that in anionic vesicles the mechanism of stabilization of MP1 either did not involve salt bridge between aspartic (D2) and lysine (K5) or that the stabilization mechanisms of these peptides are different in anionic vesicles.

The spectral changes of tryptophan, blue shift accompanied by the increase in the intensity of the fluorescence emission, indicate that the tryptophan residue migrate to a less polar environment in the bilayer, probably near the acyl chains. The partition coefficients, estimated from the changes in the intensity of the tryptophan fluorescence emission spectra, were higher in anionic vesicles indicating the importance of the electrostatic interaction to modulate the peptide-bilayer affinity. Despite this feature, K_P of the less charged peptide MP1 (Q=+2) in anionic vesicles is larger than that of the D2N mutant (Q=+3) and even than the most charged MPX (Q=+4). The higher affinity of the less charged peptide to anionic vesicle is very unusual and opposes to the expected behavior from coarse a graining model (Taheri-Araghi et al. 2011). However, it is remarkable that the CD titrations in LUVs and the relative change in the zeta potential at low [P]/[L] ratios support the order of affinities obtained from fluorescence. In zwitterionic vesicles, the K_P values decrease while the net charges increase as expected suggesting a possible repulsion of the peptides in neutral bilayer.

The free energy of partition and folding of the peptide in the zwitterionic bilayer interface showed that the energetic cost to fold the peptide is lower than that of partition suggesting that other energetic contributions may be involved in the peptide partition into the PC vesicles. In anionic vesicles, the electrostatic energetic contribution seems to play only a secondary role on the adsorption compared to the conformational free energy that is likely to be the main hydrophobic contribution to the adsorption. Although the additivity of the electrostatic and hydrophobic energies has not been shown for these peptides, other energetic contributions, with different origins, must play important role besides the coulombic and conformational components. Many other energetic contributions could be involved in the partition of the peptide to lipid bilayer (White and Wimley 1999). These contributions could be non-coulombic electrostatic due to solvation of the peptide, thermodynamic contributions of the bilayer itself., Change in lipid packing, observed previously by microscopy of GUVs (dos Santos Cabrera et al 2011), is another contribution to the affinity, that could take place in the peptide partitioning into the bilayer and contributing with the affinity order observed.

Acidic residues are very rare in antimicrobial peptides (Wang et al. 2009, Harris et al. 2013), nevertheless there are anionic antimicrobial peptides with high selectivity (Harris et al. 2009). Besides charge balance and conformational stabilization provided by salt bridge when acidic and basic residues are positioned as third and fourth nearest neighbors (dos Santos Cabrera et al. 2008), some acidic residues play important role in peptides as observed in cyclotides by Herrman et al. (2006). These authors observed that methylation of E2 of cycloviolacin O_2 reduced drastically the activity of the peptide in cell cancer. We showed here that the D2 also play a key role in the selectivity of MP1 by enhancing its affinity conferring high selectivity to this peptide, which is in a very good agreement with our previous observation that the D2N substitution impaired the selectivity (Leite et al 2011).

In conclusion, the aspartic acidic residue D2 in the MP1 sequence has an important contribution to the stabilization of the helical structure in contact with lipid bilayer. The charge balance provided by the extensive ion-pairing between the acidic and basic residues seems to play important role on the stabilization of this peptide in PC vesicles. Different mechanism seems to be involved in the stabilization of the helical conformation in PC/PG vesicles that could not involve ion-pairing. The energetic cost for folding the peptides in PC vesicles plays the major role in the partition of the peptides. In PC/PG vesicles the electrostatic contribution plays a minor role compared with the conformational contribution that is accounted for the main part of the hydrophobic contributions. The higher affinity of MP1 for anionic (PC/PG) vesicles in comparison to its D2N mutant is in opposition to its less favorable electrostatic (coulombic) and conformational free energies and most likely the higher affinity of MP1 is being provided by other energetic contributions. These extra energetic contributions are higher than the electrostatic (coulombic) and almost equal to the conformational energy for MP1. The D2 residue leads these extra energetic contributions more favorable for MP1 than its D2N mutant and MPX in 1.2 kcal/mol and 1.5 kcal/mol respectively.

References

Almeida PF, Ladokhin A and White SH (2012) Hydrogen-bond energetics drive helix formation in membrane interfaces. Biochim. Biophys. Acta. 1818: 178-182.

Andreu D and Rivas L (1999) Animal antimicrobial peptides: an overview. Biopolymers 47:415–433

Arbuzova A and Schwarz G (1999) Pore-forming action of mastoparan peptides on liposomes: a quantitative analysis. Biochim.Biophys.Acta 1420:139-152.

Blondelle SE, Forood B, Houghten RA and Perez-Paya E (1997) Secondary structure induction in aqueous vs membrane-like environments. Biopolymers 42: 489-498.

dos Santos Cabrera MP, Costa STB, Souza BM, Palma MS, Ruggiero JR and Ruggiero Neto J (2008) Selectivity in the mechanism of action of antimicrobial mastoparan peptide Polybia-MP1. Eur. Biophys. J. 37: 879-891.

dos Santos Cabrera MP, Alvares DS, Leite NB, Souza BM, Palma MS, Riske KA and Ruggiero Neto J (2011) New insight into the mechanism of action of wasp mastoparan peptides: lytic activity and clustering observed with giant vesicles. Langmuir 27: 10805-10813.

dos Santos Cabrera MP, Arcisio-Miranda M, Gorjão R, Leite NB, de Souza BM, Curi R, Procopio J, Ruggiero Neto J and
Palma MS (2012) Influence of the Bilayer Composition on the Binding and Membrane Disrupting Effect of Polybia-MP1, an Antimicrobial Mastoparan Peptide with Leukemic T-Lymphocyte Cell Selectivity. Biochemistry 51:4898-908.

Fairman R, Shoemaker KR, York EJ, Stewart JM and Baldwin RL (1989) Further studies of the helix dipole model: effects of a free α-NH_3^+ or α-COO^- group on helix stability. Proteins: Struct. , Funct. Genetics 5:1-7.

Harris F, Dennison SR and Phoenix DA (2009) Anionic peptides from eukaryotic organisms. Curr. Protein Pep. Sci. 10: 585-606.

Harris F, Dennison SR, Singh J and Phoenix DA (2013) On the selectivity and efficacy of defense peptides with respect to cancer cells. Med. Res. Rev. 33: 190-234.

Herrmann A, Svangard E, Claeson P, Gullbo J, Bohlin L and Goransson U (2006) Key role of glutamic acid for the cytotoxic activity of the cyclotide cycloviolacin O2. Cell Mol Life Sci. 63:235–245.

Hunter R.J (1981) Zeta Potential in Colloid Science ***Principles and Applications***. Academic Press, London. Chapter2.

Jaysinghe S, Hristova K, Wimley W, Snider C, White SH (2009) http://blanco.biomol.uci.edu/MPEx

Ladokhin AS and White H (1999) Folding of amphipathic helices on membranes: energetics of helix formation by melittin. J. Mol. Biol. 285:1363-1369.

Ladokhin AS, Jayasinghe S and White SH (2000) How to measure and analyze the tryptophan fluorescence in membrane properly and why bother. Analytical Biochemistry 285:235- 245.

Ladokhin AS and White SH (2001) Protein chemistry at membrane interfaces: Non-additivity of electrostatic and hydrophobic interactions. J. Mol. Biol. 309: 543 – 552.

Ladokhin AS, Fernández-Vidal M and White SH (2010) CD spectroscopy of peptides and proteins bound to large unilamellar vesicles. J. Membrane Biol. 236: 247 – 253.

Leite NB, Costa LC, Alvares DS, dos Santos Cabrera MP, Souza BM, Palma MS and Ruggiero Neto J (2011) The effect of acidic residues and amphipathicity on the lytic activities of mastoparan peptides studied by fluorescence and CD spectroscopy. Amino Acids 40:91-100.

Marqusee S and Baldwin RL (1987) Helix stabilization by Glu^{-}... Lys^{+} salt bridges in short peptides of ***de novo*** design. Proc. Natl. Acad. Sci.USA 84: 8898-8902.

Mckeown AN, Naro JL, Huskin LJ and Almeida PF (2011) A thermodynamic approach to the mechanism of cell-penetrating peptides in model membranes. Biochemistry 50: 654-662.

Nakajima T, Uzu S, Wakamatsu K, Saito K, Miyazawa T, Yasuhara T, Tsukamoto Y, and Fujino M (1986) Amphiphilic peptides in wasp venom. Biopolymers 25, 115−121.

Palma MS (2006) In: Handbook of Biologically active peptides "Insect venom peptides" Kastin A. ed. Elsevier/Academic Press San Diego. USA 409-417.

Persson D, Thorén PEG and Nordén B (2001) Penetratin-induced aggregation and subsequent dissociation of negatively charged phospholipid vesicles. FEBS Letters. 505:307-312.

Rohl CA and Baldwin RL (1998) Deciphering rules of helix stability in peptides. Methods in Enzymol. 295: 1-26.

Rouser G, Fleischer S and Yamamoto A. (1970) Two Dimensional Thin Layer Chromatographic Separation of Polar Lipids and Determination of Phospholipids by Phosphorus Analysis of Spots. Lipids 5:494-496.

Scholtz JM, Qian H, Robbins VH and Baldwin RL. (1993) The energetics of ion-pair and hydrogen-bonding interactions in a helical peptide. Biochemistry 32: 9668-9676.

Schwarz G, Stankowski S and Rizzo V (1986) Thermodynamic analysis of incorporation and aggregation in a membrane. Application to the pore forming peptide alamethicin. Biocim. Biophys. Acta 861: 141-151.

Schwarz G and Reiter R (2001) Negative cooperativity and aggregation in biphasic binding of mastoparan X peptide to membranes with acidic lipids. Biophys.Chem. 90:269- 277.

Sforça ML, Oyama Jr. S, Canduri F, Lorenzi CCB, Pertinhez TA, Konno K, Souza BM, Palma MS, Ruggiero Neto J, de Azevedo Jr, WF and Spisni A (2004) How C-terminal carboxyamidation alters the biological activity of peptides from the venom of the Eumenine solitary wasp. Biochemistry 43:5608.

Souza BM, Mendes MA, Santos LD, Marques MR, Cesar LMM, Almeida RNA, Pagnocca FC, Konno K and Palma MS (2005) Structural and functional characterization of two novel peptide toxins isolated from the venom of the social wasp ***Polybia paulista.*** Peptides 26: 2157-2164.

Souza BM, Silva AR, Resende VMF, Arcuri HA, dos Santos Cabrera MP, Ruggiero Neto J and Palma MS (2009) Characterization of two novel polyfunctional mastoparan peptides from the venom of the social wasp ***Polybia paulista.*** Peptides 30: 1387-1395.

Taheri-Araghi S, Ha B-Y (2007) Physical basis for membrane charged selectivity of cationic antimicrobial peptides. Phys Rev. Lett. 98:168101

Wang GS, Li X and Wang Z (2009) APD2. The updated antimicrobial peptide database and its application in peptide design. Nucleic Acids Res. 37: D933- D937.

Wang K, Yan J, Zhang B, Song J, Jia J, Jia P and Wang R (2009) Novel mode of action of Polybia-MP1 a novel antimicrobial peptide in multidrug resistant leukemic cells. Cancer Lett. 278:65-72.

Wang KR, Zhang BZ, Zhang W, Yan JX, Li J, Wang R. Antitumor effects and cell selectivity and structure-activity relationship of a novel antimicrobial peptide Polybia-MP1. Peptides 2008;29:2320-2327.

White SH and Wimley WC. (1999) Memebrane protein folding and stability: physical principles. Annu. Rev. Biophys. Biomol. Struct.28: 319-365.

Wimley WC (2010) Describing the Mechanism of Antimicrobial Peptide Action with the Interfacial Activity Model, ***ACS Chem. Biol.*** 5(10)905-17.

Yandek LE, Pokorny A and Almeida PFF (2009) Wasp mastoparan follow the same mechanism as the cell-penetratin transportan 10. Biochemistry 48:7342-7351.

Yeaman MR, Yount NY (2003) Mechanisms of antimicrobial peptide action and resistance. Pharmacol Rev. 55:27-55.

Chapter 5

Mechanistic insight into the chemotherapeutic activity of an antimicrobial peptide

Natália Bueno Leite[1], Anders Aufderhorst-Roberts[2], Mario Sergio Palma[3], Simon D. Connell[2], João Ruggiero Neto[1,*], Paul A. Beales[4,*]

[1] Department of Physics IBILCE – São Paulo State University -UNESP;

[2] School of Physics and Astronomy and Astbury Centre for Structural Molecular Biology, University of Leeds, Leeds, UK

[3] Center of Studies of Social Insects/Dept. Biology/ IB – São Paulo State University – UNESP.

[4] School of Chemistry and Astbury Centre for Structural Molecular Biology, University of Leeds, Leeds, UK

Article in Preparation

Summary

MP1 has been shown to inhibit cancer (prostate and bladder) cell proliferating being a promise antitumor agent (Wang et al. 2008 and 2009). The presence of anionic phosphatidylserine in the outer monolayer of cancer cells could be the origin of its selectivity to cancer cells. Recently, it was observed that in apoptotic and tumor endothelial cells PE lipids are also externalized as well as PS due to the fact that both lipids are co-regulated by the same transporters (Stafford and Thorpe 2011). These authors observed that the exposure to the outer monolayer of one of these phospholipids leads to the exposure of the other (Stafford and Thorpe, 2011). Changes in lipid composition are responsible for differences on membranes charge and fluidity, and it affects directly the interaction of ligands, such as, bioactive peptides. In this work, we investigated the effects of PS and PE, separately, and in mixtures with PC on the lytic activity of MP1 in single giant unilamellar vesicles (GUVs), as a manner to understand the influence of lipid composition on the peptide affinity for tumor cells. By monitoring dye entrance through confocal microscopy, we used three different sized fluorescent probes (with molecular weights of 0.37, 3.0 and 10.0 kDa) to quantify the peptide's effects on GUVs in terms of percentage of dye influx and membrane permeability changes.

The presence of PS and PE highly affected the permeation kinetics of MP1. PS helped the peptide-lipid interaction due to electrostatic attraction, which was reflected on the kinetics by the smallest lag times while PE vesicles allowed the equal entrance of the three dyes until the equilibrium with the background be reached. The average permeability induced by the peptide in GUVs was estimated from the time dependent influx of dyes and showed that PE increases the membrane permeation. In PC/PE/PS vesicles the average permeability values were about one order of magnitude bigger than those found without PE. The average permeability and relative permeable area of the vesicles were also evaluated and showed to be independent of the size of the dyes in the presence of PE. Requenching experiments of ANTS by DPX were performed with LUVs by fluorescence spectroscopy. These experiments revealed the all-or-none mechanism of leakage by MP1 in all the tested lipid compositions. It suggests that this peptide permeates the membrane trough the formation of pore like structures long lived enough to the fluorescent probes internalize in the vesicles. Atomic Force Microscopy imaging further confirms the importance of PE for formation of larger pores and reveals a difference in pore formation mechanism dependent on PE content.

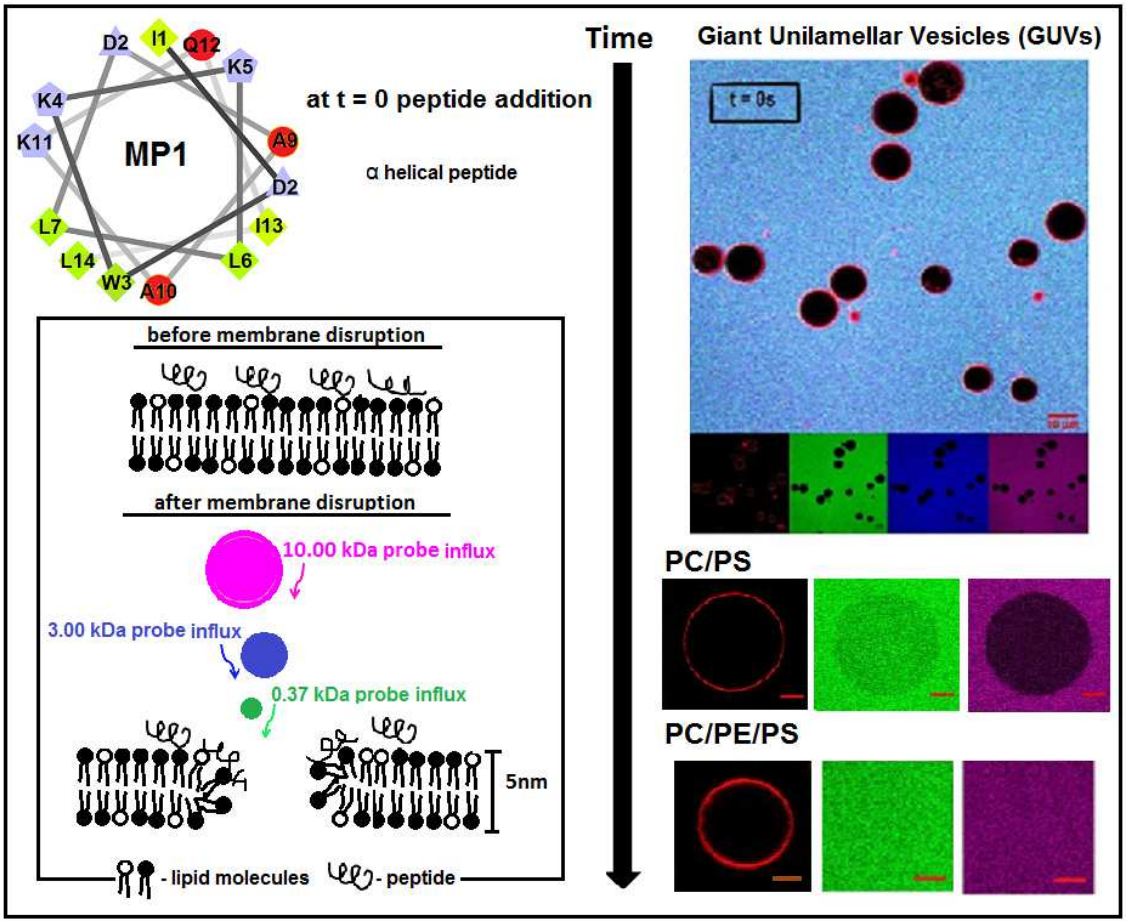

Figure 5.1 - Schematic representation of the studied system. The helical peptide MP1 is shown according to the helical wheel projections. The amino acids in blue are polar with charge, in green are the non polar, and in red are the uncharged polar. Confocal microscopy was performed to investigate the efflux of three dyes with distinct sizes in GUVs in the presence and absence of PE lipids. The peptide interacts with the GUVs disturbs its structure and enables the passage of fluorescent dyes by formation of pore like structures.

Negative curvature stress has been shown to enhance the formation of toroidal lipid pores within a membrane by stabilizing the curvature of these structures (Bergstrom et al. 2013). Therefore PE would be expected to favours the formation of pore-like defects in the membrane, consistent with the order of magnitude increase in membrane permeability that we find for PE-containing membranes upon interaction with MP1. Recently, it was showed by Schmidt et al. (2011) that this type of membrane curvature is generated by peptides with specific amino acid residues such as arginines, lysines and the hydrophobic ones. Arginines can create the Gaussian curvature due to the formation of multidentate H-bonding between the lipids

polar groups and the guanidine groups (Schmidt et al. 2011b). While lysines are able to create negative curvature only in one direction and the hydrophobic residues were observed to induce positive membrane curvature (Matsuzaki 1999; Matsuzaki et al. 1998b; MacMahon and Gallop 2005). Since MP1 does not present arginines but has 3 lysines and a percentage of 57% of hydrophobic residues, we hypothesize that the combination between, lysines and the hydrophobic amino acids can generate the negative Gaussian curvature, which is favoured due to the addition of one more inductor agent of negative curvature strain (PE).

This study, correlates the enhanced tumour inhibitory effects of MP1 with the pathological change in plasma membrane lipid composition, where the upregulation of PS and PE lipids can synergistically enhance its membrane permeabilising activity. This membrane permeabilisation is likely to be the primary mechanism of cancer cell death induced by the anti cancer peptides. This suggests that MP1 might be a candidate therapeutic for development of novel cancer therapies, or at least guide the development of novel lead compounds for treatment of these diseases.

5.1 Introduction

The antimicrobial peptide Polybia-MP1 (IDWKKLLDAAKQIL-NH2), or simply MP1, has unexpectedly been shown to have selective inhibition against several types of cancerous cells that could prove advantageous in the development of novel chemotherapies. Extracted from the Brazilian wasp ***Polybia paulista***, MP1 has a broad spectrum of bactericidal activities against Gram negative and Gram positive bacteria without being hemolytic and cytotoxic (1). Surprisingly, MP1 also shows a selective inhibitory effect on proliferating bladder and prostate cancer cells (2), and against multidrug resistant leukemic cells (3). Recently, it has been observed that this peptide is cytotoxic against leukemic T lymphocytes and very selective in recognizing these cells compared to healthy lymphocytes (4).

Cancer cell membranes are now known to lose the asymmetric transmembrane distribution of phospholipids that is observed in healthy cells (5,6). In healthy mammalian cells, the anionic aminophospholipids, phosphatidylserine (PS), are predominant in the inner membrane leaflet and zwitterionic phospholipids in the outer leaflet of the membrane. In these cells, the phospholipid asymmetry is maintained by a family of aminophospholipid translocases, catalyzing the transport of PS from the outer to the inner membrane leaflets (7). However in apoptotic and cancer cells, PS is found to also be located in the outer monolayer of the plasma membrane in significant proportions (5,6).

Changes in the distribution and/or composition of lipids (e.g. PS) within the plasma membrane of malignant cells could be the origin of MP1's cancer selectivity. This is a reasonable hypothesis based upon the well-established selectivity of antimicrobial peptides for bacterial membranes over eukaryotic membranes due to their higher anionic lipid content. Recently, the effect of PS on the pore-forming activity of MP1 was investigated by multiple techniques: conductance measurements in planar bilayer lipid membranes, binding assays, and lytic activity on large unilamellar vesicles (4). Although an increase in affinity and lytic activity of MP1 for lipid vesicles containing PS was observed, MP1's pore-formation activity in BLM showed no difference between phosphocholine (PC) and mixed PC/PS bilayers. However it was recently reported that, in apoptotic and tumor endothelial cells, PE lipids are also externalized to the outer monolayer of the plasma membrane due to both PS and PE lipids being co-regulated by the same transporters (7). These authors observed that the exposure to the outer monolayer of one of these phospholipids leads to the exposure of the other.

In this work we study the effects of MP1 on the structure and permeability of model membranes. Primarily we study the permeability of giant unilamellar vesicles (GUVs) at the single vesicle level. We investigate the dependence of lipid composition on membrane perturbation by exploring the effect of PS and PE lipids within DOPC (PC) membranes, both separately and in combination: DOPC/POPS 80:20 (PC/PS), DOPC/DOPE 90:10 (PC/PE), and DOPC/DOPE/POPS 70:10:20 (PC/PE/PS). Fluorescence confocal microscopy was used to determine the size-dependent macromolecular permeability of lipid membranes in GUV model systems by analysing the influx of three fluorescent dyes with molecular weights of 0.37, 3.0 and 10.0 kDa into these vesicles (Fig. 1). We show that PE imparts the most significant contribution to the rate and extent of membrane permeabilisation by MP1, allowing the opening of larger membrane defects than in bilayers containing only PC and PC/PS. Ensemble fluorescence spectroscopy experiments provide further evidence for pore formation initiated by MP1 by demonstrating the all-or-none mechanism of vesicle leakage for these membrane compositions.AFM imaging supports the conclusion that PE is important for the formation of larger transmembrane pores and reveals differences in pore formation mechanism for PE-containing membranes compared to membranes that lack this lipid.

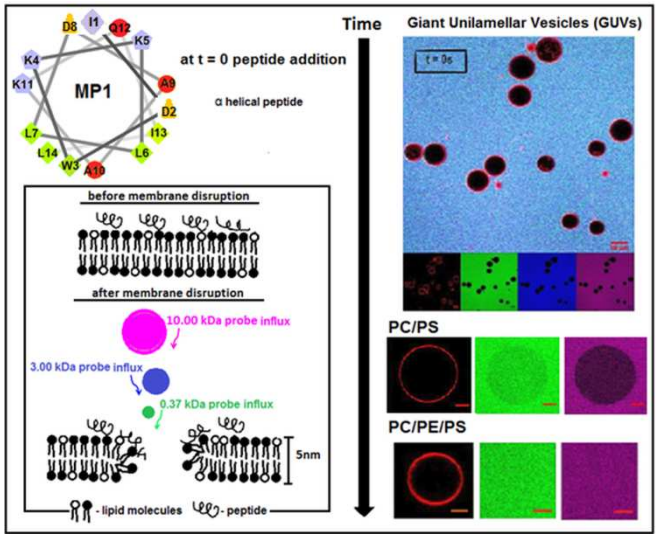

Figure 1 - Schematic representation of membrane disruption by peptides and our experimental system. The helical peptide Polybia MP1 is shown according to the helical wheel projections. The amino acids in blue are the polar with positive net charge, in purple are the polar with negative net charge, in green are non polar, and in red the polar non charged. Confocal microscopy was performed to investigate the influx of three dyes with distinct sizes in GUVs in the presence and absence of PE lipids: 0.37 kDa CF (green), 3k-CB (blue), 10k-AF647 (magenta) and the red bars correspond to 10μm. Lipid membranes are labeled with Rh-DOPE (red). The peptide interacts with the GUVs, disturbs its structure and enables the passage of fluorescent dyes by formation of pore like structures.

5.2 Materials and Methods

Materials

1,2-dioleoyl-***sn***-glycero-3-phosphocholine (DOPC), 1,2-dioleoyl-***sn***-glycero-3-phosphoethanolamine (DOPE), 1-palmitoyl-2-oleoyl-***sn***-glycero-3-phosphoserine (POPS) and 1,2-dioleoyl-***sn***-glycero-3-phosphoethanolamine-N-(lissamine rhodamine B sulfonyl) (ammonium salt) (Rh-DOPE) were purchased from Avanti Polar Lipids (Alabaster, AL). 10 kDa Alexa Fluor© 647-labelled dextran (10k-AF647), 3 kDa Cascade Blue-labelled dextran (3k-CB), 8-aminonaphtalene-1, 3, 6-trisulfonic acid sodium salt (ANTS), and p-xylenebis (pyridinum) bromide (DPX) were purchased from Invitrogen Molecular Probes. Diphenylhexatriene (DPH), Carboxyfluorescein (CF) (370 MW) and all other reagents were purchased from Sigma Aldrich. ***Buffer:*** 10mM Hepes and 150mM NaCl pH 7.4.

Peptide synthesis and purification

Polybia-MP1 (MP1) was synthesized, as described (1, 2) by step-wise manual solid-phase synthesis using N-9-fluorophenylmethoxycarbonyl (Fmoc) chemistry. The crude product was purified by reverse-phase HPLC and the homogeneity and sequence was assessed by analytical HPLC and electrospray ionization mass spectrometry (ESI-MS).

Mass spectrometry analyses

The homogeneity of peptide preparations were ascertained by mass spectrometry. Samples were analyzed on a triple quadrupole mass spectrometer, model QUATTRO II, equipped with a standard electrospray ionisation (ESI) probe (Micromass, Altrincham), adjusted to ca. 250 µl/min. During all experiments the source temperature was maintained at 80°C and the needle voltage at 3.6 kV, applying a drying gas flow (nitrogen) of 200 L/h and a nebulizer gas flow of 20 L/h. The mass spectrometer was calibrated with intact horse heart myoglobin and its typical cone-voltage induced fragments. The molecular masses were determined by ESI-MS, adjusting the mass spectrometer to give a peak width at half-height of 1 mass unit and the cone sample to skimmer lens voltage, controlling the ion transfer to the mass analyzer, was set to 38 V. About 50 pmol (10 µL) of each sample was injected into the electrospray transport solvent. The ESI spectra were obtained in the multi-channel acquisition mode; the mass spectrometer data acquisition and treatment system was equipped with MassLynx and Transform software for handling spectra.

Giant Unilamellar Vesicles (GUVs) Formation

GUVs composed respectively of 100% DOPC (PC), 80% DOPC and 20% POPS (PC/PS), 90% DOPC and 10% DOPE (PC/PE) and 70% DOPC, 10% DOPE and 20% POPS (PC/PE/PS) were formed by the electroformation method. Chloroform stock solutions of the lipid mixture and the fluorescent lipid Rh-DOPE (0.5 mol%) were prepared at a total lipid concentration of 1.0 mM. 50 µl of lipid solution was added drop-wise onto the platinum wires of the electroformation chamber and dried under vacuum from 2-4 hours. The chamber was then filled with a 300 mM sucrose solution and the peak-to-peak voltages of 6.5 V a.c., for zwitterionic lipid mixtures, or 4.5 V a.c., for anionic lipid mixtures, was applied across the platinum wires at distinct frequencies: 10 Hz for 30 mins, 3.0 Hz for 15 mins, 1.0 Hz for 7 mins, and 0.5 Hz for 7 mins. The GUVs were prepared at room temperature. Once formed, GUV

solutions were harvested from the electroformation chamber and stored in foil-wrapped plastic vials prior to imaging.

Large Unilamellar Vesicles (LUVs) Preparation

LUVs composed of the same lipid mixtures as the GUVs were prepared according to general procedures with slight modifications. Briefly, phospholipids dissolved in chloroform were dried under N_2 flow in a round bottom flask. The lipid film was completely dried under vacuum for at least three hours and afterwards hydrated either with 25 mM CF solution prepared in bidistilled water for leakage experiments, or with ANTS 5mM and DPX 8mM both prepared in Hepes buffer for the re-quenching assay. In both preparations the final lipid concentration was around 10 mM. The suspension was submitted to two extrusion steps using an Avanti Mini-Extruder (Alabaster, AL) and double stacked polycarbonate membrane (Nuclepore Track-etch Membrane, Whatman): firstly 6 times through 0.4 μm and then 11 times through 0.1 μm membranes. The dye-entrapped LUVs were separated from unencapsulated fluorophores by gel filtration on a Sephadex G25M column (Amersham Pharmacia, Upsala, Sweden). Vesicles were used within 48 hours of preparation. The lipid concentrations were determined by phosphorus analysis (3).

Confocal Microscopy

Vesicle samples were imaged at room temperature by using the Zeiss LSM 510 META (Jena, Germany) inverted confocal microscope. The objective lens used was a 63×/1.4 N.A. Oil Plan-Apochromat. The Rhodamine probe was excited by a DPSS laser at 543 nm, the CF probe was excited with the 488 nm line of an Argon laser, the Cascade Blue was excited at 405 nm with a Diode Laser and the Alexa Fluor 647 was excited with the 633 nm line of a Helium Neon laser. Small plastic Petri dishes with glass coverslips on the bottom (MatTek Corporation P35G-1.5-14-C) were used as observation chambers. The glass was treated with a 10% Bovine Serum Albumin solution (10 min.) and then washed with deionized water to avoid vesicle adhesion to the glass (4). 20 μL of GUV solution and 75 μL of buffer were incubated for 15 minutes prior to imaging to allow the GUVs to sediment to the bottom of the sample. This is due to the higher density of the sucrose solution inside the GUVs in contrast to the surrounding buffered saline solution.

CF, 3k-CB and 10k-AF647 were diluted in Hepes buffer to obtain solutions of 3 to 30 μM final concentration and were added carefully to the top of the sample. Images and movies of the vesicles in the mixture with buffer and the three dyes were recorded as a control experiment.

For the quantitative analysis of the dye influx process, the concentration of dye in the interior of the vesicles was normalized on a scale of 0-1 according to the equation $c(t) = (b_{interior,\ t} - b_{interior,\ control}) / (b_{exterior} - b_{interior,\ control})$. $b_{exterior}$ is the average pixel intensity in a region of the bulk solution; $b_{interior\ t}$ is the average pixel intensity of dyes in the interior of GUVs after t seconds after peptide addition and $b_{interior,\ control}$ is the average pixel intensity of the dyes in the interior of GUVs in the unleaked control samples (i.e. the background signal). This procedure allowed us to monitor leakage events of individual GUVs for a period of up to 30 min. after peptide addition and to quantify the permeability of GUVs during leakage events.

Analysis of Confocal Images and Movies

Confocal images and movies were analyzed by using ImageJ software. As a criterion, aggregated and multilamellar vesicles and also vesicles with diameter smaller than 8μm, were excluded from the analysis and the remaining vesicles were used on the experiments. Images of GUVs were obtained after 30 minutes of MP1 addition at total final concentrations 4nM, 40nM, 0.4μM, 1.2μM and 4.0μM. This was done to investigate the influx percentage of different sized dyes as a function of peptide concentration (C_P). The percentage of dye influx was obtained by converting dye influx fraction c in terms of percentage: % of dye entrance=100%c. In the movies, single vesicles were monitored over time immediately after peptide addition, at a fixed Cp=4.0μM, during 30 minutes or until the vesicle could be perfectly focalized. For vesicles that moved in the course of the movie, the region of interest was moved to keep it within the vesicle interior and the average background intensity was monitored over time by selecting an external region near the vesicle of interest. Vesicle permeability (P_m) was estimated according to the proposed by (5,6). To obtain P_m we considered that the concentration of dye outside the vesicles,c_{ext}, is constant and equal to 1. The concentrationinside the vesicles is a variable dependent of time, c(t), which can be described after a time interval dtas follows:

$$c(t + dt) = c(t) + \frac{dN_{ext\rightarrow int} - dN_{int\rightarrow ext}}{V_i} \quad (5.1)$$

where$dN_{ext\rightarrow int}$ and $dN_{int\rightarrow ext}$ are the numbers of fluorophore molecules crossing the vesicles from outside to the inner side and from inner side to outside, V_i is the vesicle volume. The concentration can be substituted by the ratio between the number of particles and the volume, c=N/V:

$$c(t + dt) = c(t) + \frac{1-c(t)}{V_i} dV = c(t) + \frac{1-c(t)}{V_i} P_m A dt \quad (5.2)$$

sincethe vesicles are spheres $A=4\pi R^2$ and $V=4/3\pi R^3$, and assuming c(t+dt) – c(t) = dc(t)the equation can be rewritten as:

$$dc(t) = 3P_m \frac{1-c(t)}{R} dt. \quad (5.3)$$

The integration of both sides by considering that at t=0 the vesicles are completely empty and c(0)=0 results in:

$$-\ln(1-c(t)) = \frac{3P_m}{R} tandP_m t = -\frac{R}{3}\ln(1-c(t)) \quad (5.4)$$

From this we conclude that P_m is taken as the gradient of the log-linear plot of the time dependent observed influx as –R/3 ln (1 – c) against time t (5,6).

Dye leakage

Lytic activity of the peptide was investigated in dye leakage experiments induced by peptide in LUVs containing entrapped dye. This was monitored by the de-quenching of the CF fluorescence due to the dye release into the extravesicular medium. In these experiments an aliquot of the LUV suspension was injected into a 1 cm quartz cell, containing magnetically stirred peptide solutions in buffer. The peptide concentrations ranges were from 0.25 to 50 µM, according to the permeabilizing efficiency, to reach around 100% leakage within 20 to 30 minutes of peptide action. CF release from the vesicles was monitored by fluorimetrically using a ISS PC1 spectrofluorometer (Champaign, IL, USA) at 520 nm, 0.5 nm slit width, (excited at 490 nm, 1 nm slit width) at 25°C. Percentage of dye leakage was determined after regular time intervals, and calculated with the equation: % of leakage = $(f - f_0) / (f_{100} - f_0) \times 100$, where f is the observed fluorescence intensity, f_0 and f_{100} correspond, respectively, to the fluorescence intensities in the absence of peptides and to 100 % leakage, as determined by the addition of 20 µl of 10% Triton X-100 solution. f_{100} has been corrected for the corresponding dilution factor.

ANTS/DPX re-quenching measurements

LUVs with entrapped 5 mM ANTS and 8 mM DPX in Hepes buffer, pH 7.4 were prepared. In this assay ANTS works as a fluorescent dye and DPX works as a quencher. The LUVs were submitted to the MP1 interaction to establish the mechanism of leakage for the used lipid compositions. It is possible by determining the dependence of the quenching of ANTS inside the vesicles (Q_{in}) in function of the ANTS fraction outside the vesicles (f_{out}), as proposed by (7). If Q_{in} relies constant and around 0.2 as f_{out} increases, than the peptide exhibits all or none mechanism of leakage, once that a population of vesicles leaked all their content and another

population did not leaked. But, if Q_{in} increases with f_{out}, then it shows a dilution of both ANTS and DPX in the whole set of vesicles, suggesting the gradual mechanism of leakage. The fluorescence intensity was collected with ISS PC1 spectrofluorometer(Urbana Champaign, IL, USA) for 600 seconds with excitation at 355 nm and emission at 520 nm. Excitation and emission bandwidth were set at 1.0 and 2.0 nm respectively. At first, a calibration curve was performed by titrating DPX 25 mM in a sample containing 100μM of lipid and 0.25% Triton X-100. The Triton disrupted the vesicles and all the inner content was released and re-quenched at each DPX addition. This procedure gave to us the quenching of all the ANTS free in solution, Q_{out},evaluated by the ratio between,F_{obs}, the observed fluorescence signal at each DPX addition and,F^{max}, the maximum fluorescence signalobserved i.e. the fluorescence measured before the addition of DPX. After that, different samples were prepared containing100 μM of lipid, buffer and increasing peptide concentrations ranging from 0 to 40 μM.Each peptide sample remained 2 hours in equilibration until the fluorescence signal stabilize, to make sure that MP1 had its activity completed.The peptide addition enabled the leakage of ANTS, which was re-quenched by the titration of four aliquots of DPX 25 mM. At the end, to obtain the fluorescence signal corresponding to the complete leakage, 25 μl of 10% Triton X-100 was added to each sample.The fluorescence intensity was normalized by the fluorescence signal obtained after 10% Triton X-100 addition, $F_{norm}= F_{obs}/F_{triton10\%}$,and then converted to Q_{total}, which is given by the ratio between F_{norm} and F^{max}. The plot of Q_{total} ***versus*** Q_{out} is a linear curve according to:

$$Q_{total} = Q_{out}f_{out} + Q_{in}(1 - f_{out}) \tag{5.5}$$

and the behavior of Q_{in} as a function of f_{out} can be described by the plot of Q_{in} ***versus*** f_{out}.

Atomic Force Microscopy (AFM)

Lipids and cholesterol were purchased in dry form from Avanti Polar Lipids and solvated to 5 mM in chloroform. Supported bilayers were formed from these lipids by the vesicle fusion method. Specifically, solvated lipids were mixed in a glass vial to the correct molar proportion, dried under a gentle stream of N_2 and then placed under vacuum overnight to ensure no chloroform remained. The mixture was then hydrated using the buffer solution to a lipid concentration of approximately 0.5 mg/ml. The suspension was then tip-sonicated until the solution clarified, indicating formation of SUV's. The buffer solution used throughout bilayer preparation and imaging was 125 mM NaCl and 10 mM HEPES at pH7.4.

100 μl of the lipid vesicle solution was pipetted onto a freshly cleaved mica substrate along with 50 μl of a solution of 10 mM $MgCl_2$ in order to aid vesicle fusion and create a perfect defect free supported bilayer. The sample was then incubated in a humid environment at

50 ºC for approximately 1 hour, allowing the vesicles to sediment and rupture on the surface to form a continuous bilayer. The bilayer was then rigorously rinsed ten times with 100 µl warm (50 ºC) buffer using a Gilson pipette, the wash directed parallel to the bilayer surface in order to remove adhering vesicles.

AFM experiments were carried out using a Multimode 8 AFM on a Nanoscope V controller (Bruker), and equipped with a fluid cell. Bruker NP-A probes ($k \approx 0.35 Nm^{-1}$) were operated in contact mode. Although tapping mode in fluid often produces sharper images, it was found that the erosion of the bilayer by the anti-microbial peptide caused debris from the bilayer to float freely in solution, compromising the interactions between tip and sample. Contact mode is generally less susceptible to these effects and thus was more suited. It is also faster than Peak Force Tapping mode, important when attempting to capture dynamics. Following acquisition of several images of the clean bilayer without peptide, the antimicrobial peptide was added manually to the bilayer using a Gilson pipette. A quantity of 150 mM peptide in buffer was added such that the final peptide concentration within the cell was 4 mM or 10 mM. Many different regions of the each bilayer were imaged to ensure a representative view of the sample was obtained, unless time resolved experiments were taking place, when the imaging region was fixed for the whole of one experiment in order to see the direct effect of peptide injection. Maximum scan size = 13 µm. Each preparation of peptide on each lipid mixture was carried out at least three times, and usually five times, to assure reproduceablity. Temperature was not controlled, but would stabilise between 25.5-26.0 ºC within 20 minutes of injection.

5.3 Results

MP1 dose-response studies reveal that PE and PS lipids enhance membrane permeability at lower peptide concentrations.

Membrane permeability of GUV model membranes to macromolecules was characterized by confocal fluorescence microscopy. Fluorescent passive leakage markers of different sizes were simultaneously employed: 0.37 kDa carboxyfluorescein (CF), 10 kDa dextran labeled with Alexa Fluor 647 (10k-AF647) and 3 kDa dextran labeled with Cascade Blue (3k-CB). GUVs were composed of PC, PC/PS, PC/PE, or PC/PE/PS. The dose-response of the membranes to the addition of MP1 was characterized for each membrane composition and passive leakage marker by evaluating the normalized fluorescence intensities of the probes in the intravesicular lumen of the GUVS after 30 minutes incubation time (Fig. 2). Each data point

in Fig. 2 shows the mean leakage of 50 individual GUVs from a minimum of two independent experiments. For determining the percentage of leaked vesicles (Fig. 2c,d), a threshold of 20% leakage (normalized to the background probe concentration) was used to define a filled vesicle.

The integrity of membranes containing both PE and PS lipids is perturbed by lower concentrations of MP1 peptide than the other membrane compositions we investigated. PC/PE/PS GUVs show significant (40-65%) leakage to the CF probe at 0.4 μM and 1.0 μM MP1 concentrations whereas other membrane compositions studied leaked <30% within this concentration range (Fig. 2a). This enhancement in membrane disruption is even more evident when considering the fraction of leaked vesicles (Fig. 2c), with >25% leaked vesicles at MP1 concentrations as low as 4 nM for both membrane compositions containing 10% PE.

Larger pore defects are shown to be significantly enhanced in membranes containing 10% PE. Almost all GUVs (98%) containing PE lipids are observed to leak the larger 10k-AF647 probe when in the presence of 4.0 μM MP1, compared to <25% of GUVs for other membrane compositions at the same peptide concentration (Fig. 2d). Therefore at this MP1 concentration these membranes would be susceptible to the leakage of biological macromolecules such as small proteins and RNAs. This is the most significant enhancement in perturbation selectivity for specific lipid membrane compositions observed within the dose-response data in Fig. 2.

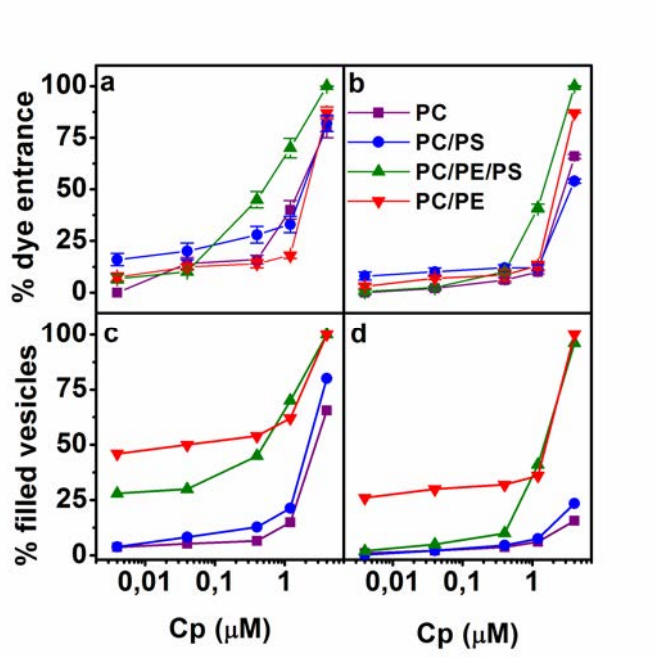

Figure 2 a- % of dye entrance of CF (0.37 kDa) after 30 minutes incubation time of MP1. b- % of dye entrance of 10k-AF647 after 30 minutes incubation time of MP1. 50 GUVs were used to construct each data point. c- % of filled vesicles by CF after 30 minutes incubation time of MP1. d-% of filled vesicles by 10k-AF647 after 30 minutes incubation time of MP1. All vesicles presenting more than 20% of dye entry were accounted. Vesicles are composed of PC, PC/PS, PC/PE and PC/PE/PS.

The lipid composition-dependent potency of MP1 was confirmed using a CF fluorescence dequenching leakage assay conducted on 100 nm diameter large unilamellar vesicles (LUVs): this gives greater statistics for the mean vesicle leakage compared to GUV studies, but lacking sensitivity to the distribution of leakage events within a given sample. CF is loaded inside LUVs at high, self-quenching concentrations; leakage of CF from these vesicles is quantified by the increase in fluorescence when CF dequenches upon dilution in the extravesicular medium. The dose-response curves in Fig. 3 give IC50 values for LUV leakage of 4.6 μM, 5.7 μM and 13.5 μM for PC/PE/PS, PC/PS and PC/PE membrane compositions respectively. This compares with estimated IC50 values from the GUV leakage data in Fig. 2a of 0.5 μM, 1.8 μM and 2.1 μM for PC/PE/PS, PC/PS and PC/PE, respectively. Therefore the trend in permeabilisation efficacy with respect to membrane composition is the same despite the

approximately two orders of magnitude difference in membrane curvature between GUVs (typical diameter >5 μm) and LUVs (average diameter of 0.1 μm). Different absolute values of these apparent IC50s can be attributed to the difference in lipid concentrations between LUV experiments (100 μM) and GUV experiments (~2 μM), therefore not allowing a direct comparison between these numbers. It should be noted that a membrane curvature dependence on the efficacy of MP1-induced leakage cannot be unambiguously deduced from a comparison of these two different experimental systems.

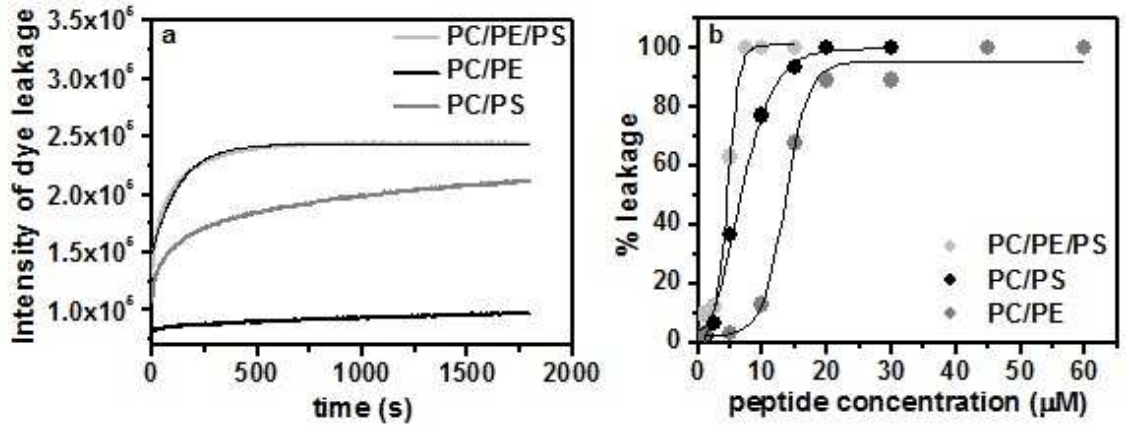

Figure 3. Carboxyfluorescein leakage assay of LUVs of PC/PE/PS (70:10:20), PC/PE (90:10) and PC/PS (80:20) at 100 μM total lipid concentration. a- Kinetic profiles for dye release at 10 μM peptide total concentration. The black line on PC/PE/PS data represents the first-order kinetics fit $I=I_0-I_i\exp(-\kappa t)$ b- Dose response curves 30 minutes after peptide addition.

Synergistic enhancement of GUV leakage kinetics by PE and PS lipids

Analysis of the time delay from the start of the experiment to observations of GUV leakage reveals a synergistic reduction in this lag time for PC/PE/PS membranes (table 1 and Fig 4). In our GUV experiments, we added 4.0 μM MP1 to our samples and monitored the time taken for initial leakage events of GUVs to the 0.37 kDa CF probe to occur. The onset of leakage occurs approximately twice as quickly for PC/PE/PS GUVs than for other membrane compositions, with only a very slight increase in kinetics for PC/PS membranes compared with PC/PE and PC GUVs. Therefore this is not a purely electrostatic effect from the interaction of the cationic peptide with anionic PS-containing membranes, and requires the presence of PE to significantly increase the susceptibility of the membrane to permeabilisation.

Table 1 ***Time delays between the leakage of each dye and the time interval before the leakage takes place.***

<Time delays> (s)				
	PC/PE	**PC/PE/PS**	**PC/PS**	**PC**
$\mathbf{T_{CF} - T_{3k\text{-}CB}}$	1.8 ± 0.6	1.5 ± 0.3	26.4 ± 3.6	162.0 ± 108.0
$\mathbf{T_{3k\text{-}CB} - T_{10k\text{-}AF647}}$	4.2 ± 1.5	2.0 ± 0.4	51.6 ± 6.0	222.0 ± 66.0
$\mathbf{T_{3k\text{-}CB} - T_{10k\text{-}AF647}}$	2.7 ± 0.9	1.4 ± 0.4	9.6 ± 1.2	60.0 ± 42.0
$\mathbf{<time>_{CF\ leakage\ start}}$	1600.0 ± 110.0	760.0 ± 120.0	1440.0 ± 60.0	1600.0

Once the initial leakage event has occurred, PE-containing GUVs rapidly became leaky to fluorescent probes of larger sizes (3 kDa and 10 kDa). For PC/PE/PS and PC/PE membranes, GUVs become leaky to larger 3k-CB than 10k-AF647 passive leakage markers within seconds of permeabilisation to the smallest CF-0.37kDa probe (table 1). The consecutive delay times between CF and 3k-CB probes and 3k-CB and 10k-AF647 probes were approximately an order longer for PC/PS membranes, and almost two orders of magnitude longer for purely PC membranes. This strongly implies that the presence of PE significantly enhances the favorability and rate of formation of larger membrane defects or pores.

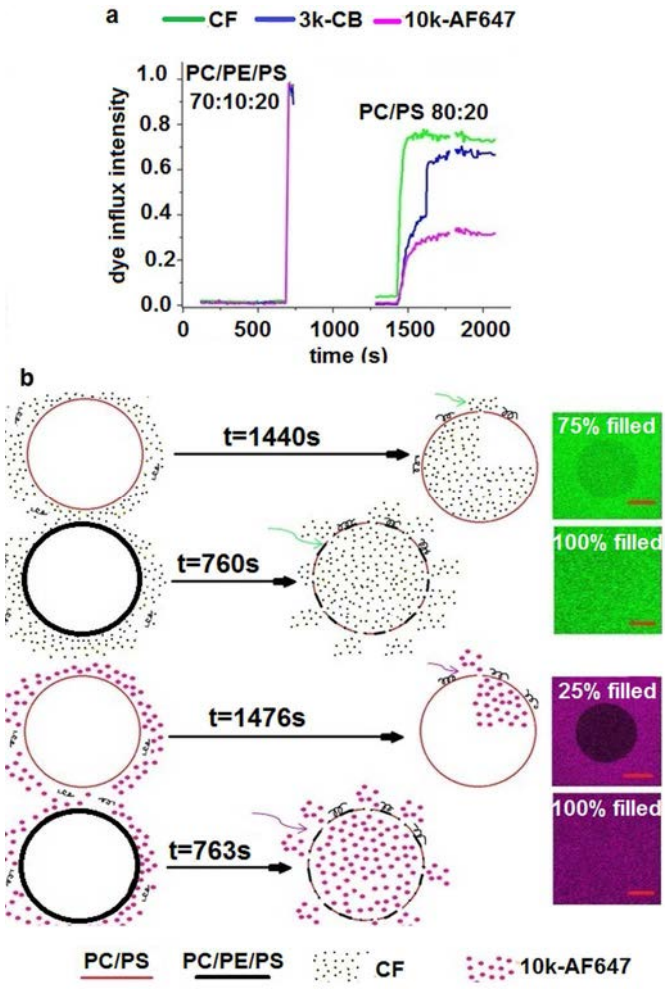

Figure 4 a- Comparison between dye influx kinetics of three distinct dyes (CF-0.37kDa, 3k-CB and 10k-AF647) in the presence and absence of PE after MP1 addition. b- Schematic vision of the dye influx kinetics for PC/PS and PC/PE/PS GUVs in the presence of CF and 10k-AF647.

Confirmation of the pore formation hypothesis in lipid vesicles

The fluorescence re-quenching method (8) enables us to distinguish whether all-or-none or gradual leakage mechanisms are induced by MP1 for our lipid compositions under investigation. The all-or-none mechanism is where some vesicles release all of their internal contents while the others remain intact and is attributed to pore formation mechanisms of membrane perturbation. The gradual leakage mechanism is where vesicles only release a fraction of their encapsulated contents during a leakage event and is associated with transient perturbations of the membrane. A fluorophore (ANTS) and a quencher (DPX) are encapsulated within lipid vesicles at high concentrations such that the fluorescence is initially quenched; vesicle leakage results in the release of both ANTS and DPX, however quenching is decreased

due to dilution of these probes. The externalized ANTS fluorescence can be suppressed by additional titration of DPX such that the remaining fluorescence signal is only due to the ANTS inside intact vesicles. The data can be represented by a plot of degree of quenching (Q_{in}) against the released ANTS fraction, (f_{out}). In the case of an all-or-none leakage mechanism, the concentration-dependent ANTS fluorescence inside the vesicles will remain constant, independent of the fraction of vesicles that have leaked their contents, and so the plot of Q_{in} vs f_{out} will be a horizontal line. In contrast, the gradual leakage mechanism causes release of only a fraction of the encapsulated contents within individual vesicles and so Q_{in} increases with increasing f_{out} (9).

Different from antimicrobial peptides mastoparans X and mastoparan MP (9), MP1 shows the all-or-none leakage mechanism for all the lipid compositions studied. Figure 5 shows that the values of Q_{in} remain constant with the increase of f_{out} and the consequent increase of peptide:lipid molar ratios. This is related to peptide-induced pore formation (10-13), since the vesicles are able to release all their internal contents through pore-like structures that are sufficiently long-lived (13-18). Furthermore, pore-like activity of MP1 has previously been identified from electrophysiology measurements in planar lipid bilayers composed of chicken egg PC and PC/PS (70:30) (4). Our fluorescence requenching results show that stable pores form with a lifetime that persists long enoughfor the dye efflux to reach equilibrium in LUV systems. However this does not discount the possibility that pores might self-heal over longer timescales, for example during the leakage of much larger vesicles such as GUVs.

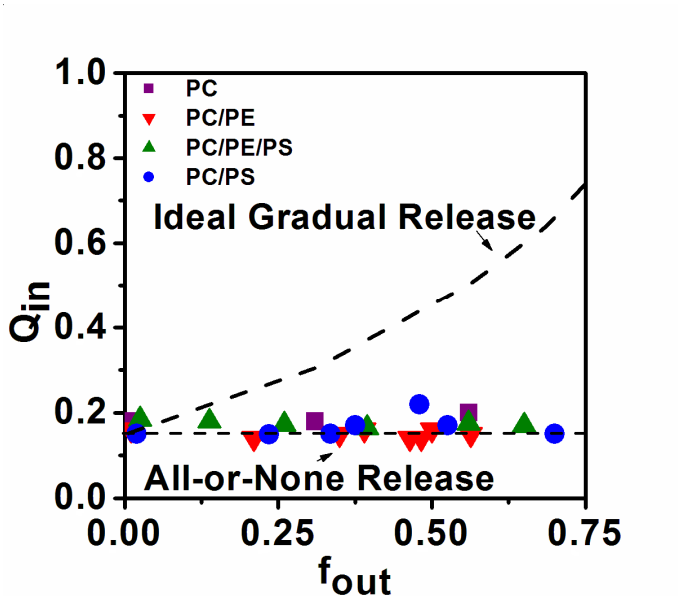

Figure 5. Fluorescence requenching assay curve for MP1 in the four used lipid compositions. MP1 exhibited a horizontal line of Q_{in} vs f_{out} which is in agreement with the all-or-none mechanism of dye release. The lines represents the theoretical curves for ideal graded and all-or-none dye release (8).

PE lipids significantly enhance pore size and membrane permeability

Time-series confocal microscopy imaging was used to quantify the membrane permeability of GUVs during initial leakage. Quantification of the fluorescence intensity of the leakage markers in the intravesicular and extravesicular medium allowed us to calculate the fractional leakage of individual GUVs as a function of time. The leakage kinetics of individual GUVs were monitored for up to 30 min. after the addition of 4.0 μM MP1. These experiments were conducted on GUVs of all four membrane compositions under investigation using the CF, 3k-CB and 10k-AF647 leakage markers simultaneously such that the time evolution of membrane permeability to different molecular sizes could be simultaneously measured for individual GUVs (Fig. 4a and Fig. 6). To the best of our knowledge, this is the first example of simultaneous size-dependent permeability measurements in GUVs for three different sized leakage markers.

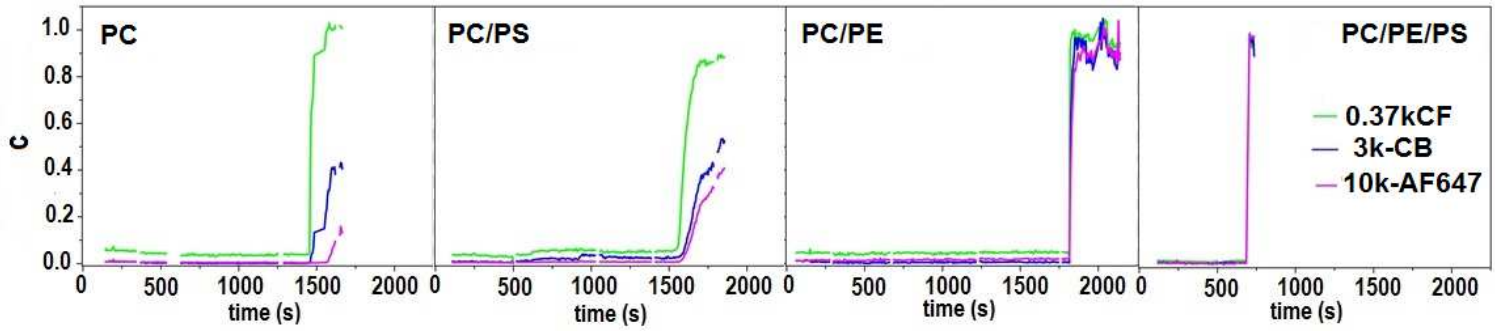

Figure 6. Example profiles for the typical kinetics of single vesicle permeation due to the addition of MP1 at 4.0μM final concentration in four lipid compositions: by PC, PC/PS, PC/PE and PC/PE/PS.

Typical leakage kinetic profiles for different membrane compositions and probe sizes are shown in Fig. 6 and Fig. 4a. It can be qualitatively seen from these example profiles that membrane compositions containing 10% PE exhibit full and rapid membrane leakage to all three sizes of leakage marker, consistent with the leakage kinetics data in table 1, which is also outlined at Fig 4b. For membrane compositions lacking PE, membrane self-healing events followed by later phases of increased leakage can be observed, particularly for the 3k-CB and 10k-AF647 leakage probes. Therefore the membrane permeability for PC and PC/PS GUVs, in particular, can change dynamically during the observed leakage events as the lipid bilayer and peptides compete to maintain their barrier properties and induce membrane pores/defects, respectively (Fig.7a).

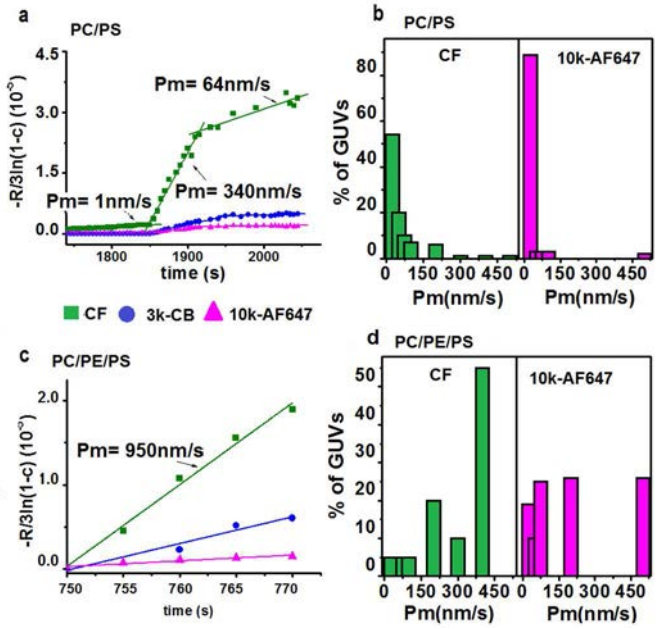

Figure 7 a- Typical log-linear plot of time dependent dye influx: –R/3ln(1-c) ***vs*** time, for the three dyes in a single GUV of PC/PS. b- Distributions of the obtained permeabilities in single GUVs composed by PC/PS. c- Typical log-linear plot of time dependent dye influx: –R/3ln(1-c)(10^{-6}) ***vs*** time, for the three dyes in a single GUV of PC/PE/PS. d- Distributions of the obtained permeabilities in single GUVs composed of PC/PE/PS. The permeabilities were obtained from the slopes of the log-linear plots of the time dependent influx of dyes into single GUVs (fig. S3).

Our leakage kinetic profiles were used to calculate the membrane permeability to the different sized probes using a diffusional model for membrane translocation (23); the membrane permeability is the gradient of the log-linear plot as seen in the example data in Figure 7a,c. Average permeability values for each membrane composition to each probe size during the initial leakage events are shown in table 2. It can be seen that, for all membrane compositions tested, average permeability decreases with increasing probe size. However the most significant finding from this data is the large, order of magnitude increase in membrane permeability for membrane compositions containing 10% PE. This can be observed for all three leakage markers studied. It can also be seen that the presence of PS in the membrane imparts a modest, but significant, increase in permeability on the membranes upon perturbation by MP1. This effect can be seen further in Figure 7b,d, which show the distributions of permeability measurements for PC/PS and PC/PE/PS GUVs to the CF and 10k-AF647 leakage markers, respectively. For both probe sizes, the majority of permeability measurements for PC/PS membranes were in the 0-25 nm/s range, whereas when PE was included in the membrane formulations, a large proportion of permeability measurements were >500 nm/s.

The permeability data was used to calculate the effective fractional permeable area of the membrane for each probe size using the expression (19):

$$\frac{A_p}{A_v} = \frac{P_m}{D_0}\delta$$

Where $\boldsymbol{A_p}$ is the permeable area of membrane on a GUV, $\boldsymbol{A_v}$ is the total area of the vesicle, $\boldsymbol{P_m}$ is the permeability and δ is the thickness of the membrane. The Stokes-Einstein diffusion constant of the leakage marker, $D_0 = kT/6\pi\eta R_0$, where kT is the thermal energy, η is the solvent viscosity and R_0 is the hydrodynamic radius of the fluorescent dye that was estimated with the relation: $\boldsymbol{R_0} = 0.0332(M_W)^{0.463}$, in nm (20), M_W is molecular weight of the dye. Values of the fractional permeable areas are shown in table 2. The fractional permeable areas were also found to be an order of magnitude greater for membrane compositions containing PE than those which did not. Note that slightly larger permeable areas were measured for the larger leakage markers as these represent a later time point in the membrane disruption of GUVs by MP1 as the smaller leakage markers translocate the membrane at earlier times (table 1). This extended delay time therefore allows for a greater area of membrane disruption to occur prior to the initiation of leakage to the larger M_w dyes.

Table 2 ***Average permeability values (<P_m>) and the average fractional permeated area per vesicle (<A_p>/<A_v>) obtained from the average permeability values for each probe size and membrane composition.***

	<P_m> CF (nm/s)	<A_p>/<A_v> CF (10^{-6})	<P_m> 3k-CB (nm/s)	<A_p>/<A_v> 3k-CB (10^{-6})	<P_m> 10k-AF647 (nm/s)	<A_p>/<A_v> 10k-AF647 (10^{-6})
PC	46 ± 14	0.45 ± 0.14	17 ± 6	0.50 ± 0.16	8 ± 2	0.44 ± 0.08
PC/PS	59 ± 12	0.58 ± 0.12	29 ± 6	0.90 ± 0.20	23 ± 4	1.30 ± 0.20
PC/PE	466 ± 143	4.60 ± 1.40	207 ± 102	6.50 ± 3.40	158 ± 53	8.80 ± 2.90
PC/PE/PS	589 ± 142	5.80 ± 1.40	333 ± 73	10.40 ± 2.80	169 ± 52	9.40 ± 2.90

Besides the order of magnitude increase in membrane permeabilisation in the presence of PE lipids, we found an interesting correlation between PE content and membrane morphological response to MP1. Without PE, PC and PC/PS GUVs exhibited bright spots of fluorescent lipids at specific locations on the membrane surface in the presence of 4.0 μM MP1 (Fig. 8). We attribute these observations to local aggregation of peptides and lipids at the GUV surface. These peptide-induced lipid aggregates may be in competition with the pore/defect forming activity of the peptides. Such dense lipid structures were not seen on GUVs containing PE (PC/PE and PC/PE/PS) upon introduction of the peptide. Therefore we speculate that the PE suppresses the intramembrane lipid aggregation by more easily facilitating the poration of the membrane.

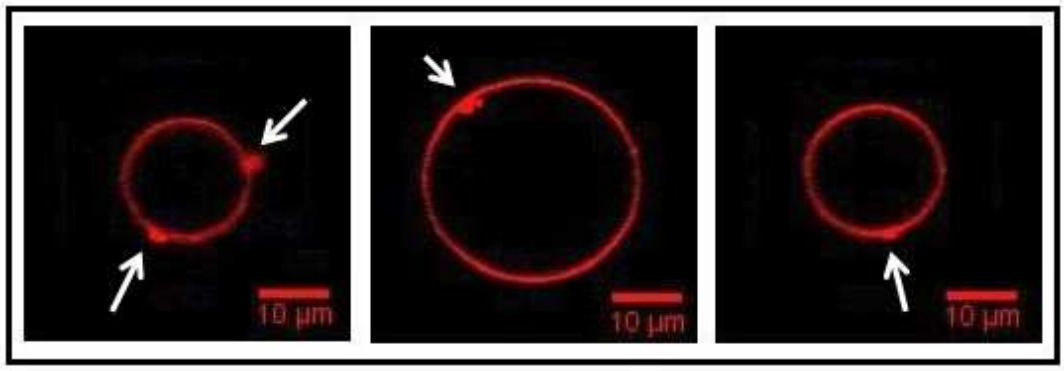

Figure 8. Images of local lipid aggregation at the GUV surface (bright localised spots of fluorescence) seen after peptide addition (Cp= 4.0μM). This effect is frequently observed in PC and PC/PS GUVs, but not for the lipid mixtures containing 10 mol% PE.

AFM imaging of supported lipid bilayers confirms the role of PE in potentiating the formation of larger transmembrane pores. MP1 was added at 10 μM concentration; resultant pores/defects were observed to be much larger in PC/PE/PS membranes compared to PC/PS (Fig. 9). Similar sized transmembrane pores were observed in PC/PE/PS and PC/PE membranes, however significantly fewer defects formed in PC/PE membranes. No pores were evident in PC membranes 2 hr after peptide addition (Fig. 9), however pores would need to be several nm in diameter to be observable by AFM, considerably larger than those that can be detected by passive dye influx into GUVs that we have used to investigate the early stages of GUV poration.

Figure 9. AFM images of the 4 different membrane compositions 2 hr. after the addition of 10 μM MP1. Large pores can clearly be seen in PC/PE/PS and PC/PE membranes with a larger number of pores in the former. PC/PS shown much smaller defects, while no membrane perturbation was resolvable by AFM for PC membranes.

Our AFM studies also clearly show a difference in pore formation and growth mechanisms dependent on the presence of PE. The large transmembrane pores in PC/PE/PS and PC/PE membranes are seen to grow by the step-wise loss of lipid aggregates from the edge of the pore, implying that vesicle micellisation is important for pore growth in the these membranes (Fig. 10). Conversely, in PC/PS membranes, raised areas of lipid are first seen to form on the membrane (Fig. 11), which may correlate to the dense lipid structures observed in Fig. 8. These raised areas of membrane later evolve into comparatively small pores; many of the

defects seen in Fig. 9 (bottom left panel) only span half the bilayer, with only the centre of a few of these showing full bilayer pores (Fig. 12). This indicates that pores in these membranes may form via a half membrane intermediate state. Finally the timescale for observation of membrane defects by AFM was much faster for PC/PE/PS membranes than for other lipid mixtures, with defects observed almost immediately after peptide addition (Fig 10), compared with a few 10s of min. for other mixtures.

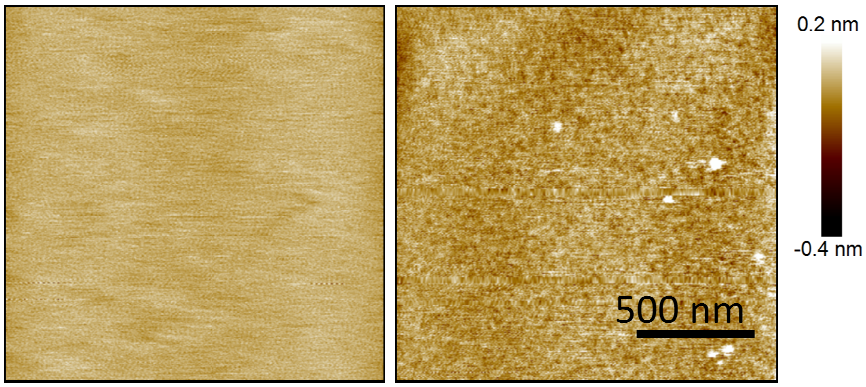

Figure 10. AFM images of a DOPC membrane 80 min. after addition of 10 μM MP1. No clear defects can be observed, but a textured, puckered image can be seen if the z-scale is strectched by a factor of 10.

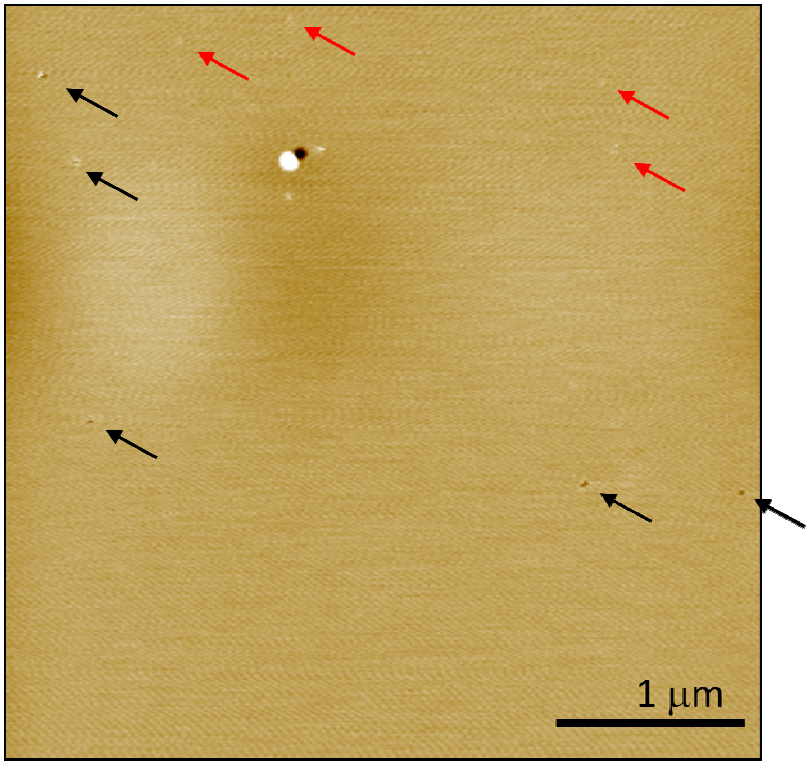

Figure 11. AFM image showing 10-20 nm pin-holes (black arrows) in PC/PE/PS membranes in the first scan, 5 min. after addition of 10 µM MP1. In addition feint "blisters" (some depicted by red arrows) can be seen, which will later develop into pores. A larger pore can be seen top centre-left with a vesicle forming at the edge; vesicle micellisation at the pore rim was observed to be the quantized growth mechanism of larger pore defects.

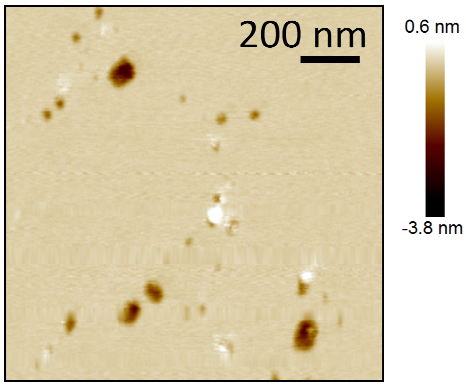

Figure 12. AFM image showing the structural details of pores in PC/PS membranes. Half-bilayer defects (mid-brown) can be observed, along with pores containing full-bilayer pores in their centre (black).

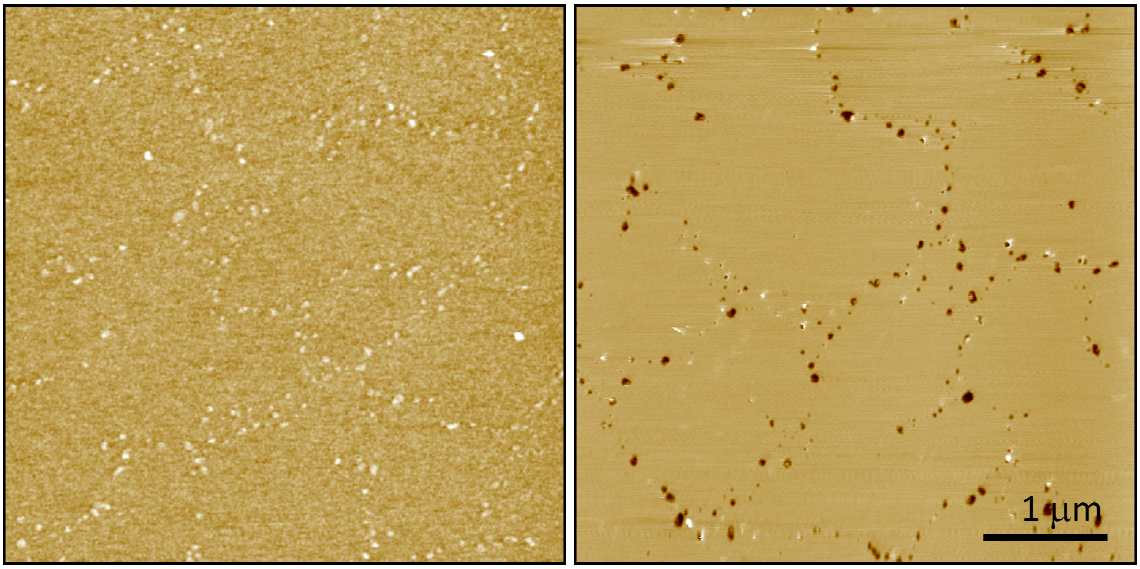

Figure 13. AFM images of PC/PS membranes. (Left) 5-10 min. after addition of 10 μM MP1 "blisters" can be observed in the membrane that will eventually for pores. (Right) Pores observed in the membrane approximately 1 hr. after peptide addition. Interestingly, note that the blisters and pores appear to form along a network of lines on the membrane, implying that there may be some cooperativity between the occurrences of neighboring membrane defects.

5.4 Discussion

Biophysical implications for MP1 – lipid membrane interactions

We have shown a synergistic enhancement of the rate and extent of membrane permeabilisation by MP1 peptides when PE and PS lipids are present in the lipid membrane. PE has the greatest effect on membrane permeability, which is increased by an order of magnitude when 10 mol% PE is present in the membrane compositions under investigation. The combined effect of PE and PS lipids also showed a synergistic enhancement in the rate of permeabilisation of GUVs containing these lipids, with onset of leakage times a factor of 2 quicker than other compositions that were studied.

Changes in lipid composition are responsible for differences in membrane properties such as charge, fluidity, lateral pressure profiles and mechanical moduli. Changes in these fundamental membrane properties directly affect their interactions with extraneous compounds, such as antimicrobial peptides. The cationic nature of the MP1 peptide is likely an important component in the initial step of peptide action, in which the peptide recognizes the target

membrane due to electrostatic interactions and binds to it in a structured form, most of the time as a helix. Therefore the inclusion of PS lipids in our GUV membranes would be expected to increase these electrostatic interactions with the MP1 peptide (net charge = +2$\boldsymbol{e}$). Next, insertion of the peptide into the bilayer likely takes place due to the hydrophobic effect, where non-polar MP1 residues insert into the bilayer core, and defects may then be opened within the membrane structure, leading to its disruption. Furthermore, taking account of the fact that MP1 is a short peptide (14 amino acids) and hence not long enough to form a bilayer spanning barrel stave pore (9, 21), we anticipate that these pores will be disorganized toroidal structures formed by lipids and peptides, as described by many molecular dynamics studies (22-24).

PE is known to significantly modulate the lateral pressure profile through membranes and thereby induce negative curvature stress in the bilayer. Negative curvature stress has been shown to enhance the formation of toroidal lipid pores within a membrane by stabilizing the curvature of these structures (25). Therefore PE would be expected to favor the formation of pore-like defects in the membrane, consistent with the order of magnitude increase in membrane permeability that we find for PE-containing membranes upon interaction with MP1 peptides. Membrane negative Gaussian curvature (positive and negative curvatures along the two perpendicular principal directions) is a necessary condition for toroidal pore formation. Recently, it was showed by Shmidt et al (26) that this type of membrane curvature is generated by peptides with specific amino acid residues such as arginines, lysines and hydrophobic side groups. Arginines can create the Gaussian curvature due to the formation of multidentate hydrogen bonding between the lipid polar groups and the guanidine groups (27). Conversely, lysines are able to create negative curvature only in one direction and the hydrophobic residues were observed to induce positive membrane curvature (28-30). The insertion of hydrophobic residues into the membrane increases the hydrophobic volume of the perturbed lipid monolayer by inducing positive curvature (26). Since MP1 does not present arginines but has 3 lysines and 57% hydrophobic residues, we hypothesize that the combined effect of the lysines and hydrophobic amino acids can generate negative Gaussian curvature. In the presence of PE this structure is favored due to the addition of one more inductor agent of negative curvature strain, clearly reflected from our results. There are another 1080 antimicrobial peptides which are able to form negative Gaussian curvature (26), among them is magainin-2, similar to MP1, which does not present arginines but is rich in lysines and contains 39% hydrophobic residues (27).

Implications for the chemotherapeutic potential of MP1 peptides

The MP1 peptide has been shown to have selective inhibition against numerous cancer lines compared to healthy cells (2,3). Such malignant cells are also known to have increased expression of PS and PE lipids on their outer plasma membrane (5-7). This study strongly

correlates the enhanced tumour inhibitory effects of these peptides with this pathological change in plasma membrane lipid composition, where the upregulation of PS and PE lipids can synergistically enhance the membrane permeabilising activity of MP1. This membrane permeabilisation is likely to be the primary mechanism of cancer cell death induced by these peptides.

This suggests that MP1 might be a candidate therapeutic for development of novel cancer therapies, or at least guide the development of novel lead compounds for treatment of these diseases. One challenge for the application of antimicrobial peptides in medicine is that they often do not show high enough selectivity to their target cells to result in a favorable therapeutic index for these compounds (31). However MP1 does not exhibit hemolytic activity to rat erythrocytes but presents chemotaxis for polymorphonucleated leukocytes and potent antimicrobial action against Gram-positive and Gram-negative bacteria (32), suggesting it could potentially have a favourable selectivity. It may also be of interest to test MP1 in a combination therapy with other chemotherapeutics that have intracellular targets. The selectivity of the MP1 peptide to disrupt the membranes of cancer cells may act synergistically with these other chemotherapeutics to significantly enhance the potency of the therapy. Therefore the therapeutic potential of this and other membrane-active peptides within the field of oncology is worthy of further investigation.

References

1. Souza BM et al. (2009) Characterization of two novel polyfunctional mastoparan peptides from the venom of the social wasp ***Polybia paulista.*** Peptides 30(8): 1387-1395.
2. Wang KR, Zhang BZ, Zhang W, Yan JX, Li J, Wang R (2008) Antitumor effects, cell selectivity and structure-activity relationship of a novel antimicrobial peptide Polybia-MP1. Peptides 29(6):963-968.
3. Wang K et al. (2009) Novel mode of action of Polybia-MP1 a novel antimicrobial peptide in multidrug resistant leukemic cells. Cancer Letters 278(1):65-72.
4. dos Santos Cabrera MP et al. (2012) Influence of the Bilayer Composition on the Binding and Membrane Disrupting Effect of Polybia-MP1, an Antimicrobial Mastoparan Peptide with Leukemic T-Lymphocyte Cell Selectivity. Biochemistry 51(24):4898-908.
5. Zwaal RFA, Comfurius P and Bevers EM (2005) Surface exposure of phosphatidylserine in pathological cells. CMLS 62(9): 971-988.
6. Schweizer F (2009) Cationic amphiphilic peptides with cancer-selective toxicity. European J. Pharmacology 625: 190-194. DOI: 10.1016/j.ejphar.2009.08.043

7. Stafford J H and Thorpe (2011) Increased exposure of phosphatidylethanolamine on the surface of tumor vascular endothelium. Neoplasia 13(4): 299–308.
8. Ladokhin AS, Wimley WC, and White SH (1995) Leakage of membrane vesicle contents: Determination of mechanism using fluorescence requenching. Biophys. J. 69(5): 1964-1971.
9. Arbuzova A and Schwarz G (1999) Pore-forming action of mastoparan peptides on liposomes: a quantitative analysis. Biochim. et Biophys. Acta 1420(1-2): 139-152.
10. Nicol F, Nir S, Francis C, and Szoka J (1996) Effect of Cholesterol and Charge on Pore Formation in Bilayer Vesicles by a pH-Sensitive Peptide. Biophys. J. 71(6): 3288-3301.
11. Apellániz B, Nir S, and Nieva JL (2009) Distinct mechanisms of lipid bilayer perturbation induced by peptides derived from the membrane-proximal external region of HIV-1 gp41. Biochemistry 48(23): 5320-5331.
12. Apellániz B, Nieva JL, Schwille P, and García-Sáez AJ (2010) All-or-None versus Graded: Single-Vesicle Analysis reveals Lipid Composition Effects on Membrane Permeabilization. Biophys. J. 99(11):3619-3628.
13. Fuertes G et al. (2010) Pores formed by Baxα5 to a smaller size and keep at equilibrium. Biophys. J. 99(9): 2917-2925.
14. Matsuzaki K, Murase O, Miyajima K (1996) An antimicrobial peptide, magainin 2, induced rapid flip-flop of phospholipids coupled with pore formation and peptide translocation. Biochemistry 35(35): 11361–11368.
15. Matsuzaki K, Murase O, and Miyajima K (1995) Translocation of a channel-forming antimicrobial peptide, magainin 2, across lipid bilayers by forming a pore. Biochemistry 34(19): 6521–6526.
16. Rathinakumar R and Wimley WC (2008) Biomolecular engineering by combinatorial design and high-throughput screening: small, soluble peptides that permeabilize membranes. J. Am. Chem. Soc. 130(30): 9849–9858.
17. Gregory SM, Pokorny A, and Almeida PFF (2009) Magainin 2 revisited: a test of the quantitative model for the all-or-none permeabilization of phospholipid vesicles. Biophys. J. 96(1): 116–131.
18. Rex S and Schwarz G (1998) Quantitative studies on the melittin-induced leakage mechanism of lipid vesicles. Biochemistry 37(8): 2336–2345.
19. Nelson P. 2004. Biological Physics: Energy, Information, Life (Freeman, New York).

20. Needham D, Park Ji-Y, Wright AM and Tongx J (2013) Materials characterization of the low temperature sensitive liposome (LTSL): effects of the lipid composition (lysolipid and DSPE–PEG2000) on the thermal transition and release of doxorubicin. Faraday Discuss 161: 515–534. DOI: 10.1039/c2fd20111a.
21. Huang HW (2000) Action of Animicrobial Peptides: Two-State Model. Biochemistry 39(29):8347-8352.
22. Sengupta D, Leontiadou H, and Marrink SJ (2008) Toroidal pores formed by antimicrobial peptides show significant disorder. Biochim. Biophys. Acta 1778(10): 2308–2317.
23. Lee MT, Hung WC, and Huang HW (2008) Mechanism and kinetics of pore formation in membranes by water-soluble amphipathic peptides. Proc Natl Acad Sci USA 105(13): 5087–5092.
24. Leontiadou H, Mark AE, and Marrink SJ (2006) Antimicrobial peptides in action. J Am Chem Soc 128(37): 12156–12161.
25. Bergstrom CL, Beales PA, Lv Y, Vanderlick TK, and Groves J (2013) Cytochrome c causes pore formation in cardiolipin-containing membranes. Proc Natl Acad Sci USA. 110(16): 6269-6274.
26. Schmidt NW et al. (2011) Criterion for Amino Acid Composition of Defensins and Antimicrobial Peptides Based on Geometry of Membrane Destabilization. Journal of the American Society Chemical Society 133(17): 6720-6727.
27. Schmidt NW (2011) Deterministic Design of Peptide-Membrane Interactions. Dissertation for the degree of Doctor of the University of Illinois at Urbana-Champaign.
28. Matsuzaki K (1999) Why and how are peptide-lipid interactions utilized for self-defense? Magainins and tachyplesin as archetypes. Biochim Biophys Acta-Biomembranes 1462(1-2): 1–10.
29. Matsuzaki K, Sugishita K-i, Ishibe N, Ueha M, Nakata S, Miyajima K, and Epand R M (1998) Relationship of Membrane Curvature to the Formation of Pores by Magainin 2. Biochemistry 37(34): 11856–11863.
30. McMahon HT and Gallop JL (2005) Membrane curvature and mechanisms of dynamic cell membrane remodeling. Nature 438: 590-596. DOI:10.1038/nature 04396.
31. Matsuzaki K (2009) Control of cell selectivity of antimicrobial peptides**.** BBA Biomembranes 1788(8): 1687-1692.
32. Souza BM et al. (2005) Structural and functional characterization of two novel peptide toxins isolated from the venom of the social wasp ***Polybia paulista.*** Peptides 26(11): 2157-2164.

Chapter 6

Final Considerations

The study of mechanisms of action of bioactive peptides is a wide field of interest, since they can work as good agents against bacteria, fungus and cancer cells and their action is directly related to the lipid portion present on the cellular surfaces of these organisms. The most relevant characteristic in this system is the signaling mechanism that promotes the peptide interaction with the target cells. Once that, the peptides has positive net charges and the prokaryotic cells have surfaces with negative density of charge while the mammalian healthy cells are electrically neutral; in the case of cancer cells especially prostate, bladder and leukemic ones the presence of anionic lipids on the outer leaflet is increased due to the sickness evolution. Then, the presence of both cationic molecules (peptides) and anionic surfaces (prokaryotic or cancer cells) in the same environment, allows their interaction by electrostatic attraction. Independently of any chemical receptor these peptides are seen as promising drugs not subject to mutations that lead to acquired resistance of the aim organism. Even with this importance the mechanisms of action of bioactive peptides is not well understood and the purpose of this thesis was study many aspects involved in the peptide-lipid interaction in search of new findings about it.

In the first part, we used five mastoparan peptides with distinct charges and mean hydrophobicity interacting with zwitterionic and anionic lipid bilayers. To test their membranes affinity and activity, we used circular dichroism and fluorescence spectroscopy. The peptides with lower net charges showed higher lytic activity and affinity in zwitterionic membranes. All the used peptides showed increased activity in anionic environment. The presence of acidic residues showed an important role in modulating the activity of the peptides dependent of the <H>, especially demonstrated in the helix stabilization of Polybia MP1.

In the second part, we used three of the initially used mastoparan peptides with charges +2, +3 and +4 interacting with zwitterionic and anionic lipid bilayers. To estimate the free energies of peptide to lipid interaction we used spectroscopy fluorescence, electrophoretic mobility measurements and circular dichroism data. The results showed higher affinity in both anionic and zwitterionic environments for the peptides with lower net charge, i.e. presenting acidic residues on their amino acid sequence. The estimative of free energy were obtained separately according to each experiment. The partition free energy was evaluated from the partition coefficients resulted from fluorimetric titrations. The electrostatic free energy was obtained from zeta potential results and increased with the peptide charges and the conformational free energy from circular dichroism data. The sum of electrostatic and non-

electrostatic contributions was incompatible with the total free energy (the partition free energy) given origin to an excess free energy. From this, even with lower electrostatic and conformational contributions MP1 exhibited the major affinity for anionic vesicles. The excess free energy for this peptide was the bigger observed and it is likely due to other energetic contributions related to the presence of the acidic residue on the second position of the amino acid sequence.

Since we have obtained interesting results for MP1 and a lot have been explored about this peptide as an antitumor agent, we observed the MP1 interaction with distinct lipid compositions to understand its affinity by cancer cells and the effect of the acidic residue D2 in this action. For this,giant and large unilamellar vesicles were formed in specific lipid compositions (PC, PC/PE, PC/PE/PS and PC/PS). The giant vesicles were observed by confocal microscopy, which enabled us to monitor the vesicles separately and study how the peptide could affect the membrane structure taking account the size of the defects opened through the use of three different sized dyes. The presence of PS and PE highly affected the permeation kinetics of MP1. PS helped the peptide-lipid interaction due to electrostatic attraction, which was reflected on the kinetics by the smallest lag times. Vesicles with PE allowed the equal influx of the three dyes until reach the equilibrium with the background. Experiments with large unilamellar vesicles (LUVs) were made by fluorescence spectroscopy. The re-quenching results allowed us observe the all-or-none mechanism of leakage exhibited by MP1 in all the tested lipid compositions, which means that this peptide permeates the membrane trough the formation of pore like structures. The possibility of the acidic residue D2 on MP1 is related to the strong activity with vesicles containing PE and PS was investigated by leakage experiments in LUVs with MPX, fig.6.1. Since MPX has no acidic residues on its amino acid sequence, we observed the activity in the presence and in the absence of PE and compared it with MP1 results. From this result, we could see the importance of the acidic residue on this interaction because MPX even with charge +4 did not show de same affinity as MP1 in the presence of PE and PS. The lipid compositions with PE showed to relieve the stress due to MP1 action easily due to the fact that PE induces negative curvature in the bilayer while PC and PS favor positive curvatures and toroidal pores are composed by regions of positive and negative curvatures. Since the same was not observed for MPX, we suggest that this effect is not attributed to the lipid composition and the elastic/torsional properties of the membrane only, but the complex peptide/lipid has a fundamental role in potentiate the interaction. Particularly for MP1 the acidic residue D2 was shown to be a differential by stabilizing the helical structure and by increasing the partition free energy. From this, we suggest that this amino acid residue is one of the responsible for its high activity observed in PE vesicles.

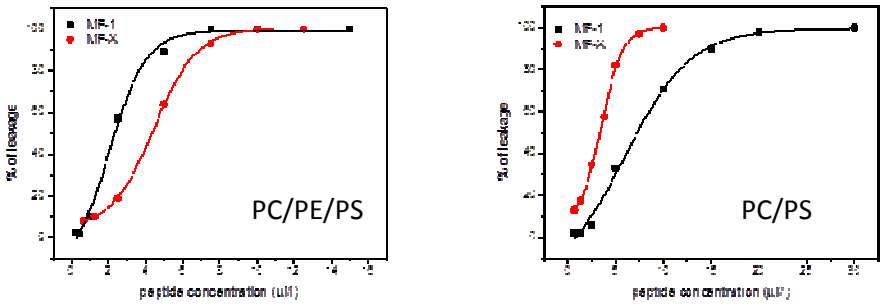

Figure 6.1. Tests with fluorescence spectroscopy of CF leakage due to MP1 and MPX action in large unilamellar vesicles.

In conclusion, from this whole study we could explore the aspects involved in the peptide to lipid interaction such as: peptide net charge, mean hydrophobicity, amino acid and lipid compositions by using different experimental techniques. From this, MP1 was highlighted due to its low net charge and the abundance of acidic residues, which played an important role in modulating its structuration and activity in a wide range of lipid compositions, by equilibrating electrostatic and non-electrostatic contributions giving basis to understand its action as bioactive peptide.

CONCLUSIONS

- The lytic activity increased with the reduction of the peptides net charge in zwitterionic vesicles;
- All the peptides showed increased affinity for anionic lipids in relation to the zwitterionic ones;
- The acidic residues played an important role in modulating the peptides affinity depending on their mean hydrophobicity;
- MP1 presented the most stable helical conformation due to the acidic residues and the lowest mean hydrophobicity;
- The electrostatic, the conformational, the excess and the partition free energies were evaluated for MP1, D2N-MP1 and MPX and the electrostatic free energy increased with the peptides net charge;
- Even with lower electrostatic and conformational free energies MP1 showed the highest affinity for anionic lipids exhibiting the biggest excess free energy, which is related to the presence of the acidic residue D2;
- The presence of PE and PS highly influenced the rate and the extent of membrane permeation by MP1;
- MP1 showed an all-or-none mechanism of leakage for all the lipid compositions, by confirming the formation of pore like structures;
- The pores sizes are dependent on the lipid composition;
- The peptide lipid interaction is modulated by peptides and lipids characteristics such as: peptides' net charge, mean hydrophobicity, and amino acid/lipid compositions.
- MP1 is a potent bioactive peptide due to its high activity in a wide range of lipid compositions attributed to the balance between the electrostatic and non-electrostatic interactions.

REFERENCES

Bahar AA, and Ren D (2013) Antimicrobial Peptides. Pharmaceuticals (Basel). 2013 Nov 28;6(12):1543-75. doi: 10.3390/ph6121543.

Bergstrom C.L., Beales P.A., Vanderlick Y.L.T.K, and Groves J. (2013) Cytochrome c causes pore formation in cardiolipin-containing membranes. PNAS. DOI: 10.1073/pnas.1303819110.

Claxton NS, Fellers TJ, and Davidson MW (2006) Microscopy, Confocal. Enciclpedia of medical devices and instrumentation. DOI: 10.1002/0471732877.emd291.

Cronan JE (2003) Bacterial Membrane lipids: where do we stand? Annu Rev Microbiol, 57: 203-224.

Dathe M, Wieprecht T (1999) Structural features of helical antimicrobial peptides: their potencial to modulate activity on model membranes and biological cells. Biochim.Biophys.Acta 1462: 71-87.

Deber CM, Li S-C (1995) Peptides in membranes: Helicity and hydrophobicity. Biopolymers 37: 295-318.

Demegen Pharmaceuticals (2010) Pharmaceutical products.Productprofiles.Novel candidiasis therapy. www.demegen.com/pharma/candidiasis.htm

dos Santos Cabrera MP, Alvares DS, Leite NB, Souza BM, Palma MS, Riske KA and Ruggiero Neto J (2011) New insight into the mechanism of action of wasp mastoparan peptides: lytic activity and clustering observed with giant vesicles. Langmuir 27: 10805-10813.

dos Santos Cabrera MP, Arcisio-Miranda M, Gorjão R, Leite NB, de Souza BM, Curi R, Procopio J, Ruggiero Neto J and Palma MS (2012) Influence of the Bilayer Composition on the Binding and Membrane Disrupting Effect of Polybia MP1, an Antimicrobial Mastoparan Peptide with Leukemic T-Lymphocyte Cell Selectivity. Biochemistry 51:4898-908.

Epand RM, Epand RF(2009) Lipid domains in bacterial membranes and the action of antimicrobial agents. Biochim Biophys Acta. 1788:289–294.

Eisenberg D, Schwarz E, Komaromy M, Wall R (1984) Analysis of membrane and surface protein sequences with the hydrophobic moment plot. J. Mol. Biol. 179:125-142.

Fairman R, Shoemaker KR, York EJ, Stewart JM and Baldwin RL (1989) Further studies of the helix dipole model: effects of a free α-NH_3^+ or α-COO^- group on helix stability. Proteins: Struct. , Funct. Genetics 5:1-7.

Freire JM et al. (2011) Using zeta-potential measurements to quantify peptide partition to lipid membranes. Eur Biophys J 40:481–487.

Gazit E, et al. (1996) Structure and orientation of the mammalian antibacterial peptide cecropin P1 within phospholipid membranes. J Mol Biol. 258:860–870.

Hancock RE and Lehrer R (1998) Cationic Peptides: A New Source of Antibiotics. Trends Biotechnol. 1998 Feb;16(2):82-8.

Haugland, R.P. The handbook of fluorescent probes and research chemicals. 6. ed. Spencer. Eugene, USA (1996).

Henriques ST, Melo MN, and Castanho MARB (2006) Cell-penetrating peptides and antimicrobial peptides:how different are they? Biochem. J. 399:1–7

Hoskin DW, and Ramamoorthy A (2008) Studies on anti- cancer activities of antimicrobial peptides. Biochim. Biophys. Acta 1778: 357–375.

Huang H.W. (2000) Action of Animicrobial Peptides: Two-State Model. Biochemistry 39:8347-8352.

Holthuis JCM, and Menon AK (2014) Lipid landscapes and pipelines in membrane homeostasis. Nature 510, 48–57.

Hunter R.J (1981) Zeta Potential in Colloid Science ***Principles and Applications***. Academic Press, London. Chapter2.

KALKERT C and KAISER J. Laser double velocimetry, Phys 137, San Diego

Kazemzadeh-Narbat M et al (2010) Antimicrobial peptides on calcium phosphate-coated titanium for the prevention of implant-associated infections. Biomaterials 31:9519–9526.

Klocek G, Schulthess T, Shai Y, and Seelig J (2009) Thermodynamics of Melitin Binding to lipid Bilayers. Aggregation and Pore Formation. Biochemistry 48:2586-2596.

Koskimaki J E, Karagiannis E D, Rosca E V, Vesuna F, Winnard P T, Raman V, et al. (2009) Peptides derived from type IV collagen, CXC chemokines, and thrombospondin- 1 domain-containing proteins inhibit neovascularization and suppress tumor growth in MDA- MB-231 breast cancer xenografts. Neoplasia 11, 1285–1291. doi: 10.1593/neo.09620

Lakowicz, J. R. Principles of Fluorescence Spectroscopy. Kluwer Academic/Plenum, New York, (1999).

Ladokhin AS, Jayasinghe S and White SH (2000) How to measure and analyze the tryptophan fluorescence in membrane properly and why bother.Analytical Biochemistry 285:235- 245.

Ladokhin AS, Fernández-Vidal M and White SH (2010) CD spectroscopy of peptides and proteins bound to large unilamellar vesicles. J. Membrane Biol. 236: 247 – 253.

Leite NB, Costa LC, Alvares DS, dos Santos Cabrera MP, Souza BM, Palma MS and Ruggiero Neto J (2011) The effect of acidic residues and amphipathicity on the lytic activities of mastoparan peptides studied by fluorescence and CD spectroscopy. Amino Acids 40:91-100.

Ludtke SJ, et al. (1996) Membrane pores induced by magainin. Biochemistry 35:13723–13728.

Marconescu A, and Thorpe PE (2008) Coincident exposure of phosphatidylethanolamine and anionic phospholipids on the surface of irradiated cells. Biochim Biophys Acta 1778 (10):2217-24.

Matsuzaki K, Sugishita K, Ishibe N, Ueha M, Nakata S, Miyajima K, and Epand RM (1998) Relationship of membrane curvature to the formation of pores by magainin 2. Biochemistry 37: 11856–11863.

Matsuzaki K, Sugishita K-i, Ishibe N, Ueha M, Nakata S, Miyajima K, and Epand R M (1998b) Relationship of Membrane Curvature to the Formation of Pores by Magainin 2. Biochemistry 37(34): 11856–11863.

Matsuzaki K (1999) Why and how are peptide-lipid interactions utilized for sel-defense? Magainins and tachyplesins as archetypes. Biochim Biophys Acta-Biomembranes 1462: 1–10. DOI: 10.1016/S0005-2736(99)00197-2.

Mckeown AN, Naro JL, Huskin LJ and Almeida PF (2011) A thermodynamic approach to the mechanism of cell-penetrating peptides in model membranes. Biochemistry 50: 654-662.

McMahon HT and Gallop JL (2005) Membrane curvature and mechanisms of dynamic cell membrane remodeling. Nature 438: 590-596. DOI:10.1038/nature04396.

Melo MN, Dugourd D, Castanho MA (2006) Omigananpentahydro- chloride in the front line of clinical applications of antimicrobial peptides. Recent Pat Antiinfect Drug Discov 1:201–207.

Nelson DL, and Cox M (2011) Lehninger: Principles of Biochemistry. (W.H. Freeman and Company, New York and BasingStoke).

Ostolaza H, et al (1993) Release of lipid vesicle contents by the bacterial protein toxin a-haemolysin. Biochim Biophys Acta 1147:81–88. [PubMed: 7682112].

Ourth D D (2011) Antitumor cell activity in vitro by myristoylated-peptide. Biomed. Pharmacother. 65: 271–274.

Papo N, and Shai Y (2005) Host defense peptides as new weapons in cancer treatment. Cell. Mol. Life Sci. 62: 784–790.

Pasupuleti M, Schmidtchen A, and Malmste M (2012) Antimicrobial peptides: key components of the innate immune system. Critical Reviews in Biotechnology, 32: 143-171.

Qian S, Wang W, Yang L, and Huang HW (2008). Structure of the alamethicin pore reconstructed by x-ray diffraction analysis. Biophys J, 94, 3512–3522.

Rapaport D, Shai Y (1991) Interaction of fluorescently labeled pardaxin and its analogues with lipid bilayers. J Biol Chem 266:23769–23775

Santos N, Castanho M (2002) Fluorescence spectroscopy methodolo- giesonthestudy ofproteinsand peptides. Onthe 150th anniversary of protein fluorescence. Trends Appl Spectrosc 4:113–125.

Santos NC, Prieto M, Castanho MARB (2003) Quantifying molecular partition into model systems of biomembranes: an emphasis on optical spectroscopic methods. Biochim Biophys Acta 1612(2): 123–135

Schoemaker KR, Kim PS, Brems DN, Marqusee S, York EJ, Chaiken IM, Stewart JM, Baldwin RL (1985) Nature of the charged group effect on the stability of the C-peptide helix. Proc Natl. Acad. Sci USA 82:2349-2353.

Schmidt NW et al. (2011) Criterion for Amino Acid Composition of Defensins and Antimicrobial Peptides Based on Geometry of Membrane Destabilization. Journal of the American Society Chemical Society 133(17): 6720-6727.

Schmidt NW (2011b) DETERMINISTIC DESIGN OF PEPTIDE-MEMBRANE INTERACTIONS. Dissertation for the degree of Doctor of the University of Illinois at Urbana-Champaign.

Schweizer F (2009) Cationic amphiphilic peptides with cancer-selective toxicity. European J Pharmacology 625: 190-194. DOI: 10.1016/j.ejphar.2009.08.043.

Sengupta D, Leontiadou H, Mark AE, and Marrink S-J (2008) Toroidal pores formed by antimicrobial peptides show significant disorder. Biochim Biophys Acta. 1778:2308–2317.

Souza BM, (2007) Estrutura a função de mastoparanos dos venenos de vespas. Dissertation. Universidade Estadual Paulista, Rio Claro, Brazil.

Souza BM, Mendes MA, Santos LD, Marques MR, Cesar LMM, Almeida RNA, Pagnocca FC, Konno K and Palma MS (2005) Structuralandfunctionalcharacterizationoftwo novel peptidetoxinsisolatedfromthevenomofthe social wasp***Polybia paulista.*** Peptides 26: 2157-2164.

Souza BM, Silva AR, Resende VMF, Arcuri HA, dos Santos Cabrera MP, Ruggiero Neto J and Palma MS (2009) Characterization of two novel polyfunctional mastoparan peptides from the venom of the social wasp ***Polybia paulista.***Peptides 30: 1387-1395.

Souza BM, Silva AR, dos Santos Cabrera MP, Ruggiero Neto J and Palma MS (2010) Investigating the effect of different positioning of lysine residues along the peptide chain of mastoparans for thier secondary structures and biological activities. Amino Acids 40(1):77-90.

Sforça ML, Oyama Jr. S, Canduri F, Lorenzi CCB, Pertinhez TA, Konno K, Souza BM, Palma MS, Ruggiero Neto J, de Azevedo Jr, WF and Spisni A (2004) How C-terminal carboxyamidation alters the biological activity of peptides from the venom of the Eumenine solitary wasp. Biochemistry43:5608.

Stafford J. H. and Thorpe P.E.(2011)Phosphatidylethanolamine on Tumor Endothelium. Neoplasia, vol. 13, pp. 299–308.

Taheri-Araghi S, Ha B-Y (2007) Physical basis for membrane charged selectivity of cationic antimicrobial peptides. Phys Rev. Lett. 98:168101.

Tossi A, Scocchi M, Skerlavaj B, and Gennaro R (1994). Identification and characterization of a primary antibacterial domain in CAP18, a lipopolysaccharide binding protein from rabbit leukocytes. FEBS Lett, 339:108–112.

Uematsu N, Matsuzaki K (2000) Polar angle as a determinant of amphipathic alpha-helix-lipid interactions: a model peptide study. Biophys J 79: 2075–2083.

Wang Y S, Li D, Shi H S, Wen Y J, Yang L, Xu N, et al. (2009a). Intratumoral expression of mature human neutrophil peptide-1 medi- ates antitumor immunity in mice. Clin. Cancer Res. 15: 6901–6911.

Wang GS, Li X and Wang Z (2009b) APD2. The updated antimicrobial peptide database and its application in peptide design. Nucleic Acids Res. 37: D933- D937.

Wang K, Yan J, Zhang B, Song J, Jia J, Jia P and Wang R (2009c) Novel mode of action of Polybia MP1 a novel antimicrobial peptide in multidrug resistant leukemic cells. Cancer Lett. 278:65-72.

Wang KR, Zhang BZ, Zhang W, Yan JX, Li J, Wang R.(2008) Antitumor effects and cell selectivity and structure-activity relationship of a novel antimicrobial peptide Polybia MP1. Peptides 29:2320-2327.

White SH and Wimley WC (1999) Memebrane protein folding and stability: physical principles. Annu. Rev. Biophys. Biomol. Struct.28: 319-365.

Wimley WC and White SH (1996) Experimentally determined hydrophobicity scale for proteins at membrane interfaces. Nat Struct Biol. 3(10):842-8.

Wimley WC (2010) Describing the Mechanism of Antimicrobial Peptide Action with the Interfacial Activity Model, ***ACS Chem. Biol.*** 5(10)905-17.

Wimley WC and Hristova K (2011) Antimicrobial Peptides: Sucesses, Chalenges and Unanswered Questions. J Membrane Biol 239:27-34.

Yandek LE, Pokorny A, Florén A, Knoelke K, Langel U, and Almeida PFF (2007) Mechanism of the Cell-Penetrating Peptide Transportan 10 Permeation of Lipid Bilayers. Biophysical Journal 92: 2434–2444.

Yandek LE, Pokorny A and Almeida PFF (2009) Wasp mastoparan follow the same mechanism as the cell-penetratintransportan 10. Biochemistry 48:7342-7351.

Yeaman MR, Yount NY (2003) Mechanisms of antimicrobial peptide action and resistance. Pharmacol Rev. 55:27-55.

Yount NY, Yeaman MR (2005) Immunocontinuum: perspectives in antimicrobial peptide mechanisms of action and resistance. Protein Pept Lett 12:49–67.

Zwaal RFA, Comfurius P and Bevers EM (2005) Surface exposure of phosphatidylserine in pathological cells. CMLS 62(9): 971-988.

Zasloff M (2002) Antimicrobial peptides of multicellular organisms. Nature 415:389-95.